Influence of amphiphile composition on properties of model primitive membranes and its implications for the origins of early cellular life

A Thesis

Submitted in partial fulfilment of the requirements

for the degree of

Doctor of Philosophy

By

Susovan Sarkar

20152017

Indian Institution of Science Education and Research (IISER) Pune

DEDICATION

I dedicate this work to my mother Shima Sarkar

and my brother Sasank Konakamchi

CERTIFICATE

Certified that the work incorporated in the thesis entitled "Influence of amphiphile composition on properties of model primitive membranes and its implications for the origins of early cellular life" submitted by Susovan Sarkar was carried out by the candidate, under my supervision. The work presented here or any part of it has not been included in any other thesis submitted previously for the award of any degree or diploma from any other University or institution.
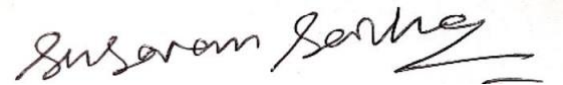
Dr. Sudha Rajamani

14.06.2022

DECLARATION

I declare that this written submission represents my ideas in my own words and where others' ideas have been included, I have adequately cited and referenced the original sources. I also declare that I have adhered to all principles of academic honesty and integrity and have not misrepresented or fabricated or falsified any idea/data/fact/source in my submission. I understand that violation of the above will be cause for disciplinary action by the Institute and can also evoke penal action from the sources, which have thus been properly cited, or from whom proper permission has not been taken when needed.

Susovan Sarkar

14.06.2022

ACKNOWLEDGEMENTS

Table of Content

List of Figures

List of Tables

Synopsis

Influence of amphiphile composition on properties of model primitive membranes and its implications for the origins of early cellular life

Susovan Sarkar, B.Sc., Calcutta University

Introduction:

Semipermeable boundaries composed of amphiphiles are considered to be crucial for the emergence of cellular life on the early Earth[2-4]. In this context, protocells have been studied as the earliest forms of cellular life, which are suggested to be composed of heritable polymers (presumably RNA) and minimal metabolic reactions that are encapsulated within vesicular compartments[1-2]. Unlike the contemporary biological membranes, model protocellular membranes are thought to have been relatively simpler and composed of single chain amphiphiles (SCAs)[3-5]. These SCAs could have come about on the early Earth either by endogenous synthesis, or via exogenous delivery[6-7]. In this context, fatty acids have been studied extensively because of their prebiotic relevance, ability to assemble into cell-sized vesicles and the capacity to encapsulate different kinds of solutes[4-5, 8]. Unlike diacyl phospholipids, fatty acid vesicles possess properties such as high permeability to solutes and increased fluidity due to their unique dynamic nature, which are crucial to support the emergence and sustenance of protocells[9]. However, self-assembly of fatty acids is known to be really sensitive to the changes in its environment[10]. Thus, they can undergo structural transitions in response to different environmental conditions[10-11]. Towards this, in my doctoral studies, I used a combinatorial approach to construct model protocellular membrane systems using fatty acids and other SCAs. I characterized the self-assembly behaviour and physicochemical properties of these composite systems under different environmental conditions as discussed in Chapter 2. Next, I evaluated the structural and chemical stability of these mixed model protocellular membranes under multiple wet-dry cycles, a geological feature with important implications for life's origins as discussed in Chapter 3. Following this, I delineated the self-assembly behaviour and membrane-forming ability of mono-n-dodecyl phosphate (DDP; an alkyl phosphate), a novel prebiotically relevant SCA (an alternative for fatty acid-based membranes), as detailed in Chapter 4.

Chapter 1: Model protocellular membrane compartments (Sarkar et. al, 2020; The Journal of Membrane Biology)

Fatty acid monomers can assemble only in a narrow pH regime near to the pKa of acid head group and possess high critical bilayer concentrations (CBCs); this is the threshold concentration at which the monomers start assembling into bilayer structures[10-12]. Fatty acids are also cation sensitive detergents, i.e. in the presence of cations, they form soap-crystals[13]. However, nucleic acids like self-replicating ribozymes that are at the crux of the RNA world hypothesis, require Mg^{2+} for their catalytic activity[14]. This makes pure fatty acid based membranes incompatible to support protocellular life forms. Towards this end growing literature suggests that the lack of stability of fatty acid membranes can be compensated by adding additional supporting co-surfactants[2-5, 15-16]. However, earlier studies have largely overlooked the probable complexity of protocell membranes and predominantly focussed on binary membrane systems. It is fair to assume that the physicochemical properties of protocellular membrane compartments would have largely been influenced by the early Earth environment[4, 17-18]. Various environmental conditions (e.g. pH variations, presence of ions, rainfall and flooding events leading to dilution, wet-dry cycles etc) would have acted in concert, as a combination of prebiotic selection pressures, shaping the evolutionary landscape of prebiological membranes[18-19]. Towards this end, I aimed to discern how prebiotically pertinent environmental constraints would have acted as important selection pressure(s) to shape the evolution of protocellular systems. Further, I also evaluated the membrane-forming ability of mono-n-dodecyl phosphate (DDP), a prebiotically relevant SCA, as a prebiotically viable alternative for fatty acid-based membranes.

Chapter 2: Influence of compositional diversity on the self-assembly, membrane stability and survivability of model protocellular membrane compartments (Sarkar et al. 2020; SciRep)

First, we aimed to understand the influence of protocell membrane composition on the self-assembly behaviour, membrane stability and physicochemical properties of the compartments, under different environmental conditions. We set out to characterize the physicochemical properties of composite binary and tertiary membrane systems. These systems comprised of a fatty acid, fatty alcohol and

glycerol monoester of the fatty acid in varying ratios, to address how compositional diversity can influence protocellular membrane properties. Fatty acids of two different chain lengths, i.e. oleic acid (OA, C18) and undecylenic acid (UDA, C11), were mixed with their corresponding alcohol and/or glycerol monoester derivatives, and used as a proxy for mixed membrane protocellular systems. Fatty alcohols and glycerol monoester derivatives were chosen because of their prebiotic relevance[15-20]. The prebiotically relevant physical parameters that were characterized included their formation under neutral to alkaline pH, their critical bilayer concentration (CBC), ionic stability and the permeability of all the aforesaid systems. Our results demonstrate that the mixed membrane systems are indeed more stable and robust under diverse environmental selection conditions. Therefore, we make a case for how these would have been more suitable to support protocellular life forms. Systems containing different derivatives possess different survival rates when subjected to a specific selection pressure. Our results illustrate that the head groups of these SCAs play an important role in stabilizing the membranes under specific selection conditions. An important result of this study is the demonstration that the tertiary system, being the most heterogeneous, possessed the best chance at survival when subjected to multiple selection pressures, i.e. by combing all three conditions (i.e. alkaline pH, dilution and divalent cation exposure) in a sequential manner. When put together, these results indicate that different prebiotically pertinent selection pressures would have shaped the evolution of protocellular membranes in a manner that was predominantly determined by their composition.

Chapter 3: Influence of wet-dry cycling on the self-assembly and physicochemical properties of model protocellular membrane systems. (Sarkar et al. 2021; ChemSystemsChem)

Fluctuating environments on the prebiotic Earth that would have been driven by thermal evaporation, geyser activity, rainfall etc., give rise to wet-dry cycles[18-19]. Such naturally recurring wet-dry cycles have been demonstrated to promote formation of biopolymers form different building blocks[21-23]. Despite the imminent relevance of wet-dry cycles on the prebiotic Earth, and its undeniable role in the formation of biopolymers, its influence on the physicochemical properties of model protocellular membranes has been largely overlooked. Given this, we aimed to investigate the self-assembly, physicochemical properties and the chemical stability

of model protocellular membrane systems composed of C18 chain length, under multiple wet-dry cycles. A total of four systems, viz. the oleic fatty acid system, two binary systems containing oleic acid with either the oleyl alcohol or the monooleate derivative, and the tertiary system containing all the three components were used. The ability of preformed vesicles to reassemble into bilayer structures over multiple wet-dry cycles was evaluated. The influence of multiple wet-dry cycles on the physicochemical properties of these model membrane systems was also characterized using different solvatochromic probes. We also evaluated the encapsulation efficiency of model protocell membranes in these scenarios. The results from this study confirm that the protocell membranes composed of C18 based SCAs readily reassemble into vesicles under multiple wet-dry cycles. Furthermore, in-depth characterization of the self-assembled structures reveal changes in the composition and the physicochemical properties of these model membrane systems. Multiple wet-dry cycles were found to influence properties such as vesicle size and percentage encapsulation. Moreover, the effect of multiple wet-dry cycles on the different properties of the membranes also seem to depend on the membrane's composition. Our study indicates how multiple wet-dry cycles would have played an important role in shaping the molecular evolution of protocellular membranes.

Chapter 4: pH-responsive self-assembled compartments as tuneable model protocellular membrane systems. (Sarkar et al. 2022; bioRxiv)

The ability of SCA's to form vesicles only within a narrow pH regime, results in significant shortfalls and limits the environments that would have been suitable for the emergence of early cellular life[4-5, 24-25]. Our previous work demonstrated that addition of co-surfactants (fatty alcohol and glycerol monoester of fatty acid) can stabilize fatty acid based vesicles in alkaline pH regimes but not in acidic pH conditions. Towards this, we aimed to systematically characterize the self-assembly behaviour of mono-N-dodecyl phosphate (DDP), a prebiotically plausible amphiphile[26-27] and discern its membrane's physicochemical properties. We explored the aggregation behaviour and vesicle formation propensity of DDP from pH 2 to 10. The effect of addition of varying ratios of 1-dodecanol (DOH) on the self-assembly and membrane properties of DDP-DOH mixed systems, was also characterized. Remarkably, our results show that DDP alone can assemble into vesicles over a

wide range of pH, all the way from pH 2 to pH 10 in a pH dependent manner. Interestingly, DDP membrane properties were found to be responsive to pH changes. We also studied the high-temperature behaviour of both pure DDP and DDP-DOH mixed membranes, by varying temperature between under different pH. We also compared these properties with other conventional fatty acid based membranes. On comparing the properties of DDP membranes with different diacylphospholipid and fatty acid based membranes at pH 8, DDP membranes showed similar micropolarity as diacylphospholipid membranes. Nonetheless, DDP membrane packing was similar to that of fatty acid based membranes indicating their unique dynamic nature.

References:

1) Ruiz-Mirazo, Kepa, Carlos Briones, and Andres de la Escosura. "Prebiotic systems chemistry: new perspectives for the origins of life." *Chemical reviews* 114.1 (2014): 285-366.
2) Monnard, Pierre-Alain, and Peter Walde. "Current ideas about prebiological compartmentalization." *Life* 5.2 (2015): 1239-1263.
3) Segré, Daniel, et al. "The lipid world." *Origins of Life and Evolution of the Biosphere* 31.1 (2001): 119-145.
4) Sarkar, Susovan, et al. "Prebiological membranes and their role in the emergence of early cellular life." *The Journal of Membrane Biology* 253.6 (2020): 589-608.
5) Mansy, Sheref S. "Model protocells from single-chain lipids." *International journal of molecular sciences* 10.3 (2009): 835-843.
6) McCollom, Thomas M., Gilles Ritter, and Bernd RT Simoneit. "Lipid synthesis under hydrothermal conditions by Fischer-Tropsch-type reactions." *Origins of Life and Evolution of the Biosphere* 29.2 (1999): 153-166.
7) Lawless, James G., and George U. Yuen. "Quantification of monocarboxylic acids in the Murchison carbonaceous meteorite." *Nature* 282.5737 (1979): 396-398.
8) Monnard, Pierre-Alain, and David W. Deamer. "Preparation of vesicles from nonphospholipid amphiphiles." *Methods in enzymology*. Vol. 372. Academic Press, 2003. 133-151.
9) Mansy, Sheref S. "Membrane transport in primitive cells." *Cold Spring Harbor perspectives in biology* 2.8 (2010): a002188.
10) Fameau, Anne-Laure, Audrey Arnould, and Arnaud Saint-Jalmes. "Responsive self-assemblies based on fatty acids." *Current opinion in colloid & interface science* 19.5 (2014): 471-479.
11) Morigaki, Kenichi, and Peter Walde. "Fatty acid vesicles." *Current Opinion in Colloid & Interface Science* 12.2 (2007): 75-80.
12) Chen, Irene A., and Peter Walde. "From self-assembled vesicles to protocells." *Cold Spring Harbor Perspectives in Biology* 2.7 (2010): a002170.
13) Monnard, Pierre-Alain, et al. "Influence of ionic inorganic solutes on self-assembly and polymerization processes related to early forms of life: Implications for a prebiotic aqueous medium." *Astrobiology* 2.2 (2002): 139-152.

14) Bowman, Jessica C., et al. "Cations in charge: magnesium ions in RNA folding and catalysis." *Current opinion in structural biology* 22.3 (2012): 262.

15) Rendón, Adela, et al. "Model systems of precursor cellular membranes: long-chain alcohols stabilize spontaneously formed oleic acid vesicles." *Biophysical journal* 102.2 (2012): 278-286.

16) Jordan, Sean F., et al. "Promotion of protocell self-assembly from mixed amphiphiles at the origin of life." *Nature ecology & evolution* 3.12 (2019): 1705-1714.

17) Thomas, Jacquelyn A., and F. R. Rana. "The influence of environmental conditions, lipid composition, and phase behavior on the origin of cell membranes." *Origins of Life and Evolution of Biospheres* 37.3 (2007): 267-285.

18) Damer, Bruce, and David Deamer. "The hot spring hypothesis for an origin of life." *Astrobiology* 20.4 (2020): 429-452.

19) Damer, Bruce, and David Deamer. "Coupled phases and combinatorial selection in fluctuating hydrothermal pools: A scenario to guide experimental approaches to the origin of cellular life." *Life* 5.1 (2015): 872-887.

20) Maurer, Sarah Elisabeth, et al. "Chemical evolution of amphiphiles: glycerol monoacyl derivatives stabilize plausible prebiotic membranes." *Astrobiology* 9.10 (2009): 979-987.

21) Forsythe, Jay G., et al. "Ester-mediated amide bond formation driven by wet–dry cycles: A possible path to polypeptides on the prebiotic Earth." *Angewandte Chemie International Edition* 54.34 (2015): 9871-9875.

22) Rodriguez-Garcia, Marc, et al. "Formation of oligopeptides in high yield under simple programmable conditions." *Nature communications* 6.1 (2015): 1-7.

23) Rajamani, Sudha, et al. "Lipid-assisted synthesis of RNA-like polymers from mononucleotides." *Origins of Life and Evolution of Biospheres* 38.1 (2008): 57-74.

24) Meierhenrich, Uwe J., et al. "On the origin of primitive cells: from nutrient intake to elongation of encapsulated nucleotides." *Angewandte Chemie International Edition* 49.22 (2010): 3738-3750.

25) Steller, Luke H., Martin J. Van Kranendonk, and Anna Wang. "Dehydration Enhances Prebiotic Lipid Remodeling and Vesicle Formation in Acidic Environments." *ACS central science* 8.1 (2022): 132-139.

26) Powner, Matthew W., and John D. Sutherland. "Prebiotic chemistry: a new modus operandi." *Philosophical Transactions of the Royal Society B: Biological Sciences* 366.1580 (2011): 2870-2877.

27) Cooper, George W., Wilfred M. Onwo, and John R. Cronin. "Alkyl phosphonic acids and sulfonic acids in the Murchison meteorite." *Geochimica et Cosmochimica Acta* 56.11 (1992): 4109-4115.

ABSTRACT

Influence of amphiphile composition on properties of model primitive membranes and its implications for the origins of early cellular life

Susovan Sarkar, B.Sc., Calcutta University

Membrane compartmentalization is considered a feature fundamental to the origin, evolution, and maintenance of cellular life on Earth. Prebiotic membranes are thought to have preceded contemporary membranes and composed of single-chain amphiphiles (SCAs) such as fatty acids and their derivatives. Recent studies indicate that prebiotic environmental conditions would have directly influenced the biophysical properties of protocell membranes. Given this, I aimed to discern how prebiotically pertinent environmental constraints would have acted as important selection pressure(s) to shape the evolution of protocellular systems. I started out by generating model protocell membrane systems by mixing fatty acids of different chain lengths with other co-surfactants. The vesicle formation, its stability, and the properties of these model membrane systems were then evaluated as a function of multiple environmental factors, including varying pH, Mg^{2+} ion concentrations, dilution regimes, etc. Our results show that compositionally diverse membrane systems are amenable to readily forming compartments that are more stable and robust under multiple selection regimes. I evaluated the structural and chemical stability of these model protocellular membranes under wet-dry cycles, a geological feature with important implications for life's origins. The change in various membrane properties and their encapsulation ability were systematically characterized. The membranes investigated were found to readily reassemble into vesicles even after multiple wet-dry cycles. This cycling induced compositional changes in these membranes, which led to changes in their physicochemical properties. Pertinently, multiple wet-dry cycles were also found to increase the vesicle's encapsulation of small molecules. Finally, I evaluated the membrane-forming ability of dodecyl phosphate (DDP), a minimally studied prebiotically relevant SCA, as an alternative for fatty acid-based membranes. The self-assembly behavior of pure and mixed DDP membranes showed that DDP-based membranes are highly tuneable and would have been very suitable to support the emergence and evolution of protocellular life forms on the early Earth.

Chapter I

Introduction: Model protocellular membrane compartments.

(Adapted from, Sarkar et al., 2020; The Journal of Membrane Biology)

1.1 Introduction

How life originated on the early Earth is one of the most fascinating and as yet unsolved puzzle. It has interested scientists from all walks alike to participate in the interdisciplinary endeavour that is implicit to answering this fundamental question. Many interesting and diverse theories have been proposed over the centuries on how life would have emerged, and how the transition from non-living to living took place. A lot of effort has gone into identifying the key features of life, which are compartmentalization (that separates it from its environment), the ability to carry forward information thus undergo evolution, and to possess some sort of metabolism that produces energy and building blocks.[1] Based on that, protocells, the earliest forms of cellular life, are suggested to be composed heritable polymers (presumably RNA), metabolic reactions encapsulated within compartments[1-2] as depicted in Figure 1.1. Membrane Compartmentalization is considered crucial for the origins and evolution of cellular life as it separates internal components from the outside environment, helps in chemical enrichment and protects encapsulated material from both dilution and parasitic molecules.[2-5] Importantly, compartmentalization introduces 'selfness' to the system and provides a framework for facilitating chemical evolution[6] (without invoking the need for a genetic material). Moreover, the ubiquitous nature of the membrane compartmentalization in contemporary cellular life highlights the importance of membrane boundaries in emergence and maintenance of early life. Extant membranes are complex and are predominantly composed of double chain glycerophospholipids, sphingolipids, sterols and a large number of proteins.[7-9] Unlike the contemporary biological membranes, model protocellular membranes are thought to have been relatively simpler and composed of different single chain amphiphiles (SCAs).[2-5] Such amphiphiles have been reported to be synthesized under early Earth conditions and also found in meteoritic samples, hence, considered prebiotically plausible.[4, 10-11] Importantly, the self-assembled structures of the SCAs are generally responsive to their environment and could potentially undergo changes in terms of their composition to different environmental conditions.[12] Fatty acids have been studied extensively in this regard because of their prebiotic relevance, ability to assemble into cell-sized vesicles and the capacity encapsulate solutes.[3-6]

The ability of fatty acids to form bilayer was first explored by Hargreaves and Deamer in 1978, where they found that fatty acids, starting from nine carbon chain length, can assemble under certain conditions to result in vesicles.[13] However, there are multiple caveats associated with fatty acid membrane stability as they are extremely sensitive to change in pH, divalent cation concentration and high temperature.[5] Moreover, fatty acid possesses high critical bilayer concentration (CBC, the threshold concentration of molecules required for stable bilayer formation)[4]. In this regard, Growing literature also suggests that the lack of stability can be compensated for by the increase in heterogeneity of the system which will be discussed later.[1, 3-6] Studies carried out on model protocell membranes focused on only fatty acid based system and some with two-component system, containing fatty acid with another co-surfactant.[2, 4-5] Even though these studies set the stage for our preliminary understanding of such systems, the inherent complexity of these systems, which would result from a heterogenous prebiotic soup, has largely been overlooked. It is fair to assume that the composition and the physicochemical properties of protocellular membrane compartments would have been largely influenced by the early Earth environment.[14-16] The self-assembled structures of SCAs are responsive to their environment and would potentially undergo changes based on different environmental conditions. Hence, various environmental conditions (e.g. pH variations, presence of ions, rainfall and flooding events leading to dilution, wet-dry cycles, etc) are hypothesized to be prebiotically pertinent environmental conditions shaping the composition and properties of protocell membranes.[14, 16] Towards this end, in this chapter, I have summarizes previous literature and recent findings on model protocellular membranes to understand the emergence, composition and chemical evolution of primitive membranes in a comprehensive manner. This chapter addresses various aspects of model protocellular membrane starting from their formation on primitive Earth to emergence of model protocellular systems and the influence of various environmental constrains in this endeavour.
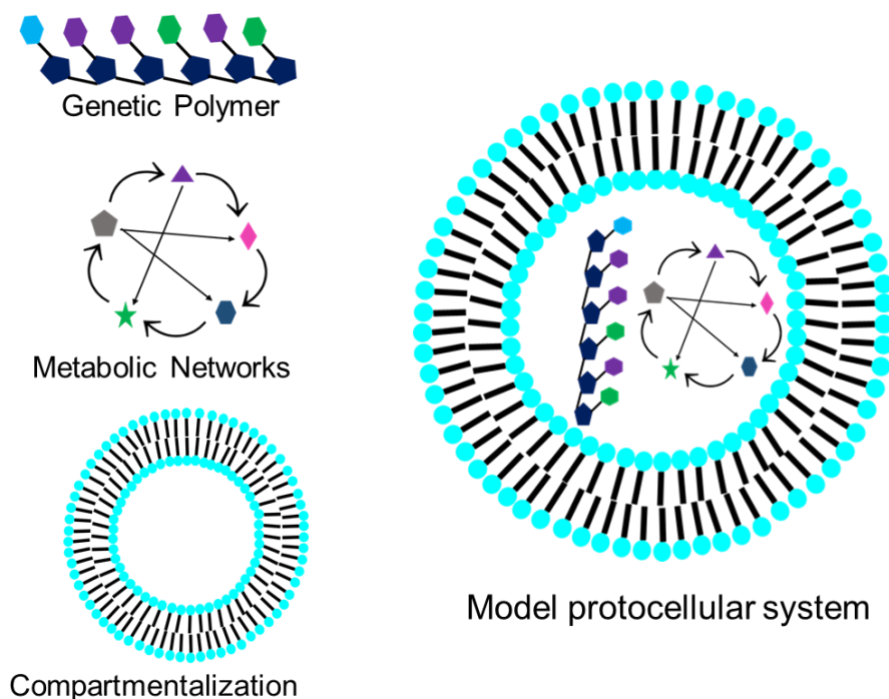
Figure 1.1: *Schematic representation of model prototocellular systems. Model protocells are thought be comprised of the three essential components as depicted in the figure. A heritable biopolymer (presumably RNA) to carry forward genetic information, metabolic reactions to produce energy and building blocks life and finally membrane bound compartments.*

1.2 **Prebiotic origins of amphiphiles:**

Model protocellular membranes are thought to have been 'simpler' both in terms of their composition and their chemical nature and composed predominantly of SCAs, and polycyclic aromatic hydrocarbons.[3-5] Several molecules come within the ambit of description of prebiotically plausible amphiphiles, which might have comprised protocell membranes as shown in Figure 1.2. Such amphiphiles could have come about on the early Earth via exogenous delivery from extraterrestrial sources (like comets and meteorites), or by endogenous synthesis in specific early Earth niches.[10-11] Fatty acids containing up to 12 carbon chain length have been observed in exogenously delivered meteoritic samples.[17] Also, polycyclic aromatic hydrocarbon (PAH) derivatives of pyrene, fluorenone, anthracene, etc., abundantly found in exogenously delivered interstellar material, have been shown to work as a cholesterol analogue in prebiotic SCA membranes.[18] Pioneering work by Deamer

and Pashley demonstrated that SCAs extracted from meteorites can assemble into vesicles under aqueous conditions.[19] Other than fatty acids, amphiphiles like alkyl sulfonic acids and alkyl phosphonic acids, containing up to four carbon atoms, have also been observed in meteoritic samples.[20] In the context of the endogenous synthetic routes, Fischer–Tropsch type (FTT) synthesis is one of the most explored pathways by which a simple carbon source can combine with hydrogen and form a diverse group of amphiphiles under primitive conditions.[10, 21-22] Reconstitution of FTT synthesis under hydrothermal experimental conditions has been shown to result in the formation of unbranched lipids such as *n*-alkanols, *n*-alkanoic acids, *n*-alkenes, *n*-alkanes and alkanones, when oxalic and formic acid were used as the starting reactants.[23] The length of the hydrocarbon chains varied from C2 to > C35. However, with increasing chain length, the abundance of the species seemed to decrease drastically. Hargreaves et al. demonstrated the possible derivatization of products of FTT synthesis, such as fatty acids and fatty aldehydes, with glycerol to result in mono-, di- and tri-glycerides, under simulated prebiotic conditions.[24] In a redox based reaction, Bachmann et al. showed the conversion of fatty alcohols to fatty acids by permanganate-mediated oxidation.[25] When a mixture of short chain alcohols (C2, C6 and C10) was heated in the presence of urea and ammonium phosphate, phosphate amphiphiles were formed wherein decyl phosphate dominated over hexyl and ethyl phosphate.[26] Results from previous literature in this regard have questioned the prebiotic relevance of phospholipids because of their low synthesis yields under prebiotic conditions.[24, 27] However, recent studies in the field have demonstrated plausible synthesis routes of diacyl phospholipids under prebiotic conditions, which reignites the possibility that diacyl phospholipids could have been present in protocell membranes. Towards this end, Bonfio et al. demonstrated the formation of diacyl phospholipids via acylation of glycerophosphates using imidazolide activated acyl chains, in organic co-solvent.[28] Recently, Liu et al. demonstrated the synthesis of diacyl phospholipids in high yields via acetylation of lysophospholipids using acyl donors under aqueous conditions.[29] These studies suggest routes by which diacyl phospholipids could have been incorporated into protocell membranes before the emergence of complex protein machineries that aid phospholipid synthesis in contemporary biology. However, it is important to mention here that incorporation of phospholipids would also adversely influence protocell functions as they limit permeability in the resulting membranes.[30] These properties

would have been absolutely critical for a protocellular system to survive, as they would have been devoid of complex protein machineries. Taken together, all of the aforementioned prebiotically plausible routes would have contributed to the diverse inventory of SCAs on the early Earth.
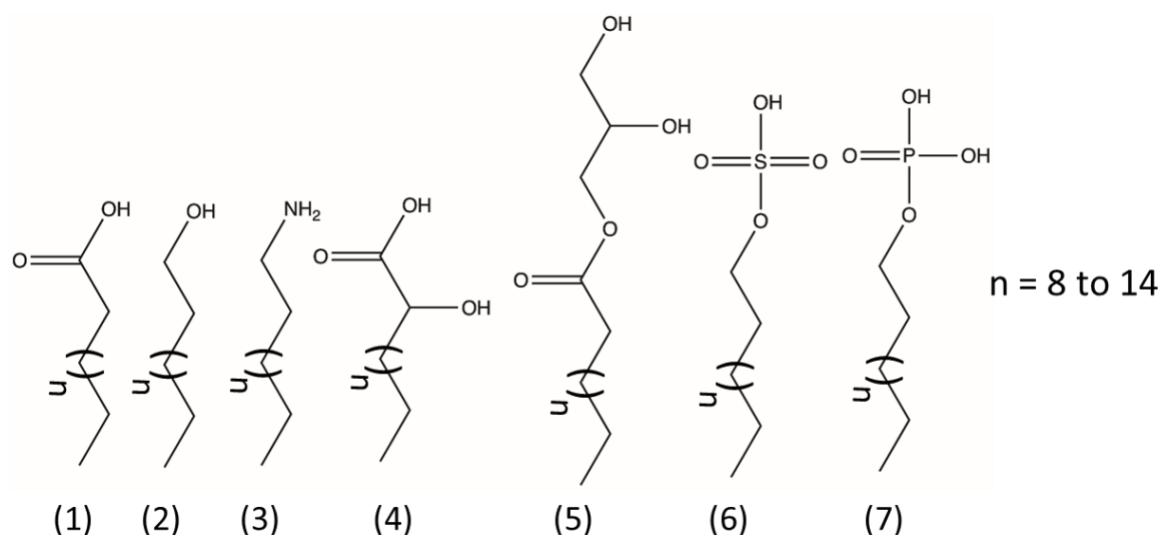
Figure 1.2: *Structures of different amphiphiles with varying head groups that will be used in the proposed studies: (1) fatty acid, (2) long chain alcohol, (3) long chain primary amine, (4) alpha-hydroxy fatty acid, (5) glycerol monoester of fatty acid, (6) aliphatic sulphate amphiphile and (7) aliphatic phosphate amphiphile. The structures were drawn using ChemDraw professional (PerkinElmer) 20.0.*

1.3 Self-assembly of prebiotically relevant amphiphiles:

The basic process that drives the formation of compartments from amphiphiles is their spontaneous self-assembly behaviour. The fundamental phenomenon governing this self-assembly in an aqueous medium is the hydrophobic effect; an entropic effect driven predominantly by the inherent tendency of water molecules to behave in a restricted manner. Other noncovalent interactions such as hydrogen bonding, electrostatic interactions among the protonated and deprotonated polar head groups, and van der Waals interactions between closely packed hydrophobic tails of the molecules, further stabilize the self-assembled structure resulting from the hydrophobic effect.[31-32] Even though these interactions are noncovalent and 'weak', (with ΔG value of 0.5–40 kcal/mol compared to 150–400 kcal/mol in case of covalent interactions),[33] when combined together they produce an overall force which is

sufficient to initiate assembly and stabilize the resultant self-assembled structures[31]. Stability of the self-assembled structure majorly depends on two factors. One is the hydration of the polar group, which is an enthalpy gain coming from ionic interaction and hydrogen bond formation. The second one is referred to as the hydrophobic effect stemming from the coming together of the hydrophobic tails of the amphiphiles, which is a gain in entropy for the surrounding aqueous solvent.[34-35] Electrostatic interactions with other solutes or ions (e.g., Mg^{2+}, Ca^{2+}) present in the bulk aqueous phase can also affect the self-assembly of amphiphiles into a bilayer.[34] Moreover, the shape and size of a given amphiphile, its concentration, along with environmental constraints such as temperature, pH and ionic strength, collectively influence the self-assembly process and the stability of vesicles, especially in the case of SCAs.[35] In order to self-assemble into bilayer structures, the amphiphiles need to reach a threshold concentration in the solution known as critical bilayer concentration (CBC).[36] The amphiphiles remain in dynamic equilibrium between the bilayer structure and the free monomers in suspension. For diacyl phospholipids, the CBC lies in the nanomolar (nM) range, resulting in the formation of the bilayer readily and with negligible monomers in the bulk solution.[30] This could be attributed to their increased hydrophobic area and tighter packing. In the case of SCA based systems like fatty acids, the CBC is in the millimolar (mM) range, resulting in membranes but with increased monomers in the bulk solution, particularly due to their lower hydrophobic surface area.[30]

1.4 Fatty acid and mixed fatty acid based model protocell membranes:

Fatty acids, starting from eight carbon chain length, have been shown to self-assemble under certain conditions to result in vesicles of varying size and shape.[13] However, pure fatty acid membranes are extremely sensitive to their environmental conditions, especially the pH variation. They can only assemble into bilayers when the surrounding pH is near the pKa of their head group, as depicted in Figure 1.3. This limits the vesicle formation to a very narrow pH regime.[2, 37] Towards this, it has been demonstrated that the addition of fatty alcohol to fatty acids enables the mixture to assemble into vesicles over alkaline pH regime.[38-39] Namani and Deamer showed that membranes composed of decanoic acid (C10) and decylamine, can form vesicles at low (pH 2) as well as high pH (pH 11), but not near neutral pH.[40] Mixtures of oleic acid (C18) with varying long chain alcohols (C6 to C18) has been

shown to assemble into vesicles over a wide range of alkaline pH.[39] Moreover, addition of the surfactant sodium dodecylbenzene sulfonate, to decanoic acid membranes, has been shown to aid the formation of vesicles even in the acidic pH regime.[41] Single chain phosphate amphiphiles with a cyclic head group, were found to form vesicles under varying pH when mixed with fatty alcohols.[42] Addition of mono acyl glycerol esters of fatty acids has been shown to facilitate the assembly of fatty acids more readily into compartments, especially in the alkaline pH regime.[43] Vesicle formation by mixed fatty acid systems over a wider pH range (especially alkaline) can be attributed to their hydrogen bonding capability. Fatty acids head groups are in a deprotonated form at a pH above their pKa. Hence, they carry a net negative charge, failing to form stable bilayers at these pHs because of the lack of hydrogen bonding as well as the electrostatic repulsion between their head groups as depicted in Figure 1.3. However, the addition of surfactants like fatty alcohol and/ or monoglyceride that have –OH as a non-dissociable head group, provides a hydrogen bond donor, which can stabilize the resulting membrane via hydrogen bonding with the deprotonated head groups of the fatty acids, while also reducing the repulsion between them. This allows mixed fatty acid systems to readily form vesicles under alkaline conditions.[5] Maurer et al. demonstrated using 8 to 18 carbon length fatty acids that mixing of their corresponding glycerol monoesters resulted in a decrease in the CBC of the system.[36] Fatty acids are cation sensitive detergents, i.e., in the presence of cations, they tend to form soap-crystals.[44] However, nucleic acids like self-replicating ribozymes, which are at the crux of the RNA world hypothesis, require divalent cations (predominantly Mg^{2+} ions) for their catalytic activity.[45] This makes pure fatty acid vesicles unsuitable to harbour prebiotic self-replicating genetic systems like RNA (in a putative RNA World). In order to circumvent the stability issue of fatty acid vesicles in the presence of high concentration of cations, two approaches have been employed, i.e., either by the addition of cation chelating agents (such as EDTA, citrate) to the solution, or by decreasing the membrane sensitivity to cations by addition of co-surfactants.[46] Binary membrane systems of fatty acids, with either fatty alcohol or its glycerol monoester derivative, are shown to be more resistant to cations.[2, 5] These studies focused on fatty acid molecules being the predominant player, with other amphiphiles being added in a smaller fraction as supporting components. Another important parameter to be evaluated in this regard is the thermostability of protocell membranes, as the early Earth temperature is

thought to be much higher than that of the contemporary Earth.[47] Terrestrial hydrothermal hot springs[48] and deep-sea hydrothermal vents[49] have been proposed as potential sites for the emergence of early cellular life on Earth. They both are characterized by elevated temperatures (about 50-90°C). Additionally, the high temperature would have been one of the important driving forces for the occurrence of many prebiotically pertinent reactions. It has been reported that mixed membrane systems made up of decanoic acid (C10) and the corresponding alcohol or glycerol monoester derivative (binary systems), and decanoic acid (C10) with both the corresponding alcohol and the glycerol monoester derivative (a tertiary system), formed more robust and thermostable vesicles than pure decanoic acid ones alone.[50] Significantly, this enhanced retention of fatty acids in the membrane alters the permeability of the mixed systems. Previously, Piedrafita et al. investigated the permeability of primitive binary mixed membrane systems and demonstrated that presence of glycerol monoester of fatty acids increases the permeability of mixed fatty acid membrane.[51] Such systems could, therefore, allow for efficiently sustaining intricate metabolic networks required for the onset of cellular life on the early Earth.
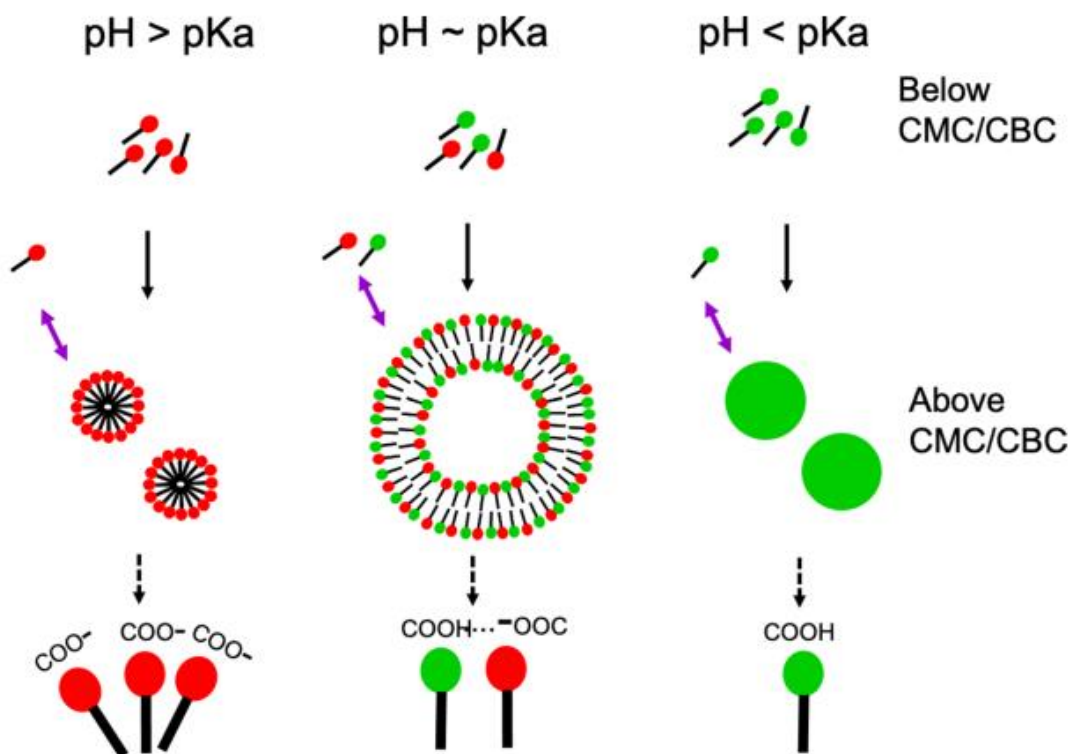
***Figure 1.3:** Schematic representation of self-assembled structures formed by fatty acid molecules in aqueous solutions. Fatty acid molecules get deprotonated (red head group) when the surrounding pH is higher than the apparent pKa of the head group. When fatty acid concentration reaches its CMC (critical micelle concentration, a threshold concentration required to from micelles) at this pH and above, they form micellar aggregates. When the surrounding pH is lower than the apparent pKa of the head group (green head group), fatty acid molecules stay protonated and form oil droplets. When the surrounding pH is equal or near the apparent pKa of the head group, both the protonated and deprotonated species are present in almost equal abundance leading to hydrogen bond formation between them, resulting in the formation of pseudodiacyl structures. At this pH, when the concentration of the fatty acid reaches its CBC and above, it predominantly forms bilayer membranes and vesicles. Significantly, in all the aforementioned scenarios, the fatty acid monomers and the higher order aggregates (micelles, vesicles, oil droplets, etc.) are always in dynamic equilibrium. (Figure adapted from Sarkar et al. 2020).*

1.5 Chemical evolution of protocell membranes: Prebiotic environmental conditions and early membrane composition

Current working model of the chemical evolution of prebiotic membranes revolves around the transition of SCAs (fatty acids) to diacyl phospholipids via mixed membranes containing both of these components as an intermediate step.[52-53] This appears to be an attractive model in the field as it tries to unify both top-down (phospholipid-based membranes) and bottom-up (fatty acid-based membranes) approaches towards understanding the chemical evolution of membranes. However, growing literature indicates that this could be an oversimplified version of the actual complicated process that would have allowed for the transition from prebiological to biological membranes.[51, 54] There are several missing links and caveats in this pathway that still need to be systematically addressed. Overall the model overlooks the complexity of the prebiotic chemical space. It is logical to assume that the environment of the protocell would have been heterogenous, which would have directly been reflected in the composition of the membranes themselves. The assumption of homogeneous fatty acid-based membranes, as an early step in membrane emergence and chemical evolution, would require that these systems managed to survive and function effectively under early Earth conditions. However, considering the susceptibility and responsiveness of fatty acid membranes to the

environmental changes, this possibility can be safely ruled out. Another major limitation of this model is that the model considers the advantage of pure phospholipid-based membranes during the process of chemical evolution. However, the negligible permeability of phospholipid-based membranes would limit them from taking up material from the surrounding environment.[30] Major drawback of this model is that it does not consider the influence of the different physical and chemical environmental constraints on the composition of protocell membranes.[54]

Living systems are known to undergo a myriad change to adapt to their surrounding environment. To restore the normal physiology of the membrane, organisms are known to modify lipid composition of their cell membranes.[55] Environmental conditions are considered to play a key role in their chemical evolution.[56] Considering different factors such as prebiotic amphiphile library, membrane stability and prebiotic environment, it is reasonable to consider that protocellular membranes would have been complex in terms of their composition. The composition of protocellular membranes would be determined by their physicochemical environment and shaped through complex interaction with multiple environmental constraints. Considering the extensive time scale available for this transition (i.e., several millions to possibly a billion years), and the changing geochemical settings of the prebiotic Earth, it is fair to assume that there might have been many intermediate stages going from prebiological to biological membranes as demonstrated in Figure 1.4. Different processes pertaining to protocells would have been influenced by complex interactions with the surrounding environment. External conditions including temperature[50], pH variations[38], presence of ions[44], wet-dry cycles[16] and unpredictable rainfall with seasonal flooding events (leading to dilution), would have influenced the composition of primitive membranes as depicted in Figure. 1.4.
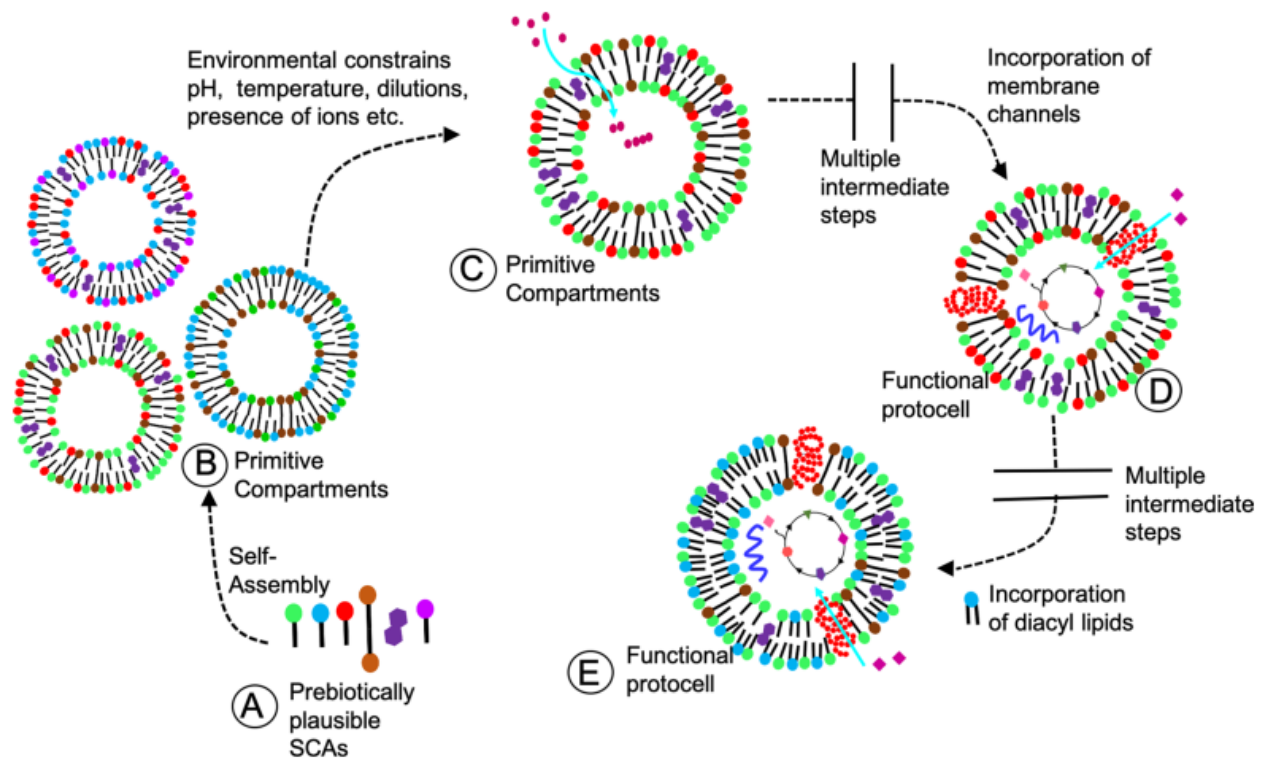
Figure 1.4: *Diagram of potential pathway for protocell membrane chemical evolution. A: Self-assembly of prebiotically plausible amphiphiles (SCAs, including PAHs, bola amphiphiles, etc.) into primitive compartments of varying compositions. B: Influence of environmental conditions such as pH, temperature, dilution, presence of ions, etc. allow for few compositions to get selected for over others because of their compositional diversity. C: Stable compartments can start accruing functions that can facilitate polymerization of building blocks and promote metabolic reactions. Without the assistance of any transmembrane channels, the exchange would have been dependent on the dynamics of the membrane. D: Chemical evolution of a functional protocell via multiple intermediate stages. Membranes become equipped with primitive membrane channels that can assist in the active exchange of matter, linking membranes with metabolic networks and genetic polymers. E: Further transition of protocellular systems via multiple intermediate stages to become more complex; get equipped with genetic material, membrane channels, reaction networks, etc. Presence of evolved transmembrane channels can counter for the decreased membrane dynamics that stems from the incorporation of diacyl lipids. At this stage, the connection between the encapsulated genetic material (genotype) and the bulk property of the protocell (phenotype) would have potentially occurred, from where the divergence into the different domains of life would have been eventually facilitated. (Figure adapted form Sarkar et al. 2020).*

Recent studies have ventured into understanding how environmental constraints would affect the transition of primitive membranes. However, the dependence and correlation between the primitive membrane chemical evolution and niche parameters are still not fully clear.[54] This long-standing problem in the field can be addressed by systematically increasing the heterogeneity of prebiotic membranes using a diverse set of prebiotically plausible amphiphiles.[2, 5] An important point worth mentioning in this regard, which is often overlooked in studies related to the transition of prebiotic membranes, is that multiple environmental conditions would have acted in a concerted fashion on prebiotic membranes to shape their composition. In this regard, no study so far have looked at the stability of mixed membranes made up of different SCAs under multiple environmental conditions. The influence of different amphiphiles on the overall stability of the membrane would depend on, the physicochemical environmental condition(s).

1.6 References:

1. Ruiz-Mirazo, Kepa, Carlos Briones, and Andres de la Escosura. "Prebiotic systems chemistry: new perspectives for the origins of life." *Chemical reviews* 114.1 (2014): 285-366.
2. Monnard, Pierre-Alain, and Peter Walde. "Current ideas about prebiological compartmentalization." *Life* 5.2 (2015): 1239-1263.
3. Segré, Daniel, et al. "The lipid world." *Origins of Life and Evolution of the Biosphere* 31.1 (2001): 119-145.
4. Sarkar, Susovan, et al. "Prebiological membranes and their role in the emergence of early cellular life." *The Journal of Membrane Biology* 253.6 (2020): 589-608.
5. Mansy, Sheref S. "Model protocells from single-chain lipids." *International journal of molecular sciences* 10.3 (2009): 835-843.
6. Szostak, Jack W., David P. Bartel, and P. Luigi Luisi. "Synthesizing life." *Nature* 409.6818 (2001): 387-390.
7. Sohlenkamp, Christian, and Otto Geiger. "Bacterial membrane lipids: diversity in structures and pathways." *FEMS microbiology reviews* 40.1 (2016): 133-159.
8. Harayama, Takeshi, and Howard Riezman. "Understanding the diversity of membrane lipid composition." *Nature reviews Molecular cell biology* 19.5 (2018): 281-296.
9. Marrink, Siewert J., et al. "Computational modeling of realistic cell membranes." *Chemical reviews* 119.9 (2019): 6184-6226.
10. McCollom, Thomas M., Gilles Ritter, and Bernd RT Simoneit. "Lipid synthesis under hydrothermal conditions by Fischer-Tropsch-type reactions." *Origins of Life and Evolution of the Biosphere* 29.2 (1999): 153-166.
11. Lawless, James G., and George U. Yuen. "Quantification of monocarboxylic acids in the Murchison carbonaceous meteorite." *Nature* 282.5737 (1979): 396-398.

12. Fameau, Anne-Laure, Audrey Arnould, and Arnaud Saint-Jalmes. "Responsive self-assemblies based on fatty acids." *Current opinion in colloid & interface science* 19.5 (2014): 471-479.
13. Hargreaves, William R., and David W. Deamer. "Liposomes from ionic, single-chain amphiphiles." *Biochemistry* 17.18 (1978): 3759-3768.
14. Thomas, Jacquelyn A., and F. R. Rana. "The influence of environmental conditions, lipid composition, and phase behavior on the origin of cell membranes." *Origins of Life and Evolution of Biospheres* 37.3 (2007): 267-285.
15. Damer, Bruce, and David Deamer. "The hot spring hypothesis for an origin of life." *Astrobiology* 20.4 (2020): 429-452.
16. Damer, Bruce, and David Deamer. "Coupled phases and combinatorial selection in fluctuating hydrothermal pools: A scenario to guide experimental approaches to the origin of cellular life." *Life* 5.1 (2015): 872-887.
17. Lai, James C-Y., et al. "Meteoritic abundances of fatty acids and potential reaction pathways in planetesimals." *Icarus* 319 (2019): 685-700.
18. Groen, Joost, et al. "Polycyclic aromatic hydrocarbons as plausible prebiotic membrane components." *Origins of Life and Evolution of Biospheres* 42.4 (2012): 295-306.
19. Deamer, David W., and R. M. Pashley. "Amphiphilic components of the Murchison carbonaceous chondrite: surface properties and membrane formation." *Origins of Life and Evolution of the Biosphere* 19.1 (1989): 21-38.
20. Cooper, George W., Wilfred M. Onwo, and John R. Cronin. "Alkyl phosphonic acids and sulfonic acids in the Murchison meteorite." *Geochimica et Cosmochimica Acta* 56.11 (1992): 4109-4115.
21. McCollom, Thomas M., and Jeffrey S. Seewald. "Carbon isotope composition of organic compounds produced by abiotic synthesis under hydrothermal conditions." *Earth and Planetary Science Letters* 243.1-2 (2006): 74-84.
22. Berndt, Michael E., Douglas E. Allen, and William E. Seyfried Jr. "Reduction of CO2 during serpentinization of olivine at 300 C and 500 bar." *Geology* 24.4 (1996): 351-354.
23. Berndt, Michael E., Douglas E. Allen, and William E. Seyfried Jr. "Reduction of CO2 during serpentinization of olivine at 300 C and 500 bar." *Geology* 24.4 (1996): 351-354.
24. Hargreaves, William R., S. J. Mulvihill, and D. W. Deamer. "Synthesis of phospholipids and membranes in prebiotic conditions." *Nature* 266.5597 (1977): 78-80.
25. Bachmann, Pascale Angelica, et al. "Self-replicating micelles: aqueous micelles and enzymatically driven reactions in reverse micelles." *Journal of the American Chemical Society* 113.22 (1991): 8204-8209.
26. Powner, Matthew W., and John D. Sutherland. "Prebiotic chemistry: a new modus operandi." *Philosophical Transactions of the Royal Society B: Biological Sciences* 366.1580 (2011): 2870-2877.
27. Rao, M., J. Eichberg, and J. Oró. "Synthesis of phosphatidylcholine under possible primitive Earth conditions." *Journal of molecular evolution* 18.3 (1982): 196-202.
28. Bonfio, Claudia, et al. "Length-selective synthesis of acylglycerol-phosphates through energy-dissipative cycling." *Journal of the American Chemical Society* 141.9 (2019): 3934-3939.
29. Liu, Luping, et al. "Enzyme-free synthesis of natural phospholipids in water." *Nature Chemistry* 12.11 (2020): 1029-1034.
30. Mansy, Sheref S. "Membrane transport in primitive cells." *Cold Spring Harbor perspectives in biology* 2.8 (2010): a002188.
31. Israelachvili, J. N. "Intermolecular and Surface Forces, Academic." (1992).

32. Cui, Xiaohong, et al. "Mechanism of surfactant micelle formation." *Langmuir* 24.19 (2008): 10771-10775.
33. Pace, C. N. "[24] Evaluating contribution of hydrogen bonding and hydrophobic bonding to protein folding." *Methods in enzymology*. Vol. 259. Academic Press, 1995. 538-554.
34. Pohorille, Andrew, and David Deamer. "Self-assembly and function of primitive cell membranes." *Research in microbiology* 160.7 (2009): 449-456.
35. Lombardo, Domenico, et al. "Amphiphiles self-assembly: basic concepts and future perspectives of supramolecular approaches." *Advances in Condensed Matter Physics* 2015 (2015).
36. Maurer, Sarah Elisabeth, et al. "Chemical evolution of amphiphiles: glycerol monoacyl derivatives stabilize plausible prebiotic membranes." *Astrobiology* 9.10 (2009): 979-987.
37. Cheng, Zhiliang, and Pier Luigi Luisi. "Coexistence and mutual competition of vesicles with different size distributions." *The Journal of Physical Chemistry B* 107.39 (2003): 10940-10945.
38. Apel, Charles L., David W. Deamer, and Michael N. Mautner. "Self-assembled vesicles of monocarboxylic acids and alcohols: conditions for stability and for the encapsulation of biopolymers." *Biochimica et Biophysica Acta (BBA)-Biomembranes* 1559.1 (2002): 1-9.
39. Rendón, Adela, et al. "Model systems of precursor cellular membranes: long-chain alcohols stabilize spontaneously formed oleic acid vesicles." *Biophysical journal* 102.2 (2012): 278-286.
40. Namani, Trishool, and David W. Deamer. "Stability of model membranes in extreme environments." *Origins of Life and Evolution of Biospheres* 38.4 (2008): 329-341.
41. Namani, Trishool, and Peter Walde. "From decanoate micelles to decanoic acid/dodecylbenzenesulfonate vesicles." *Langmuir* 21.14 (2005): 6210-6219.
42. Toparlak, Ö. Duhan, et al. "Cyclophospholipids increase protocellular stability to metal ions." *Small* 16.27 (2020): 1903381.
43. Chen, Irene A., Kourosh Salehi-Ashtiani, and Jack W. Szostak. "RNA catalysis in model protocell vesicles." *Journal of the American Chemical Society* 127.38 (2005): 13213-13219.
44. Monnard, Pierre-Alain, et al. "Influence of ionic inorganic solutes on self-assembly and polymerization processes related to early forms of life: Implications for a prebiotic aqueous medium." *Astrobiology* 2.2 (2002): 139-152.
45. Schrum, Jason P., Ting F. Zhu, and Jack W. Szostak. "The origins of cellular life." *Cold Spring Harbor perspectives in biology* 2.9 (2010): a002212.
46. Adamala, Katarzyna, and Jack W. Szostak. "Nonenzymatic template-directed RNA synthesis inside model protocells." *Science* 342.6162 (2013): 1098-1100.
47. Henderson-Sellers, A. N. N., and A. J. Meadows. "Surface temperature of early Earth." *Nature* 270.5638 (1977): 589-591.
48. Milshteyn, Daniel, et al. "Amphiphilic compounds assemble into membranous vesicles in hydrothermal hot spring water but not in seawater." *Life* 8.2 (2018): 11.
49. Kelley, Deborah S., et al. "An off-axis hydrothermal vent field near the Mid-Atlantic Ridge at 30 N." *Nature* 412.6843 (2001): 145-149.
50. Mansy, Sheref S., and Jack W. Szostak. "Thermostability of model protocell membranes." *Proceedings of the National Academy of Sciences* 105.36 (2008): 13351-13355.
51. Piedrafita, Gabriel, et al. "Permeability-driven selection in a semi-empirical protocell model: the roots of prebiotic systems evolution." *Scientific reports* 7.1 (2017): 1-10.

52. Budin, Itay, and Jack W. Szostak. "Physical effects underlying the transition from primitive to modern cell membranes." *Proceedings of the National Academy of Sciences* 108.13 (2011): 5249-5254.

53. Jin, Lin, et al. "Fatty acid/phospholipid blended membranes: a potential intermediate state in protocellular evolution." *Small* 14.15 (2018): 1704077.

54. Thomas, Jacquelyn A., and F. R. Rana. "The influence of environmental conditions, lipid composition, and phase behavior on the origin of cell membranes." *Origins of Life and Evolution of Biospheres* 37.3 (2007): 267-285.

55. Siliakus, Melvin F., John van der Oost, and Servé WM Kengen. "Adaptations of archaeal and bacterial membranes to variations in temperature, pH and pressure." *Extremophiles* 21.4 (2017): 651-670.

56. Skinner, Michael K. "Environmental epigenetics and a unified theory of the molecular aspects of evolution: a neo-Lamarckian concept that facilitates neo-Darwinian evolution." *Genome biology and evolution* 7.5 (2015): 1296-1302.

Chapter 2

Influence of compositional diversity on the self-assembly, membrane stability and survivability of model protocellular membrane compartments.

(Adapted from, Sarkar et al. 2020; SciRep)

2.1 Introduction

The earliest forms of cellular life are considered to be entities that are comprised of RNA and dynamic chemical reactions, encapsulated within amphiphilic compartments.[1,2] Protocellular membranes are thought to have been composed of SCAs.[3] These SCAs could have come about on the early Earth either by endogenous synthesis, in the form of Fisher-Tropsch Type (FTT) reactions, or via exogenous delivery.[4,5] In this context, fatty acids and their derivatives have been predominantly studied for their plausible role as early compartments.[3,6] Fatty acids are known to possess high critical vesicular concentrations (CBCs), the concentration at which the monomers assemble into higher ordered structures like vesicles.[7] Meeting this high concentration prerequisite would have been difficult on early Earth.[8,9] The pH of certain terrestrial hydrothermal pools of the early Earth is hypothesized to be neutral to alkaline[10] which can drive prebiotically pertinent reactions, including formose reaction[11], polymerization of non-activated amino acids[12], and non-canonical nucleoside or nucleotide formation.[13] However fatty acid monomers can assemble only in a narrow pH regime, near to their pKa.[6,14] Given this scenario the coexistence of the aforementioned reactions and model protocellular membranes would have been really challenging. Moreover, fatty acids are also cation sensitive moieties.[15] On the contrary, RNA molecules, which are thought to be the first biomolecules to have emerged, require divalent cations in order to efficiently replicate and carry out catalytic functions.[16–18] Such divalent cation concentrations are not compatible with fatty acid membranes.[15,19] This poses an imminent question of how RNA replicators could have coexisted with fatty acid-based membranes. Nonetheless, fatty acid membranes are in dynamic equilibrium hence can facilitate the permeation of polar molecules better.[20] Which is an essential requirement for protocells as it allows for the exchange of matter with its environment. In this regard, the self-assembly property, permeability and membrane integrity in different environmental conditions of such SCAs need to be systematically explored. Thus far, studies have predominantly focused on delineating one, or up to two of the aforesaid parameters at any given time.[3,6–9,19,21] However, the aforementioned conditions would have acted in concert as a combination of prebiotic environmental conditions , shaping the composition and properties of prebiological membranes. Previous studies have suggested that the lack of

membrane stability can be counterbalanced by increasing membrane complexity and can facilitate formation of lipid catalytic networks.[22] It is known that addition of long chain alcohols with fatty acids confers stability to the vesicles at alkaline pH.[23] Previous studies have also showed that binary systems of fatty acid and its glycerol monoester are more resistant to soluble monovalent and divalent cations.[19,24] Although insightful, the aforementioned studies predominantly looked at binary membrane systems. Given the complex nature of the prebiotic soup, and the niche parameters, it would be necessary to complexify the starting mix, to better understand how membrane related processes would have advent under 'prebiotically realistic' conditions. In this context, a membrane system composed of decanoic acid, decanol and glycerol mono-decanoate, is the only tertiary system that has been explored thus far, in terms of its thermostability and permeability.[25,26] In order to gain a deeper understanding of how compositional complexity would impinge on a membrane system's survivability, especially under multiple prebiotic environmental conditions , we set out to characterize tertiary membrane systems of selected SCAs. In the present study, fatty acids of two different chain lengths, i.e. oleic acid (OA, C18) and undecylenic acid (UDA, C11), were mixed with their corresponding alcohol and/or glycerol monoester derivatives in varying ratio, and used as a proxy for mixed membrane systems. Fatty alcohols and glycerol monoester derivatives were chosen for further experimentation because of their prebiotic relevance.[4,9] Binary membrane systems containing fatty acid with either the fatty alcohol or the glycerol monoester derivative, and tertiary systems containing all the three components, were explored for each of the chain lengths. The prebiotically relevant physical parameters that were characterized include the formation of model protocellular membranes at alkaline pH, their CBC, ionic stability and the permeability of the said systems. Our results show that the mixed membrane systems are indeed more stable, and robust under diverse environmental conditions. Therefore, these would have been more suitable to support protocellular life forms. Our results also illustrate that the head groups of the SCAs play an important role in stabilizing the membrane under specific environmental conditions. Systems containing different derivatives possess different survival rates when subjected to a specific condition. Given this interesting finding, we also attempted to delineate the contribution of individual head-groups, and the plausible mechanism that might be involved in stabilizing the protomembrane systems. An important result of this study clearly demonstrates that the tertiary

system being most complex would have possessed the best chance at survival when subjected to multiple environmental conditions.

2.2 Materials

Magnesium chloride hexahydrate (MgCl2·6 H2O, 203.30 g/mol), sodium hydroxide (NaOH, 39.997 g/mol), hydrochloric acid (HCl, 37 %, 36.46 g/mol), bicine (C6H13NO4, 163.17 g/mol), CHES (C8H17NO3S, 207.287 g/mol), calcein (622.55 g/mol) and triton X100 (647 g/mol) were purchased from Sigma Aldrich (Bangalore, India) and used without further purification. All the fatty acids mentioned in this study, namely oleic acid (cis-9, C18H34O2, 282.47 g/mol), oleyl alcohol (cis-9, C18H36O, 268.478 g/mol), glycerol 1-monooleate (cis-9, C11H40O4 356.547 g/mol), undecylenic acid (C11H20O2, 184.279 g/mol), undecylenyl alcohol (C11H22O1, 170.29), glyceryl 1-undecylenate (C14H26O4, 258.35 g/mol) and myristoleic acid (226.36 g/mol) were purchased from Nu-Chek-Prep (Elysian, MN, USA) and used without further purification. All other chemicals were purchased from Sigma Aldrich (Bangalore, India) and used without further purification. All the experiments were carried out using Nanopure (18 MΩ-cm) water.

2.3 Methods

2.3.1 Vesicle solution preparation

The vesicle solutions were prepared by dissolving the desired amount of the fatty acid and its derivatives in chloroform at a concentration of 10 mg/ml. The chloroform solution was dried under nitrogen gas flow to prepare a dry lipid film. It was then kept under vacuum for five to six hours to make sure that no trace amount of chloroform remained. Subsequently, different buffers (bicine or CHES) of desired pH were used to rehydrate the thin film to form the vesicles. This vesicle suspension was heated for one hour at 60°C to maximize vesicle formation.

2.3.2 Microscopic analysis

Lipid samples were observed under 20X and 40X magnification using a Differential Interference Contrast (DIC) microscope AxioImager Z1 (Carl Zeiss, Germany), (NA = 0.75) to observe the presence of different assemblies (vesicles, oil droplets, crystalline aggregates etc.). Typically, 10 µL of lipid solution was spread on a glass slide, followed by placing an 18X18 mm coverslip on top of it and covering the four

sides with liquid paraffin to decrease the motion of the lipid solution. Thereafter, the slide was immediately observed under the microscope.

2.3.3 CBC estimation

Three different methods were used to estimate the CBC of the membrane systems in question. The first method involved using 1,6-diphenyl-1,3,5-hexatriene (DPH), a hydrophobic fluorescent dye, that can partition into the hydrophobic region of the membrane. Upon partitioning, its fluorescence increases several folds. The increase in fluorescence is directly proportional to the lipid concentration. DPH fluorescence also depends on the kind of lipid used, the number of dissolved ions, and incubation time. The lipid solution used in the experiment was prepared by diluting a stock lipid solution with a pH appropriate buffer. For the C11 and C18 systems, 200 mM bicine buffer of pH 8, and 100 mM CHES buffer of pH 9, respectively, was used to rehydrate the dried lipid film and to prepare further dilutions. The lipid suspension was then sonicated to form a homogeneous mixture of small unilamellar vesicles. In a typical reaction, 1.8 µL of 400 µM methanol solution of DPH, was added into 180 µL of C11 lipid solution to achieve 4 µM final concentration of DPH in the solution. For all the C18 systems the final DPH concentration was decreased to 2 µM to account for reduced lipid concentration (long chain fatty acids tend to have much lower CBCs than small chain fatty acids). The lipid solutions were prepared by diluting the stock lipid solution with appropriate buffer. After adding the DPH into the lipid solution, the mixture was kept at 40°C at a constant rotation of 700 rpm for 30 minutes to increase the partitioning of DPH in to the membrane. Post-incubation, the solution was transferred to a 96-well plate. The fluorescence was measured using a 96-well plate reader on Thermo Scientific Varioskan Flash multimode reader (Thermo Scientific, Singapore) by exciting the samples at 350 nm and measuring the emitted light at 452 nm. To corroborate the CBC values obtained from this fluorescence assay, the turbidity of the lipid solution was also measured at 400 nm, which is a widely used technique in the field, for reporting CBCs. The lipid concentration at which the turbidity of the system increases sharply is considered to be an indication of formation of vesicles, and hence is considered as the CBC of the system. A UV-1800 UV-Vis Spectrophotometer (Shimadzu Scientific Instruments Inc., Columbia, USA) was used to check the turbidity of the lipid solutions, which was

indicative of higher order structure formation. The presence of vesicles was further confirmed by microscopy at 40X magnification.

2.3.4 Stability in alkaline pH regimes

The ability of different lipid systems to assemble into vesicles was evaluated from pH 7 to 11, at intervals of 0.5 pH units (e.g. pH 7, 7.5, 8 and so on). 6 mM and 60 mM lipid concentration were used for the C18 and C11 systems, respectively. Typically, the dried lipid films were hydrated with a buffer of appropriate pH so as to cover the whole pH range mentioned. This was done considering the fact that different buffers have their own range of buffering capacity. For example, 200 mM bicine was used to prepare buffers in the pH 7 to 9 regime, while 200 mM CHES was used for pH 9.5 to 11 regime. The scattering of the solution at 400 nm was used as a proxy to gauge the presence of higher order lipid assemblies that were present in the solution using UV-1800 UV-Vis Spectrophotometer (Shimadzu Scientific Instruments Inc., Columbia, USA). The same samples were subsequently observed under microscope at 40X magnification to discern the nature of the higher order assemblies (e.g. vesicles, droplets etc).

2.3.5 Stability against Mg^{2+} ion

In order to check for the stability of the vesicles in the presence of Mg^{2+} ion, Dynamic Light Scattering (DLS) spectroscopy method was used. In a typical experiment, the vesicle suspension was extruded 15 times through a 200 nm size cut-off polycarbonate membrane using Avanti mini extruder (Avanti Polar Lipids Inc., Alabaster, AL, USA). The Mg^{2+} ions were then added to the lipid solution by adding a desired volume of $MgCl_2$ stock solution, prepared in the respective buffer. 100 mM CHES buffer of pH 9 and 200 mM bicine buffer of pH 8 were used to prepare the C18 and C11 vesicle solutions, respectively. The solution was then set aside for 15 min to equilibrate, after which the average size of the particles in the solution was measured using Zetasizer Nano ZS90, (Malvern Panalytical Ltd., Malvern, UK). The average size of the population was plotted against the Mg^{2+} ion concentration, so as to estimate Mg^{2+} ion induced fatty acid aggregation. The total lipid concentration was kept at 2 mM for the four C18 based systems. 20 mM lipid solution was used for all the three heterogeneous C11 based systems to prevent concentration induced vesicle aggregation. However, for the homogenous UDA system, the lipid

concentration was kept at 60 mM due to its intrinsically high CBC. As for the microscopy analysis, the lipid concentration was kept the same as was used for the DLS experiment. Desired amount of Mg^{2+} ion concentration was obtained by adding different volumes of the $MgCl_2$ stock solution in the lipid solution. Presence of different forms of aggregates, namely, vesicles, lipid crystals and oil droplets, were checked for using DIC microscopy.

2.3.6 Zeta potential measurement of the lipid solutions

To determine the negative charge density on the vesicles, the lipid solution was extruded 15 times through a 200 nm size cut-off polycarbonate membrane using Avanti mini extruder (Avanti Polar Lipids Inc., Alabaster, AL, USA). For all the four C18 systems, a total of 2 mM lipid solution was used. In case of all the three mixed C11 systems and homogenous UDA system, 20 mM and 60 mM lipid solutions, respectively, were used. The lipid solutions were kept for one hour to equilibrate before the actual measurement was taken. Post equilibration 600 ul of lipid solution was loaded in a cuvette and the zeta potential readings were acquired using a Zetasizer Nano ZS90 (Malvern Panalytical Ltd., Malvern, UK).

2.3.7 LC-MS analysis for free fatty acid quantification

Sample preparation: In case of C11 based systems, 60 mM and 90 mM lipid concentration was used, for the UDA and the three mixed systems, respectively. This was done to keep the concentration of the fatty acid i.e. UDA constant (60 mM) across all four systems. The lipid solution was prepared in 200 mM bicine buffer of pH 8. Similarly, for the C18 systems, 20 mM and 30 mM lipid concentration was used for the homogenous OA and the three mixed systems to keep the concentration of the oleic acid constant (20 mM) across all four systems. The lipid solutions were prepared in 100 mM CHES buffer of pH 9. 500 µL of each sample was loaded onto a Vivaspin 2 centrifugal concentrator, with a molecular weight cut-off of 3 kDda and centrifuged at 5,000g for 15 min. Typically, 50 µL of the filtrate was collected. This filtrate was then acidified by adding 5 µl of formic acid. The free fatty acids present in the filtrate was then extracted by adding 400 µL of 2:1 choloroform:methanol solution. This solution also contained myristoleic acid of 10 µM as an internal standard. The extraction was carried out by vortexing the solution rigorously and then spinning it at 3000g for 2 mins. The organic phase was

withdrawn carefully and was dried under a stream of nitrogen gas, and subsequently re-dissolved into 400 ul of 2:1 choloroform:methanol. A fraction of this was loaded on to the column (details in the below section).

Fatty acid quantification: Separation of fatty acids was carried out using a Luna C18 column from Phenomenex, Torrance, CA, USA (dimensions: 4.6 X 250 mm, 5 nm particle size). The solvent system used for the liquid chromatography part was as follows: Buffer A used was 95:5 of water : methanol (vol/vol) + 0.1% ammonium hydroxide, and Buffer B was 60:35:5 of isopropanol: methanol : water (vol/vol) + 0.1% ammonium hydroxide. A typical LC run's total time was 22 minutes long. The gradient involved an increase in solvent B concentration from 5% to 100% in 4 minutes, followed by an isocratic phase of 100% of solvent B for fifteen minutes. This was followed by an equilibration phase for four minutes with solvent A, all of which was done at a constant flow rate of 0.4 mL/min. The undecylenic acid and oleic acid (from the respective reaction mixtures), and the myristoleic acid internal standard, eluted at 15.66, 15.75 and 15.84 minutes, respectively. The mass spectrometry was carried out on a Sciex X500R QTOF mass spectrometer (MS) fitted with an Exion-LC series UHPLC (Sciex, CA, USA), using Information Dependent Acquisition (IDA) scanning method. All the mass acquisitions were performed using Electron spray ionization (ESI) in the negative mode with the following parameters: turbo spray ion source, medium collision gas, curtain gas = 30 L/min, ion spray voltage = -4500 V (negative mode), at 300 °C. TOF-MS acquisition was done at declustering potential of -80 V, while using -10 V collision energy. The acquired data was analyzed using the Sciex OS software (Sciex, CA, USA; University of Florida, FL, USA). The presence of a specific species was confirmed by the presence of precursor mass within 3 ppm error range. The fatty acid was quantified by taking the ratio of the area under the corresponding fatty acid peak, with respect to the area of internal standard peak.

2.3.8 Permeability assay

In order to determine the permeability of the different C11 based membrane systems, calcein leakage assay was used. Calcein is a small polar molecule with an excitation and emission wave length of 495 and 515 nm, respectively, and it gets self-quenched at a high concentration. This property was used to carry out this study

by encapsulating calcein above its self-quenching concentration. This was done by rehydrating the dried lipid film with 200 mM bicine buffer pH 8, containing 35 mM of calcein. For all the three heterogeneous C11 based systems, 90 mM of total lipid concentration was used. However, for the homogenous UDA system, the lipid concentration was kept at 150 mM due to its relatively high CBC. Interestingly, the pH of the solution dropped after dissolving the dried fatty acid film in the aforementioned mix of buffer and calcein. Therefore, the pH of the solution was readjusted by adding NaOH solution. The solution then went through four freeze-thaw cycles to increase the encapsulation efficiency.

To confirm the encapsulation of calcein in the vesicles, the crude suspension was observed under microscope, using both, fluorescence and DIC. Thereafter, the calcein encapsulated vesicle solution was extruded 15 times through a 200 nm size cut-off polycarbonate membrane using Avanti mini extruder (Avanti Polar Lipids Inc., Alabaster, AL, USA) and was loaded on to a size exclusion column (20 cm X 1 cm) packed with Sephadex G-50 fine beads. The column was pre-equilibrated with the mobile phase, which is 200 mM bicine buffer containing just empty lipid vesicles. For each lipid system, the mobile phase contained the same lipid composition and ratio, but at a slightly higher concentration than their CBC, to prevent the lysis of the calcein encapsulated vesicles in the column. Fractions were then collected manually and loaded on to a 96-microwell plate (about 220 µL/well). The fluorescence was measured using a 96-well plate Varioskan Flash multimode reader (Thermo Scientific, Singapore), by exciting the samples at 495 nm and measuring the emitted light at 515 nm. The vesicles with encapsulated calcein eluted in the early fractions (fraction number 11 to 16), and the unencapsulated calcein eluted in the later fractions (fraction number 43 to 57), as shown in Figure S11 a. The fluorescence was monitored continuously for three hours. After that, 2 µL of Triton 100X was added in each well to rupture the vesicles and release the remaining encapsulated calcein, which led to maximum fluorescence.

The percentage of encapsulation was calculated by using the following equation:

Encapsulation (%) $= 100 * (1 - \frac{Ft-F0}{Ff-F0})$

Where, $F0$ is the fluorescence at time zero, Ft is the fluorescence at time t and Ff is the final fluorescence after the addition of Triton 100X.

2.3.9 Membrane stability under multiple environmental conditions

To evaluate the stability of protocell membranes as a function of their composition under multiple environmental conditions, C11 based membrane systems were used. Three environmental conditions, i.e. A) vesicle formation in alkaline pH regime. B) vesicle stability in dilution regimes, and C) vesicle stability in the presence of Mg^{2+} ions, were applied to the systems in a sequential manner. In order to understand if there was any effect coming from the sequence of the applied condition on the vesicle stability, the environmental conditions were applied in all possible combinations. Therefore, a total of six different sequential combinations were investigated. All the four C11 based systems were prepared in 200 mM bicine buffer at pH 8 with the lipid concentration kept at 60 mM. Typically, 300 μL of each vesicle suspension was taken in a centrifuge tube. In one of the MSPs sequence combinations tested, first the lipid solution was diluted with 200 mM bicine buffer of pH 8 in order to check the stability of the vesicles on dilution. In the next step, the pH was increased by adding desired volume of 3M NaOH solution. It was added to all the lipid solutions to bring the final pH to 10. In the final step, the stability was checked in the presence of Mg^{2+} ions by adding desired amount of $MgCl_2$ solution to reach a concentration of 14 mM Mg^{2+}. After the application of each aforesaid environmental conditions, the lipid suspension was observed under microscope at 40X magnification to check for the presence of vesicle and unordered aggregates. In the same manner, the other five MSP combinations were also tested and the membrane systems were evaluated using microscopic analysis.

2.3.10 Statistical analysis:

All statistical analysis was performed using Microsoft Excel 2016. Two-tailed t-test was used to check the significance of difference between the values within a system and also to compare between values of particular time points across systems. Values were considered statistically significant for values with $P < 0.05$.

2.3.11 Construction of mixed membrane systems

All the experiments described in this present study were conducted using binary and tertiary mixed membrane systems of C11 and C18 fatty acids. The binary systems based on the undecylenic acid (UDA, C11) fatty acid system were prepared by

mixing undecylenic acid (UDA) with either glyceryl 1-undecylenate
(UDG) or undecylenyl alcohol (UDOH). Similarly, the oleic acid based (OA, C18)
binary systems were prepared by mixing oleic acid (OA) either with glycerol 1-
monooleate (GMO), or the oleyl alcohol (OOH) derivative. The ratio of fatty acid to its
derivatives was fixed to either 4:1 or 2:1. The tertiary systems for both the chain
lengths were prepared by mixing all three respective components together, i.e.
UDA,UDG and UDOH together and OA, GMO and OOH together, in ratios of 2:1:1,
4:1:1 and 6:1:1. Figure 2.1 in the summarizes the structures of the aforesaid
amphiphiles used in this study.
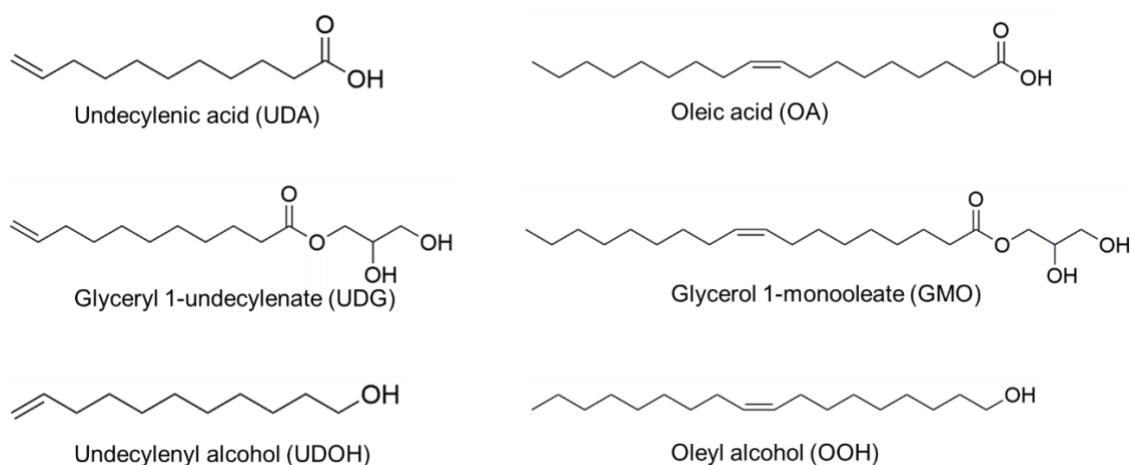
*Figure 2.1: Structures of different amphiphiles, i.e. fatty acids (C11 and C18) and their
derivatives used in the present study. The structures were drawn using ChemDraw
professional (PerkinElmer) 20.0.*

2.4 Results

2.4.1 Formation of vesicle under alkaline pH regimes

The vesicle forming ability of all different membrane system was evaluated from pH
7 to 11 at room temperature. It was observed that both the fatty alcohol and glycerol
monoester derivatives could indeed stabilize the fatty acid vesicles over a wide
range of pH. Absorption measurement of the suspension at 400 nm indicated that
UDA alone could form vesicles from pH 7.5 to 8 (Figure 2.2), which was also

confirmed using microscopy (Figure 2.3 and 2.4) that showed large multilayer vesicles (MLVs). The binary mixed UDA:UDG (2:1) system formed MLVs from pH 7 to 9, above which micelle formation occurred that resulted in a decrease in the turbidity values (Figure 2.2). On the other hand, the UDA:UDOH (2:1) binary system, formed vesicles from pH 7.5 to 11 Figure 2.3). When the ratio of fatty acid to derivative was changed to 4:1, it was observed that the UDA:UDG (4:1) and the UDA:UDOH (4:1) mixed binary systems assemble into vesicles (MLVs) from pH 7.5 to 8.5 and from 7.5 to 9 respectively (Figure 2.5). The tertiary systems of UDA:UDG:UDOH in 4:1:1 and 2:1:1 were able to form vesicles, from pH 7.5 to 11 (Figure 2.5). The tertiary system UDA:UDG:UDOH in 6:1:1 ratio formed vesicles from pH 7.5 to 9.5. As for the OA based systems, the OA itself formed vesicles from pH 8 to 9 (Figure 2.4). Below pH 8, large oil droplets were observed. The OA:OOH (2:1) binary system could form vesicles from pH 8.5 to 11. However, below 8.5 it assembled into large droplets. In the case of the OA:GMO (2:1) binary system and the tertiary system of OA:GMO:OOH in 4:1:1 ratio, vesicles were observed over a wide range of pH starting from 7.5 and up to 11 (Figure 2.4). The binary mixed system OA:GMO (4:1) and OA:OOH (4:1) formed vesicle from pH 7.5 to 10 and 8.5 to 11 respectively (Figure 2.5). In case of the tertiary systems, OA:GMO:OOH (2:1:1) and OA:GMO:OOH (6:1:1) vesicles were observed from pH 8 to 11 (Figure 2.5). Based on the observations eight different membrane systems were decided to explore further because of their robustness. Four systems were chosen for each chain length system, i.e. pure acid system, two binary systems composed of fatty acid mixed with either its corresponding alcohol or glycerol monoester in 2:1 ratio and the tertiary mixed system contains all there in 4:1:1 ratio. This way, the overall ratio of fatty acid to derivative was fixed to 2:1 to compare the membrane systems better, which also corroborates with the previous studies.[25,26]
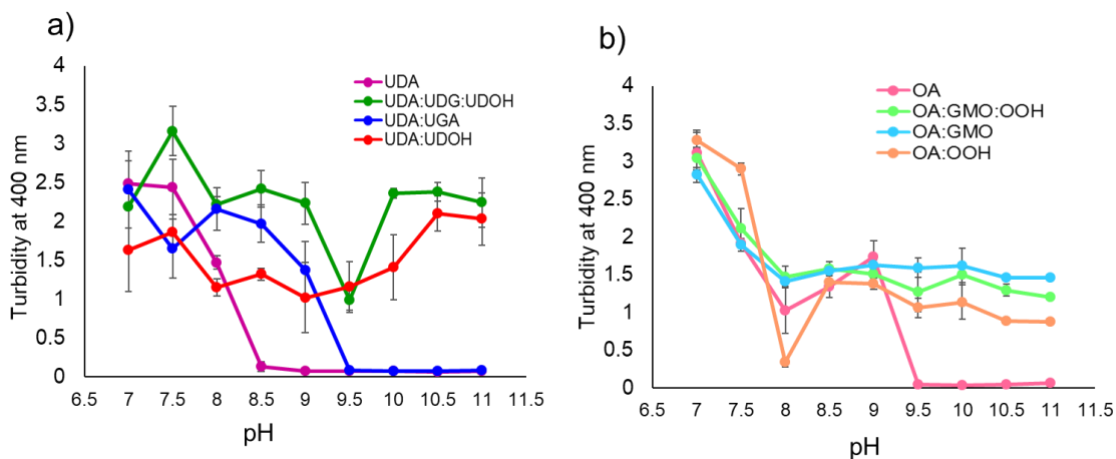
Figure 2.2: *Turbidity measurements of different C11 and C18 membrane systems at different pH. The turbidity of the systems at 400 nm is plotted as a function of the pH. Panel a and b represent the different C11 and C18 systems, respectively. Decrease in turbidity indicates the formation of micelles in the system, which cannot scatter light at 400 nm. The ratio of fatty acid to its respective glycerol monoester and/or alcohol was maintained at 2:1. N = 3; error bars represent standard deviation.*
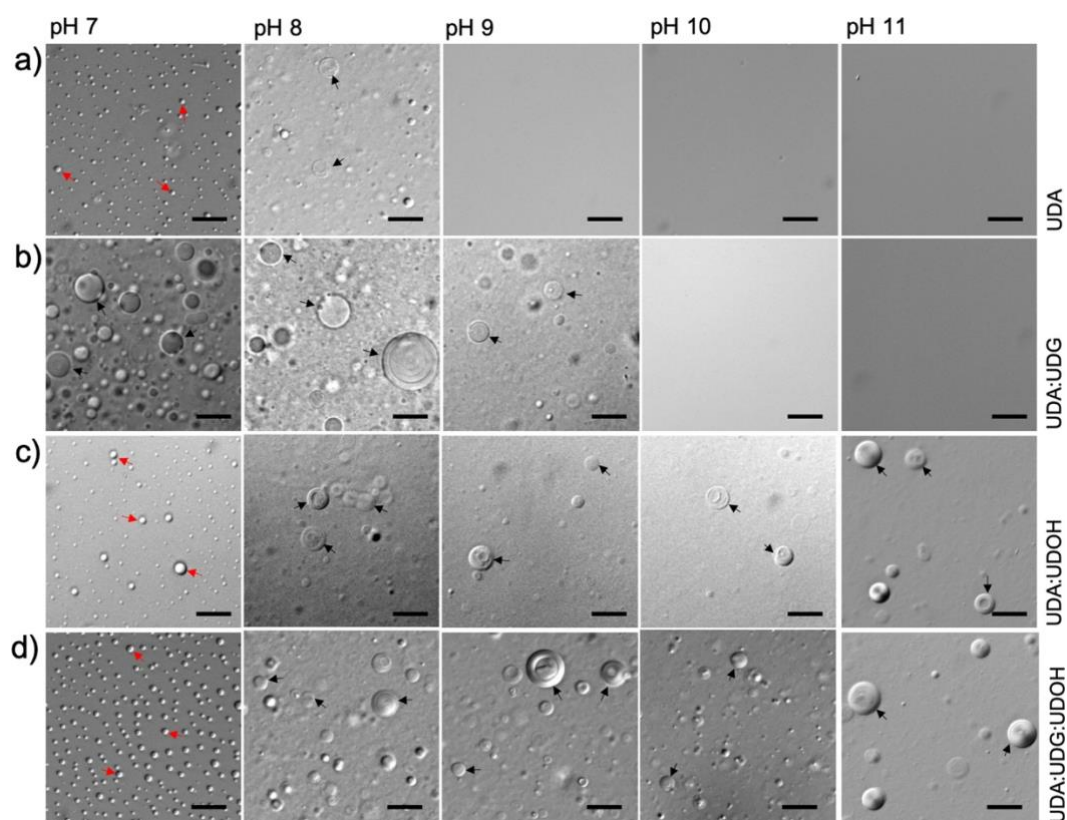
Figure 2.3: *Formation of membrane under alkaline pH regimes. Microscopic analysis of C11 based membrane systems. These images demonstrate the formation of vesicles and oil*

droplets depending on the pH of the surrounding environment. Panels (*a–d*) show the four different C11 based membrane systems. The ratio of fatty acid to its respective glycerol monoester and/or alcohol was maintained at 2:1. The black and red arrows indicate vesicles and oil droplets, respectively. The scale bar in all the images is 10 microns. N = 4.
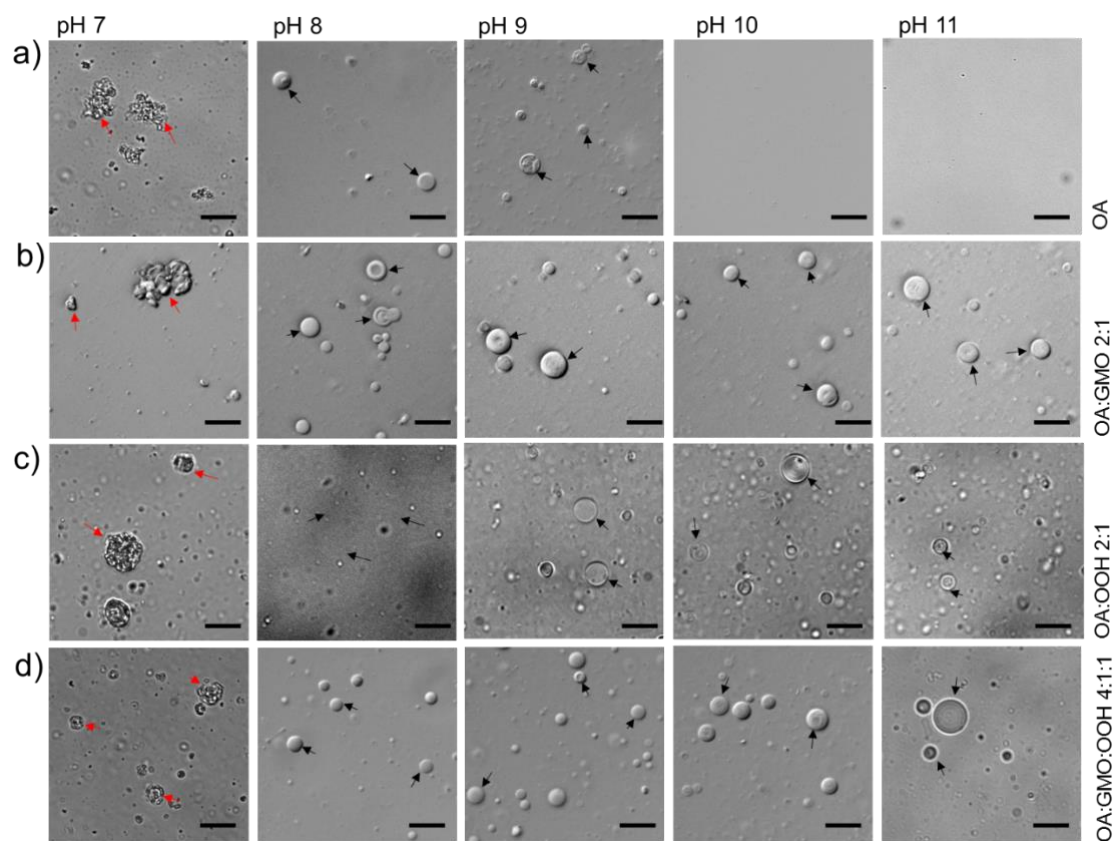
Figure 2.4: *Microscopic analysis of C18 membrane systems. These images demonstrate the formation of vesicles and oil droplets depending on the pH of the surrounding environment. Panels a to d show the four different C18-based systems. The black and red arrows indicate vesicles and aggregates, respectively. The scale bar in all the images is 10 microns. N = 4.*

		pH								
		7	7.5	8	8.5	9	9.5	10	10.5	11
UDA		□	■	■	□	□	□	□	□	□
UDA:UDG	4:1	□	■	■	■	□	□	□	□	□
	2:1	■	■	■	■	■	□	□	□	□
UDA:UDOH	4:1	□	■	■	■	■	□	□	□	□
	2:1	□	■	■	■	■	■	■	■	■
UDA:UDG:UDOH	6:1:1	□	■	■	■	■	■	□	■	■
	4:1:1	□	■	■	■	■	■	■	■	■
	2:1:1	□	■	■	■	■	■	■	■	■
OA		□	□	□	■	■	□	□	□	■
OA:GMO	4:1	□	□	■	■	■	■	■	□	■
	2:1	□	□	■	■	■	■	■	■	■
OA:OOH	4:1	□	□	□	■	■	■	■	■	■
	2:1	□	□	□	■	■	■	■	■	■
OA:GMO:OOH	6:1:1	□	□	■	■	■	■	■	■	■
	4:1:1	□	■	■	■	■	■	■	■	■
	2:1:1	□	□	■	■	■	■	■	■	■

Presence of vesicles ■
Absence of vesicles □
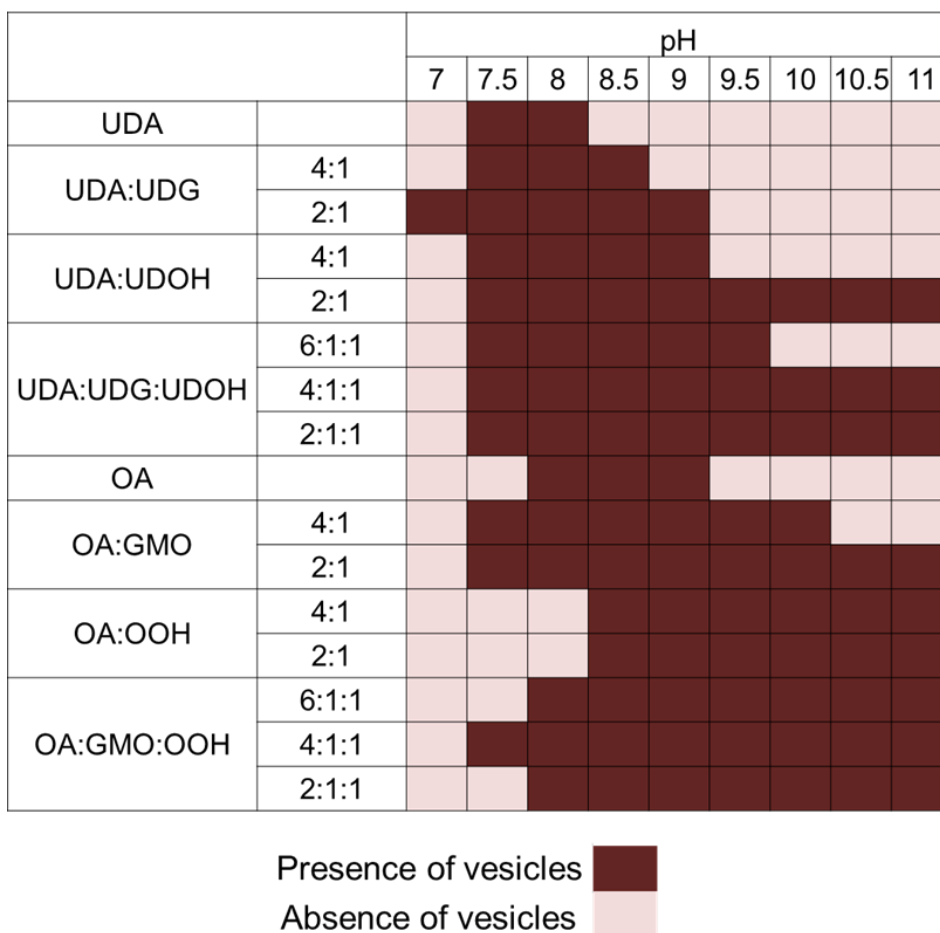
Figure 2.5: *The ability of the different membrane systems to form vesicles over varying pH regimes has been illustrated in this figure. The ability of a system to form vesicles over a range of pH is represented in the matrix. N = 4.*

2.4.2 Self-assembly of model protocellular membrane systems

The fluorescence assay using 1,6-diphenyl-1,3,5-hexatriene (DPH) revealed that the CBC of the pure UDA was around 35 mM. Upon mixing UDA with UDG, the CBC drastically decreased to 2 mM (Figure 2.6 and Table 2.1). Here the lipid concentration for the mixed systems refers to the total lipid concentration, tanking account fatty acid and the respective derivatives. For the binary system of UDA:UDOH (2:1) and the tertiary system of UDA:UDG:UDOH (4:1:1), the CBC was found to be around 4 and 2 mM, respectively (Table 2.1). Microscopic analysis of all the systems confirmed the presence of vesicles (Figure 2.7). For the pure oleic acid (OA) system, the CBC was found to be around 0.09 mM. Upon adding either the GMO or the OOH derivative (2:1 ratio), the CBC decreased to about 0.02 and 0.06

mM, respectively (Table 2.1). For the tertiary system of OA:GMO:OOH (4:1:1), the CBC was found to be around 0.02 mM. The presence of vesicle was also confirmed by measuring absorption of the (scattering) of the suspension at 400 nm. The experiments were performed at room temperature. On performing microscopy, vesicles were observed under the microscope only at a slightly higher concentration than what was expected from the fluorescence assay (Figure 2.7). This could potentially stem from the fact that light microscopy is diffraction-limited thus missing out on vesicles that are smaller than 200 nm.
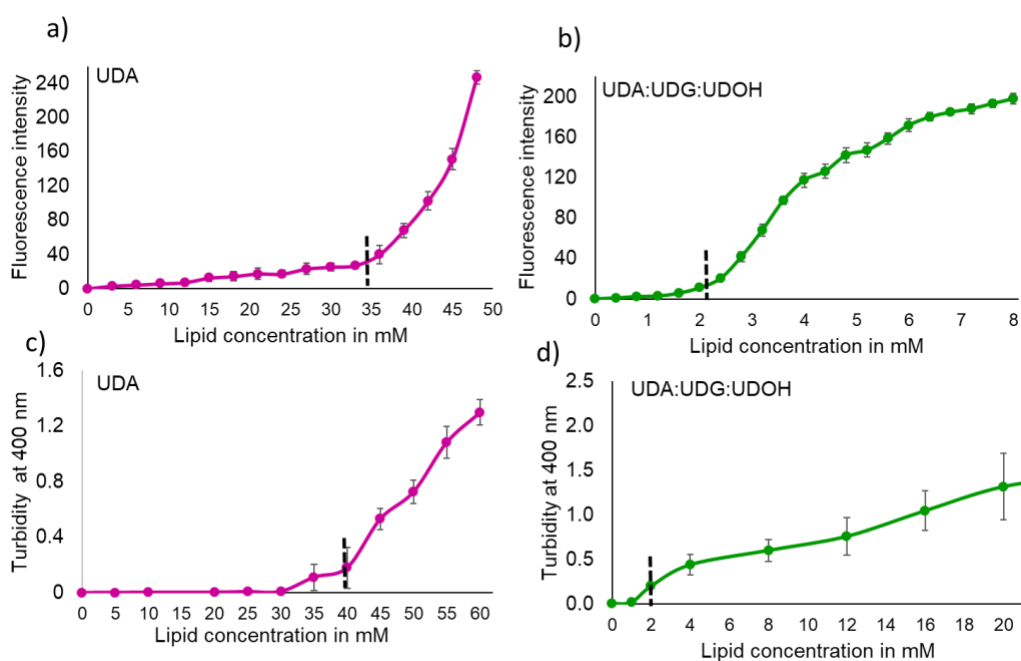
Figure 2.6: *CBC estimation of the different C11 membrane systems by fluorescence and turbidity assay. Panel a and b represent the CBC estimation of only UDA and UDA:UDG:UDOH (4:1:1) system respectively using fluorescence assay. The increase in fluorescence is plotted as a function of lipid concentration. The inflection point, which is a read out of the CBC of the system, is represented with the black dashed line. Panel c and d represent the CBC estimation of only UDA and UDA:UDG:UDOH (4:1:1) system respectively using turbidity assay. The increase in turbidity is plotted as a function of lipid concentration. The inflection point, which is a read out of the CBC of the system, is represented with the black dashed line. n = 3; error bars represent standard deviation.*

Table 2.1: *CBC estimation using fluorescence and turbidity assay. Columns 2 and 3 provide a comparison of the difference in the CBC estimation using fluorescence assay and turbidity assay, respectively.*

Apparent CBC in mM		
System used	Fluorescence Assay	Turbidity Assay
UDA	35±3	40±5
UDA:UDOH	4±0.6	8±1
UDA:UDG	2±0.4	2±0.5
UDA:UDG:UDOH	2±0.4	3±0.5
OA	0.09±0.01	0.2±0.05
OA:OOH	0.06±0.01	0.1±0.02
OA:GMO	0.01±0.005	0.1±0.02
OA:GMO:OOH	0.01±0.005	0.1±0.02
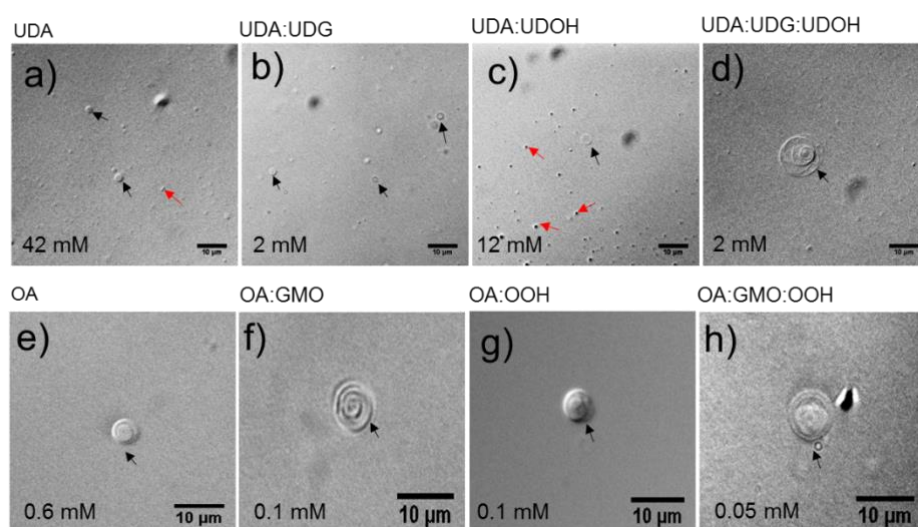
Figure 2.7: *CBC estimation using microscopic analysis. Panels a to d and e to f show the microscopic analysis of the different C11 and C18 based systems, respectively, at their*

CBC. a) 40 mM homogenous UDA, b) 2 mM of UDA:UDG, c) 12 mM of UDA:UDOH, d) 2 mM of the tertiary UDA:UDG:UDOH system, e) 0.6 mM of OA, f) 0.1 mM of OA:GMO, g) 0.1 mM of OA:UDOH, and h) 0.05 mM of OA:GMO:OOH systems. Below the aforesaid concentrations, vesicles were not observed under 40X magnification. The black and red arrows indicate vesicles and aggregates, respectively. The ratio of fatty acid to its respective glycerol monoester and/or alcohol was maintained at 2:1. Scale bar in all the images is 10 microns.

2.4.3 Stability of vesicles in the presence of Mg^{2+} ions

Dynamic Light Scattering (DLS) measurement was used to determine the stability of the vesicles in the presence of Mg^{2+} ions at room temperature. The DLS analysis showed that the UDA:UDG (2:1) binary system was the most stable one, with an Mg^{2+} ion induced-aggregation concentration (Mg^{2+}_{AIC}) (see the method section for details) of 16 mM, followed by the tertiary UDA:UDG:UDOH (4:1:1) and the binary UDA:UDOH (2:1) systems, with an Mg^{2+}_{AIC} of 14 and 8 mM, respectively (Figure 2.8). The pure UDA system was extremely labile to Mg^{2+} ions, where aggregation started even at Mg^{2+} ion concentrations of as low as 3 mM of (Figure 2.8). On microscopic analysis, large crystalline aggregates (Mg-soap) were observed in the UDA system at 4 mM Mg^{2+} ion concentration, and no vesicles were observed in the solution beyond 8 mM Mg^{2+} concentration (Figure 2.9). However, in the case of the UDA:UDG system, crystalline aggregates and collapsed vesicles started appearing at 12 mM Mg^{2+} ion concentration, and vesicles persisted even in solutions containing a Mg^{2+} ion concentration of 24 mM (Figure 2.9). Between the UDA:UDOH and the UDA:UDG:UDOH systems, the latter seemed more stable, with vesicles being observed along with some crystalline aggregates (Mg-soap) and collapsed vesicles in the presence of 12 mM Mg^{2+} ions (Figure 2.9). However, only crystalline aggregates and collapsed vesicles were found in the UDA:UDOH system at 12 mM Mg^{2+} ion concentration under the microscope (Figure 2.9). In terms of cation sensitivity among the four systems, the following order is seen:
UDA > UDA:UDOH > UDA:UDG:UDOH > UDA:UDG. Among the four C18 based systems, the OA alone system was found to be the most sensitive, with an Mg^{2+}_{AIC} of 3.5 mM (Figure 2.8). Interestingly the OA:GMO (2:1) was found to be the second most sensitive towards Mg^{2+} ions, with an Mg^{2+}_{AIC} of 5 mM. Both, the binary

OA:OOH (2:1) and the tertiary OA:GMO:OOH (4:1:1) systems showed an Mg^{2+}_{AIC} of 6 mM (using DLS) (Figure 2.8). Similar observations were confirmed using microscopy (Figure 2.10). In terms of cation sensitivity among the four systems, the following order is observed: OA > OA:GMO > OA:GMO:OOH = OA:OOH. Overall, the Mg^{2+}_{AIC} of all four C18 based systems were lower as compared to the C11 based systems because total of 2 mM lipid concentration was used for all four C18 based systems, which is much lower than what was used for C11 based systems.
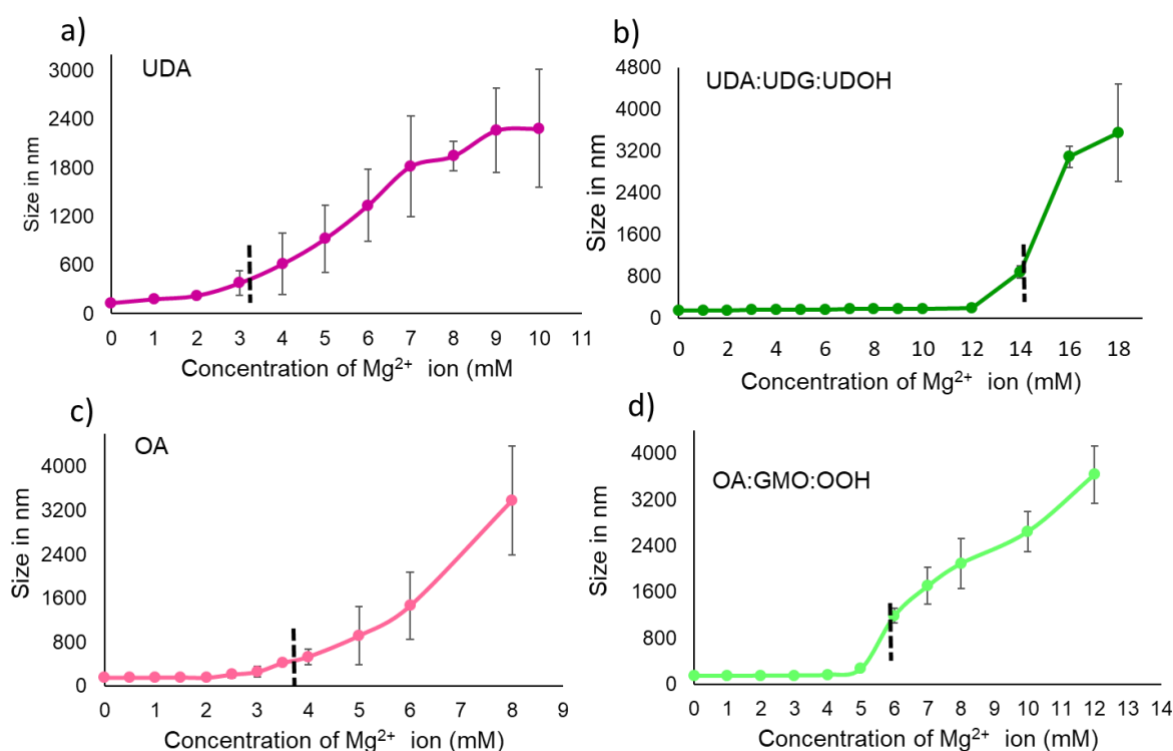
Figure 2.8: *Shows DLS measurements of the C11 and C18 membrane systems to determine Mg^{2+} ion induced aggregate formation concentration. The particle diameter (in nm) is plotted as a function of the added Mg^{2+} ion concentration. The vertical black dashed line indicates the Mg^{2+} ion induce aggregation formation concentration (Mg^{2+}_{AIC}). Panel a and b represent only UDA and UDA:UDG:UDOH (4:1:1) system. Panel c and d represent only OA and OA:GMO:OOH (4:1:1) system The ratio of fatty acid to its respective glycerol monoester and/or alcohol was maintained at 2:1. N = 3; error bars represent standard deviation.*
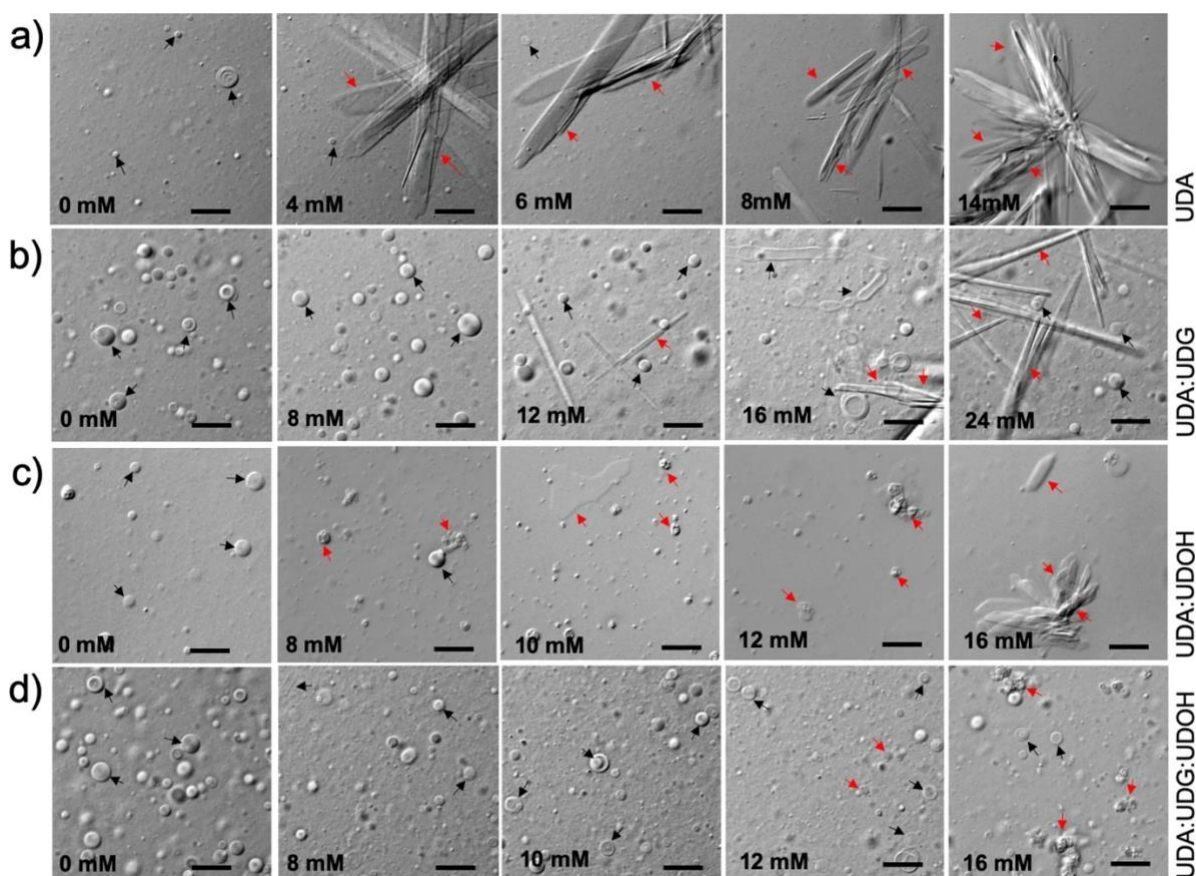
Figure 2.9: *Microscopic analysis of model protocellular membrane stability in presence of Mg²⁺ ions. Mg²⁺ ion induced aggregate (crystalline aggregates and collapsed vesicles) forming propensities of all the four UDA based systems (panels a–d). From left to right, Mg²⁺ ions concentration was increased gradually by keeping the lipid concentration constant. In terms of cation sensitivity among the four systems, the following order is seen: UDA > UDA:UDOH > UDA:UDG:UDOH > UDA:UDG. The black and red arrows indicate vesicles and aggregates (crystalline aggregates and collapsed vesicles), respectively. The scale bar = 10 microns. The ratio of fatty acid to its respective glycerol monoester and/or alcohol was maintained at 2:1.*
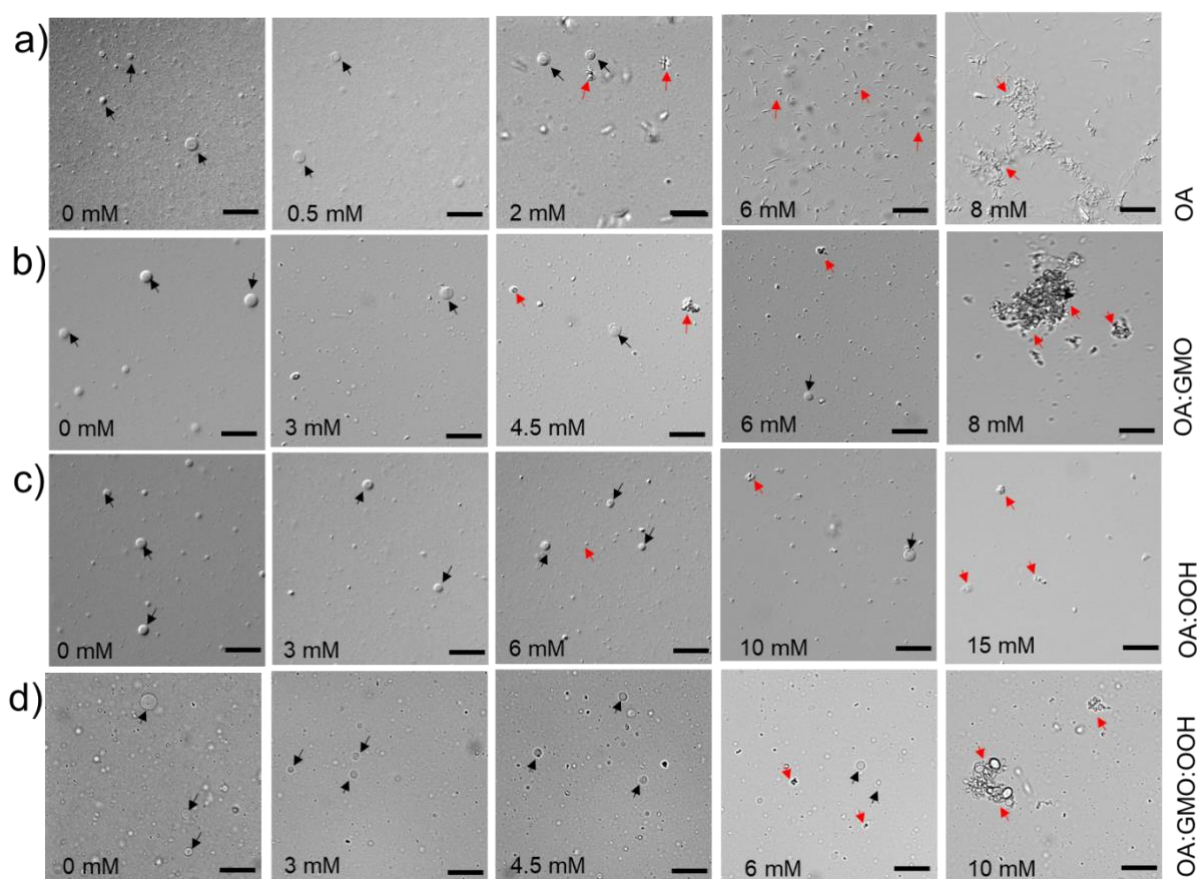
Figure 2.10: Mg^{2+} ion induced vesicle and aggregate forming properties of all the four C18 based membrane systems (panels a to d). From left to right, Mg^{2+} ion concentration was increased gradually by keeping the lipid concentration constant. The ratio of fatty acid to its respective glycerol monoester and/or alcohol was maintained at 2:1. In terms of cation sensitivity among the four systems, the following order is observed: OA > OA:GMO > OA:GMO:OOH = OA:OOH. The black and red arrows indicate vesicles and aggregates (fatty acid crystals and droplets), respectively. The scale bar in all images is 20 microns.

2.4.4 Potential mechanism by which fatty alcohol and glycerol monoester confer stability on fatty acid membranes in the presence of Mg^{2+} ions

In order to understand the mechanism behind the increased stability of fatty acid membranes towards Mg^{2+} ions in the presence of the derivatives, the charge density on the membrane and the retention of the fatty acid moieties in the membranes, was investigated. Fatty acid molecules stay in dynamic equilibrium and can therefore readily exchange between the membrane phase and the free monomers present in the solution.[28] The free negative charged monomers can interact with Mg^{2+} ions and

form crystalline aggregates, thus more amount of free fatty acids will lead to greater aggregation. Upon quantifying free fatty acid, it was observed that the UDA system possessed the highest amount of free fatty acids (Figure 2.11, Panel a). The presence of UDG and UDOH showed a decrease in the dissociation of free UDA molecules into the solution, thereby stabilizing the mixed membranes (Figure 2.11, Panel a). In case of OA based membrane systems, it was observed that both, OOH and GMO decrease the dissociation of OA into the solution, similar to what was observed in the UDA based systems (Figure 2.11, Panel c). The free Mg^{2+} ions present in the solution also tend to interact with the negatively charged fatty acid vesicles and initiate collapsing of vesicles. Therefore, a decrease in the net negative charge on the vesicle surface would lead to a weakening in the interaction with the Mg^{2+} ions. The zeta potential measurements revealed that the addition of UDG to the UDA membrane decreased the net negative charge density significantly (Figure 2.11, Panel b). The net negative charge density of the UDA:UDOH binary system was equal to that of the only UDA system (Figure 2.11, Panel b). The negative charge density on the tertiary UDA:UDG:UDOH system was found to be somewhere in between these, i.e., higher than the UDA:UDG system but lower than the UDA and UDA:UDOH system. The change in the negative charge density can be explained by considering the size of the different head groups. Because of the bulky head group of the UDG moiety, less number of deprotonated fatty acid molecules would be present in a given unit surface area as opposed to what potentially happens in the presence of UDOH. Similar pattern of zeta potential values was also observed for the oleic acid-based membranes (Figure 2.11, Panel d). Therefore, we found that both of the components, i.e. retention of fatty acid molecules in the membrane, and the change in the surface charge density, would contribute towards the increased stability of the mixed membrane systems in the presence of Mg^{2+} ions. Long chain alcohols stabilize the fatty acid membranes by retaining the fatty acid molecules in the membrane, whereas the glycerol monoester not only increases the fatty acid retention in membrane, but also decreases the overall negative charge density.
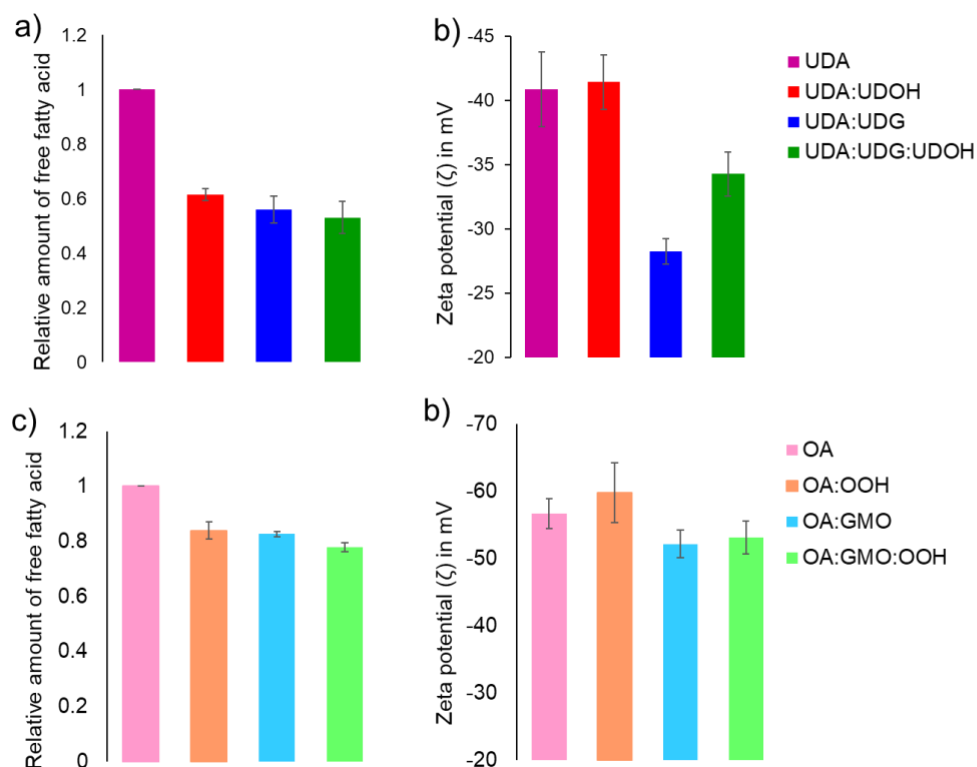
Figure 2.11: *LC-MS analysis for free acid quantification and zeta potential measurements. Panel (a) and (c) shows the relative amount of free fatty acids in the solution as a function of the membrane composition for C11 and C18 based systems respectively. N = 6; error bars represent S.D. The difference between the mean values for the pure UDA system with other three C11 mixed systems is significant based on one-tailed student t test with a p-value < 0.05. Similarly, the difference between the mean values for the pure OA system with other three C18 mixed systems is significant based on one-tailed student t test with a p-value < 0.05. Panel (b) and (d) indicates the zeta potential measurements of the different C11 and C18 based systems respectively as a function of their composition. N = 5; error bars represent S.D. The difference between the mean values for UDA with UDA:UDG and UDA:UDG:UDOH is significant based on two-tailed student t test with a p-value < 0.05. The difference between the mean values for OA with OA:GMO and OA:GMO:OOH is significant based on two-tailed student t test with a p-value < 0.05.The ratio of fatty acid to its respective glycerol monoester and/or alcohol was maintained at 2:1.*

2.4.5 Permeability of model protocellular membranes

C11 based systems were chosen to explore the effect of different composition on membrane permeability because of its smaller chain length. Previous studies have

looked at the permeability of pure OA and binary OA:GMO based system[24,25,27]. Calcein leakage assay at room temperature was used to determine the permeability of the protocell membranes. Calcein was encapsulated in vesicles above its self-quenching concentration and the vesicle encapsulated calcein was purified using size-exclusion column. The calcein encapsulated vesicle came out in early fraction as shown in Figure 2.12 panel a. All four systems were able to encapsulate calcein and the presence of vesicle encapsulating calcein was confirmed using microscopy as shown is Figure S12 panel b. From the results, it was observed that when UDG was mixed with UDA, the permeability of this mixed binary membrane system increased drastically, in comparison to the pure UDA system. Over a period of 180 min, 80 percent of the encapsulated calcein was released from the UDA:UDG system (Figure S13), whereas 22 percent of the encapsulated calcein was released in case of the pure UDA membrane system (Figure S13). This corroborates with the literature where Mansy S. et. al. showed that, addition of glycerol monoester of myristoleic acid (monomyristolein) in myristoleic acid (C14:1) system in 2:1 ratio increase the permeability of the membrane system.[25] Interestingly, the UDA:UDOH binary system was found to be impermeable to calcein, where none of the encapsulated calcein was released even after a period of 180 min (Figure S13). The tertiary system (UDA:UDG:UDOH) was found to possess moderate permeability to calcein, which was less permeable than the binary UDA:UDG binary system and the pure UDA system, but more permeable than the UDA:UDOH binary system, releasing only 14 percent of encapsulated calcein over 180 mins **(**Figure S13**)**. While presence of UDG in the membrane led to an increase in the permeability, the presence of UDOH decreased the permeability of the UDA system. The probable reason behind this observation could be explained by factoring the polar head-group size. Because of the bulky head group, the glycerol monoester is thought to hinder efficient membrane packing thereby resulting in an increase in the permeability of the system. On the other hand, UDOH possesses a small head group, which can potentially increase membrane packing, resulting in a decrease in the permeability.
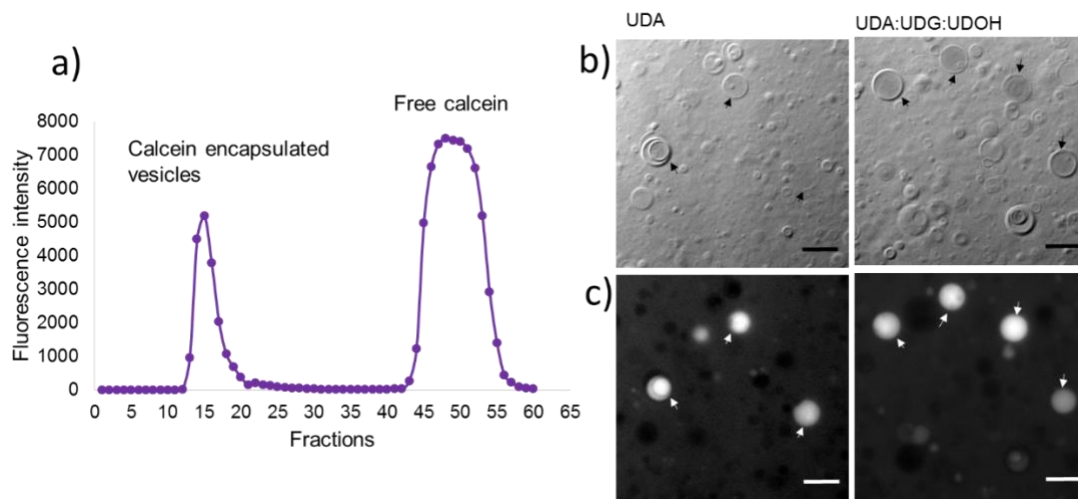
Figure 2.12: *Calcein encapsulation and size size exclusion column chromatography. Panel (a) shows the size exclusion column chromatography profile, which was used to separate vesicles with encapsulated calcein, from the unencapsulated calcein. Fluorescence at 518 nm was plotted against the fraction number. The unencapsulated calcein comes out in later fractions whereas the vesicles with encapsulated calcein elute out in the earlier fractions. Panel (b) shows the epifluorescence micrographs of calcein encapsulated vesicles from two C11 based membrane systems. The images on the top represent the Differential Interference Contrast (DIC) images, while the lower two images are of the fluorescence images of the same field of view. The scale bar in all the images is 10 microns.*
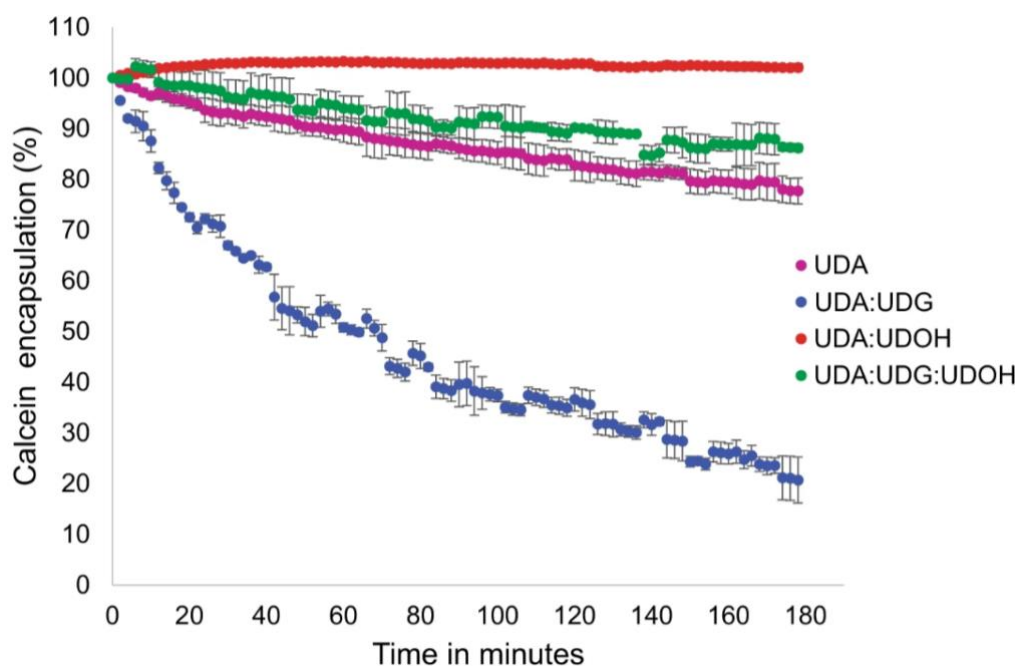
2.4.6 Multiple environmental conditions and vesicle stability of model protocell membranes as a function of their composition

The experiment (see method section and Supplementary information) revealed that even though the binary mixed systems (UDA:UDOH and UDA:UDG) could be more stable under a given environmental conditions, when all the three environmental conditions were applied sequentially, the tertiary system (UDA:UDG:UDOH) was the one that stood the best chance at survival. As shown in Figure 2.14 panel a, all four C11 based systems formed vesicles at a lipid concentration of 60 mM at pH 8. When all the four systems were diluted to a final lipid concentration of 20 mM using a buffer of pH 8, the UDA system failed to form vesicles because of its high CBC (near 35 mM), while the other three mixed systems continued to form vesicles (panel b). Next, out of the three mixed systems, only Mg-soap crystals and collapsed vesicles were observed in UDA:UDOH system when Mg^{2+} ions were added to the solution at a concentration of 14 mM (panel c). Among the other two mixed systems, UDA:UDG and UDA:UDG:UDOH, being less sensitive to Mg^{2+} ion concentration, continued to form vesicles. Finally, when the pH of the solution was adjusted to 10, the UDA:UDG system failed to assemble into vesicles. Consequently, only the tertiary system of UDA:UDG:UDOH was able to assemble into vesicles when all conditions were applied back to back (panel d). Significantly, this observation was independent of the sequence of the conditions applied. As shown in Figure 2.15 and 2.16 even after changing the chronology of the environmental conditions applied, the end result i.e. only the tertiary membrane vesicle survives does not get affected.
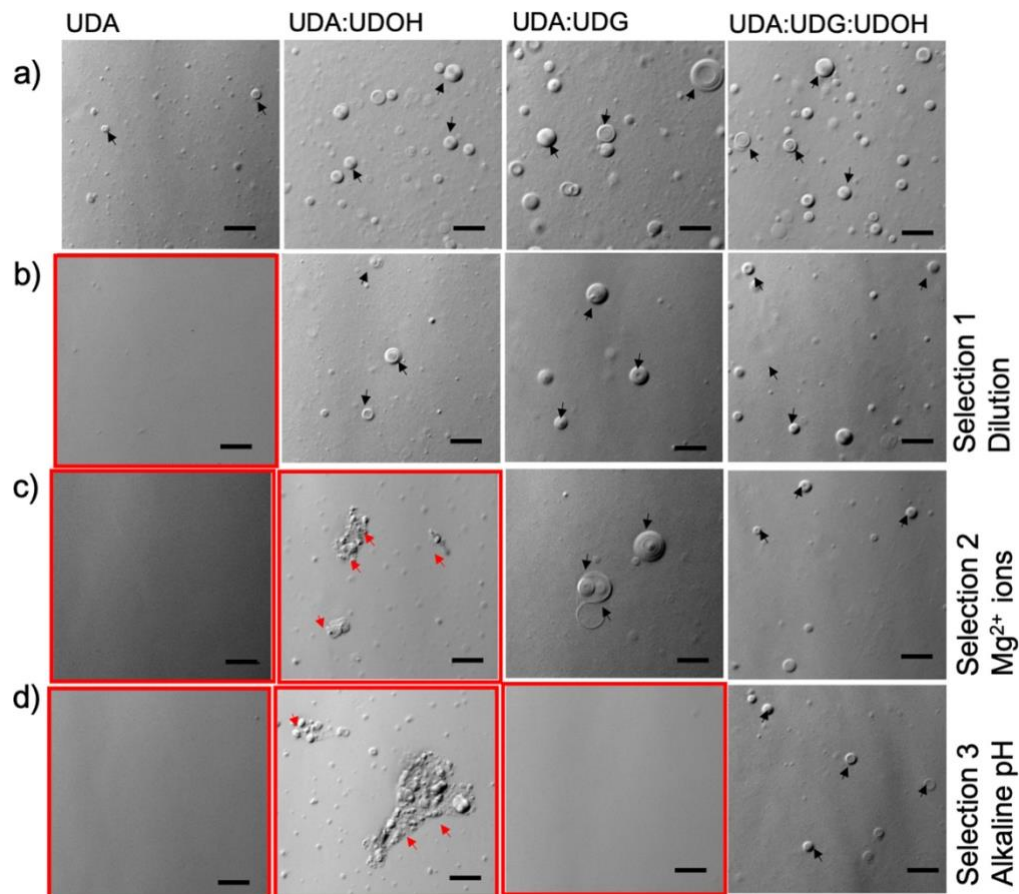
Figure 2.14: *Membrane stability under environmental conditions when applied consecutively. Panels b to d represent different prebiotically relevant conditions. a) All four C11 based systems at a concentration of 60 mM at pH 8. b) Dilution regime: All four C11 based systems diluted to a concentration of 20 mM at pH 8. c) Stability in presence of Mg^{2+} ions: All four C11 based systems at 20 mM total lipid concentration at pH 8, in the presence of 14 mM Mg^{2+}. d) Stability at alkaline pH: All systems at 20 mM total lipid concentration in the presence of 14 mM Mg^{2+} and at an alkaline pH of 10. The red enclosures indicate absence of vesicles. The black and red arrows indicate vesicles and aggregates (crystalline aggregates and collapsed vesicles) respectively. The scale bar = 10 microns.*
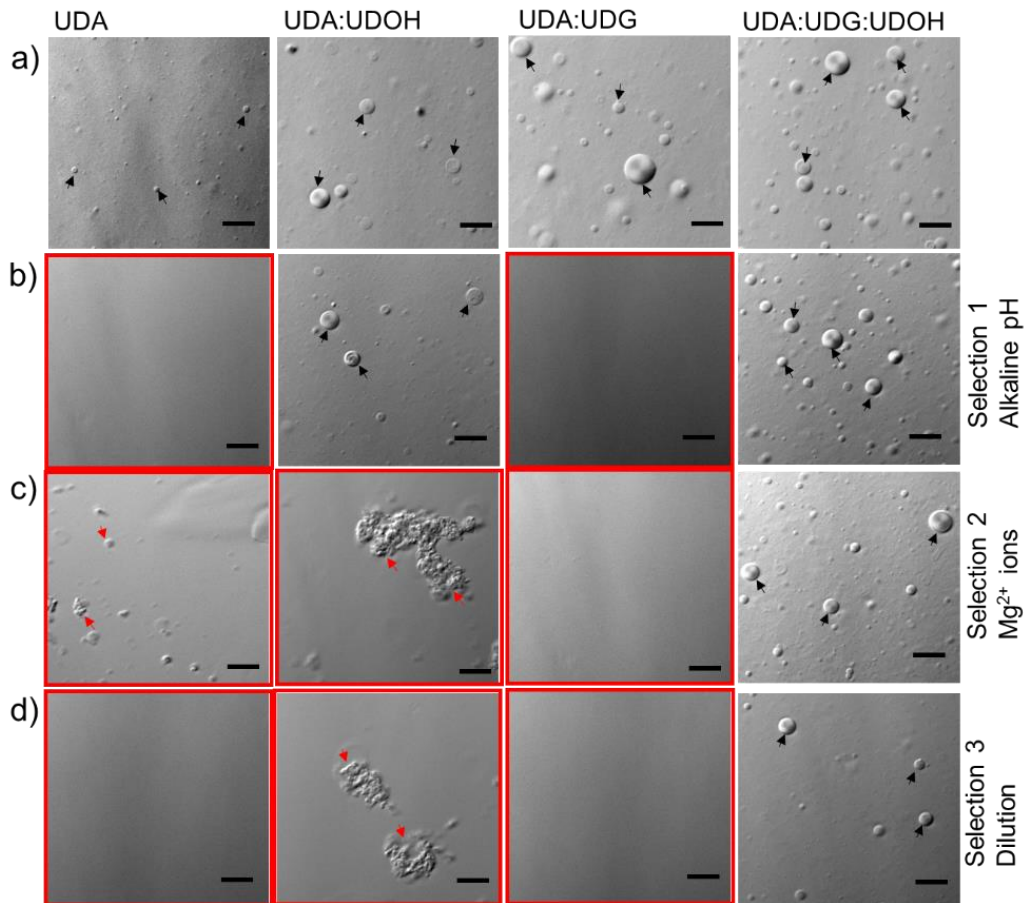
Figure 2.15: *Vesicle stability under multiple environmental conditions. Panels b to d represent the different prebiotically relevant conditions. a) All four C11 systems at a concentration of 60 mM at pH 8. b) Stability at alkaline pH as the constraining environmental condition. All systems comprised of 60 mM of lipid concentration, with the pH of the system now adjusted to 10. c) Stability in the presence of Mg^{2+} ions as selection condition . Mg^{2+} ions were added in all the systems at a concentration of 14 mM. The lipid concentration is 60 mM in all the systems, which are at pH 10. d) Dilution regime as environmental conditions in which all the four systems were diluted to concentration of 20 mM lipid concentration at pH 10 in presence of 14 mM Mg^{2+} ions. The red boxes indicate conditions where the vesicles are absent. The black and red arrows indicate vesicles and aggregates (fatty acid crystals and droplets), respectively. The scale bar in all the images is 10 microns.*
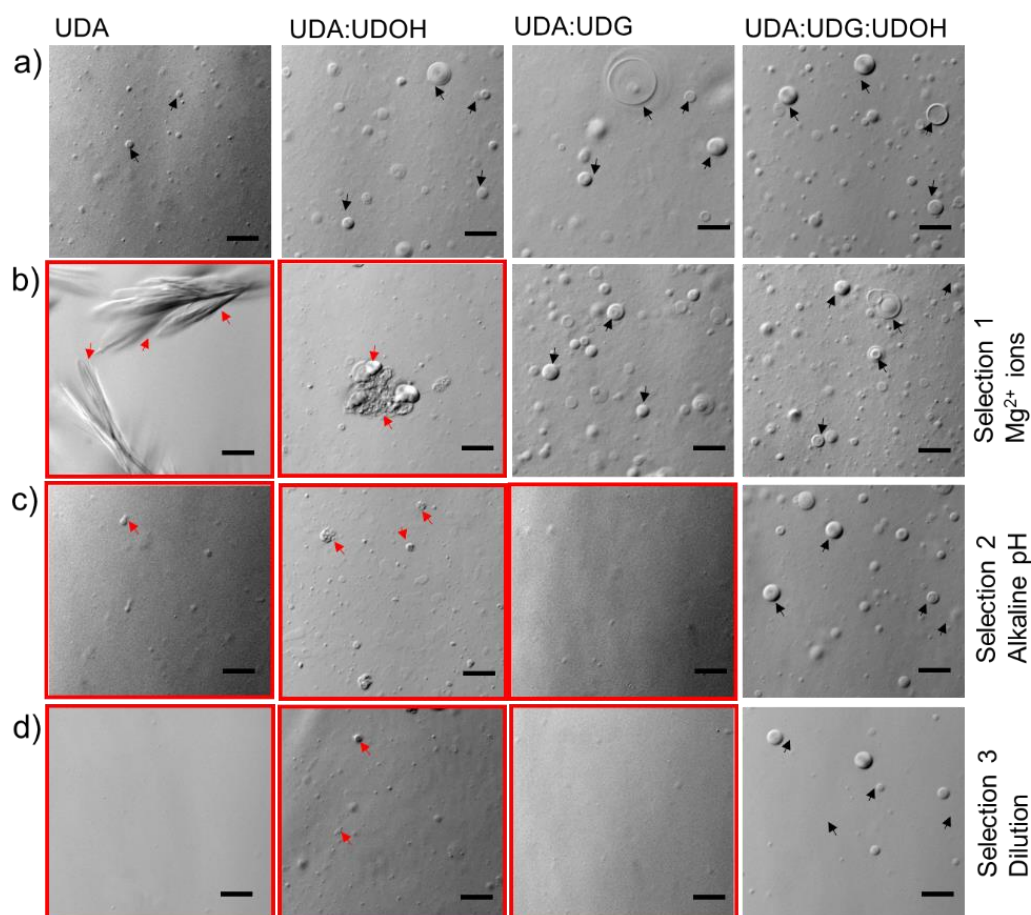
Figure 2.16: *Vesicle stability under multiple environmental conditions. Panels b to d represent the different prebiotically relevant conditions. a) All four C11 based systems at a concentration of 60 mM at pH 8. b) Stability in the presence of Mg^{2+} ions as environmental condition. Mg^{2+} ions were added in all the systems at a concentration of 14 mM. The lipid concentration is 60 mM in all the systems, which are at pH8. c) Stability at alkaline pH as a selection condition. All systems comprised of 60 mM of lipid concentration and 14 mM Mg^{2+} ions, with the pH of the system now adjusted to 10. d) Dilution regime as selection condition in which all the four systems were diluted to concentration of 20 mM lipid concentration at pH 10, in presence of 14 mM Mg^{2+} ions. The red boxes indicate conditions where the vesicles are absent. The black and red arrows indicate vesicles and aggregates (crystalline aggregates and collapsed vesicles), respectively. The scale bar in all the images is 10 microns.*

2.5 Conclusions and Discussions

When the vesicular stability of the different membrane systems was tested using dilution as the constraining environmental condition, it was observed that the incorporation of both of the derivatives, i.e. fatty alcohol and glycerol monoester moieties, decreased the CBC of the system. However, the influence of the glycerol monoester on lowering the CBC is greater than the fatty alcohol moiety. A crucial aspect to highlight here is that three different methods were employed in our study to estimate the CBC. This is because use of any of the individual techniques in isolation is not sufficient to gain an understanding of the complete picture. Thus, three techniques were combined to confidently narrow down the CBC of the systems to a precise range. As for the stability of the various systems in alkaline pH regimes, pure fatty acid systems were found to be extremely sensitive. The UDA:UDG system failed to form vesicles above a pH of 9. Whereas, the UDA:UDOH binary system and the UDA:UDG:UDOH tertiary system continued to assemble into vesicles even at pH 11. In case of the OA based systems, all three mixed systems (OA:GMO, OA:OOH, OA:GMO:OOH) were found to form vesicles even at pH 11. These observations can be explained by factoring in the protonation status of the different species. As the pH increases, the fatty acid species get deprotonated, allowing it to hydrogen bond with the hydroxyl group of the alcohol or the glycerol head group, resulting in membrane assembly.[3,6] Hence in case of UDA:UDG:UDOH tertiary system, the membrane stability predominantly seems to stem from the UDOH moiety above pH 9 as the UDA:UDG system fails to assemble into vesicles above pH 9. As for the OA:OOH system, it does not form vesicles at pH 8, while the pure OA system can. This might potentially come from the predominance of the deprotonated fatty acids species at this pH, which hampers efficient hydrogen bonding. When the stability of the membrane systems in question was evaluated against Mg^{2+} ion concentration, the UDA:UDG binary system was found to be the most resilient among the UDA based systems, followed by the UDA:UDG:UDOH. The UDA:UDOH was found to be the second most sensitive one after the pure UDA system. In the OA based systems, the OA:OOH and the OA:GMO:OOH systems were found to be equally stable towards higher Mg^{2+} ion concentrations. The OA:GMO binary system was found to be the second most sensitive one, after the only OA-based system. The greater stablizing effect of OOH, compared to that of GMO, could potentially be attributed to an

increase in the chain length. As the chain length increases, parameters like membrane thickness, membrane packing, CBC etc. also change. It has been reported that, low concentration of free Mg^{2+} ions (4 to 15 mM) can facilitate ribozyme function[19,24,33], which are compatible with the mixed membrane systems described in this study. Therefore, it seems reasonable to hypothesize that an increase in the membrane compositional heterogeneity, along with some chelation, could have provided a respite from the Mg^{2+} ion conundrum. Compartments possessing very high or very low permeability would not have been suitable to support protocellular life forms. Rather, compartments possessing moderate permeability, which would have allowed the permeability of small molecules (nucleotide monomer, dimer and amino acids etc) to the inside, without letting the internal components to permeate out, would have been more ideal. Results from our permeability experiments show that the incorporation of UDG into UDA membranes increases the membrane permeability when compared to the pure UDA membrane system. On the other hand, the addition of UDOH decreases the permeability of the system. Therefore, an optimally permeable membrane would have required a mixture of both of these derivatives, as observed in the tertiary system of UDA:UDG:UDOH. Because of the bulky head group, the glycerol monoester is thought to hinder efficient membrane packing, while also stabilizing membrane curvatures, which might have resulted from membrane solute interaction[25]. Thus, the permeability of the system increases. UDOH on the other hand, possess a small head group, which can potentially increase membrane packing, resulting in a decrease in the permeability. Basically, tuning the concentration of the various components could, in turn, enable the tuning of the permeability of a given model protocellular system that would have determined its suitability for a specific set of environmental parameters. Interestingly the C11 based tertiary system was found to possess the highest encapsulation efficiency compared to pure UDA, binary UDA:UDG and UDA:UDOH membrane systems. In conclusion, our study highlights that the stability of model protocellular membranes is not a linear property of its compositional heterogeneity. This is because, it is governed differently by different prebiotically relevant parameters. Importantly, the effect of each head group on the stability of the membrane, depends on the environmental conditions that the system is being subjected to. For example, at alkaline pH of 10 or above, the UDOH stabilizes UDA membranes, while UDG cannot. Whereas, in the presence of Mg^{2+}

ions, the UDG stabilizes the UDA membranes more than the UDOH moiety. Overall, the tertiary system was found to be more stable in the presence of all the three conditions, when they were applied sequentially.

2.6 References

1. Segré, Daniel, et al. "The lipid world." *Origins of Life and Evolution of the Biosphere* 31.1 (2001): 119-145.

2. Monnard, Pierre-Alain, and Peter Walde. "Current ideas about prebiological compartmentalization." *Life* 5.2 (2015): 1239-1263.

3. Mansy, Sheref S. "Model protocells from single-chain lipids." *International journal of molecular sciences* 10.3 (2009): 835-843.

4. McCollom, Thomas M., Gilles Ritter, and Bernd RT Simoneit. "Lipid synthesis under hydrothermal conditions by Fischer-Tropsch-type reactions." *Origins of Life and Evolution of the Biosphere* 29.2 (1999): 153-166.

5. Lawless, James G., and George U. Yuen. "Quantification of monocarboxylic acids in the Murchison carbonaceous meteorite." *Nature* 282.5737 (1979): 396-398.

6. Chen, Irene A., and Peter Walde. "From self-assembled vesicles to protocells." *Cold Spring Harbor Perspectives in Biology* 2.7 (2010): a002170.

7. Namani, Trishool, and Peter Walde. "From decanoate micelles to decanoic acid/dodecylbenzenesulfonate vesicles." *Langmuir* 21.14 (2005): 6210-6219.

8. Apel, Charles L., David W. Deamer, and Michael N. Mautner. "Self-assembled vesicles of monocarboxylic acids and alcohols: conditions for stability and for the encapsulation of biopolymers." *Biochimica et Biophysica Acta (BBA)-Biomembranes* 1559.1 (2002): 1-9.

9. Maurer, Sarah Elisabeth, et al. "Chemical evolution of amphiphiles: glycerol monoacyl derivatives stabilize plausible prebiotic membranes." *Astrobiology* 9.10 (2009): 979-987.

10. Mulkidjanian, Armen Y., et al. "Origin of first cells at terrestrial, anoxic geothermal fields." *Proceedings of the National Academy of Sciences* 109.14 (2012): E821-E830.

11. Gardner, Paul M., Klaus Winzer, and Benjamin G. Davis. "Sugar synthesis in a protocellular model leads to a cell signalling response in bacteria." *Nature chemistry* 1.5 (2009): 377-383.

12. Rodriguez-Garcia, Marc, et al. "Formation of oligopeptides in high yield under simple programmable conditions." *Nature communications* 6.1 (2015): 1-7.

13. Cafferty, Brian J., et al. "Spontaneous formation and base pairing of plausible prebiotic nucleotides in water." *Nature communications* 7.1 (2016): 1-8.

14. Morigaki, Kenichi, and Peter Walde. "Fatty acid vesicles." *Current Opinion in Colloid & Interface Science* 12.2 (2007): 75-80.

15. Monnard, Pierre-Alain, et al. "Influence of ionic inorganic solutes on self-assembly and polymerization processes related to early forms of life: Implications for a prebiotic aqueous medium." *Astrobiology* 2.2 (2002): 139-152.

16. Bowman, Jessica C., et al. "Cations in charge: magnesium ions in RNA folding and catalysis." *Current opinion in structural biology* 22.3 (2012): 262.

17. Petrov, Anton S., et al. "Bidentate RNA–magnesium clamps: on the origin of the special role of magnesium in RNA folding." *Rna* 17.2 (2011): 291-297.

18. Pyle, Anna. "Metal ions in the structure and function of RNA." *JBIC Journal of Biological Inorganic Chemistry* 7.7 (2002): 679-690.

19. Chen, Irene A., Kourosh Salehi-Ashtiani, and Jack W. Szostak. "RNA catalysis in model protocell vesicles." *Journal of the American Chemical Society* 127.38 (2005): 13213-13219.

20. Mansy, Sheref S. "Membrane transport in primitive cells." *Cold Spring Harbor perspectives in biology* 2.8 (2010): a002188.

21. Monnard, Pierre-Alain, and David W. Deamer. "Preparation of vesicles from nonphospholipid amphiphiles." *Methods in enzymology*. Vol. 372. Academic Press, 2003. 133-151.

22. Lancet, Doron, Raphael Zidovetzki, and Omer Markovitch. "Systems protobiology: origin of life in lipid catalytic networks." *Journal of The Royal Society Interface* 15.144 (2018): 20180159.

23. Rendón, Adela, et al. "Model systems of precursor cellular membranes: long-chain alcohols stabilize spontaneously formed oleic acid vesicles." *Biophysical journal* 102.2 (2012): 278-286.

24. Adamala, Katarzyna P., Aaron E. Engelhart, and Jack W. Szostak. "Collaboration between primitive cell membranes and soluble catalysts." *Nature communications* 7.1 (2016): 1-7.

25. Mansy, Sheref S., et al. "Template-directed synthesis of a genetic polymer in a model protocell." *Nature* 454.7200 (2008): 122-125.

26. Mansy, Sheref S., and Jack W. Szostak. "Thermostability of model protocell membranes." *Proceedings of the National Academy of Sciences* 105.36 (2008): 13351-13355.

27. Sacerdote, M. G., and J. W. Szostak. "Semipermeable lipid bilayers exhibit diastereoselectivity favoring ribose." *Proceedings of the National Academy of Sciences* 102.17 (2005): 6004-6008.

28. Budin, Itay, Anik Debnath, and Jack W. Szostak. "Concentration-driven growth of model protocell membranes." *Journal of the American Chemical Society* 134.51 (2012): 20812-20819.

29. Jordan, Sean F., et al. "Promotion of protocell self-assembly from mixed amphiphiles at the origin of life." *Nature ecology & evolution* 3.12 (2019): 1705-1714.

30. Adamala, Katarzyna, and Jack W. Szostak. "Nonenzymatic template-directed RNA synthesis inside model protocells." *Science* 342.6162 (2013): 1098-1100.

31. O'Flaherty, Derek K., et al. "Copying of mixed-sequence RNA templates inside model protocells." *Journal of the American Chemical Society* 140.15 (2018): 5171-5178.

32. Jin, Lin, et al. "Fatty acid/phospholipid blended membranes: a potential intermediate state in protocellular evolution." *Small* 14.15 (2018): 1704077.

33. Canny, Marella D., et al. "Fast cleavage kinetics of a natural hammerhead ribozyme." *Journal of the American Chemical Society* 126.35 (2004): 10848-10849.

Chapter 3

Influence of wet-dry cycling on the self-assembly and physicochemical properties of model protocellular membrane systems.

(Adapted from, Sarkar et al. 2021; ChemSystemsChem)

3.1 Introduction

Membrane compartmentalization is considered as one of the crucial steps towards the emergence of early cellular life and is thought to be a fundamental driver for the sustenance and transition of protocellular systems.[1-4] It is fair to assume that the physicochemical properties of such protocellular membrane compartments would have been largely influenced by the early Earth environment.[5-7] Fluctuating environments on the prebiotic Earth, driven by thermal evaporation, geyser activity, rainfall etc., give rise to wet-dry cycles.[8-9] Such naturally recurring wet-dry cycles have been demonstrated to promote formation of different building blocks of life, e.g., oligoesters[10-11], oligopeptides[12-13], nucleotides[14-15] and oligonucleotides[16-18] etc. High temperature in these niches induces water loss, which tends to concentrate dilute solutions and promote thermodynamically uphill condensation reactions.[8-9] Theoretical models have suggested that the dry phase, which is diffusion limited, helps in the formation of new bonds between monomers. Upon rehydration, the molecules get redistributed and this increases the chances of collisions, thus favouring the formation of more bonds, resulting in oligomer formation.[19-20] Repeated wet-dry cycles can create a kinetic trap and result in the formation of significantly longer polymers when compared to just prolonged dry heating.[20] When subjected to drying, phospholipid vesicles transition into a gel phase. Upon complete evaporation of the aqueous medium, phospholipids are shown to result in lamellar structures, which on rehydration (wetting) can reform into vesicles.[9] However, model protocellular membranes have been hypothesized to be largely composed of mixtures of SCAs with varying head groups, isoprenoids, polycyclic aromatic hydrocarbons etc., and devoid of complex protein machineries.[6,21] Membrane systems composed of fatty acids, and mixtures of fatty acids along with long chain alcohol and/or glycerol monoesters of fatty acids, have typically been studied as model protocellular membranes.[7, 22, 23] The reason for using these amphiphiles is their plausible availability on the early Earth and their ability to readily assemble into vesicles.[24-25] Such SCA-based model membranes have previously been shown to

encapsulate small molecules and biopolymers[7, 26] in addition to facilitating prebiotically relevant reactions such as amino acid oligomerization[27], template-directed RNA replication[26, 28], localization[29] and folding of RNA molecules[30] etc. Unlike contemporary diacyl chain-based phospholipids, self-assembly of SCAs is really sensitive to changes in its surrounding environment including pH, temperature, dilution, dissolved ions etc.[6-21]

Despite the imminent relevance of wet-dry cycles on the prebiotic Earth, and its undeniable role in the formation of biopolymers, its influence on the physicochemical properties of model protocellular membranes has been largely overlooked.[31] Given this, we aimed to investigate the self-assembly, physicochemical properties and the chemical stability of model protocellular membrane systems composed of C18 chain length SCAs, under multiple wet-dry cycles. As a first step, the ability of preformed vesicles to reassemble into bilayer structures over multiple wet-dry cycles was evaluated. The influence of multiple wet-dry cycles on the physicochemical properties of the model membrane systems was also characterized using different solvatochromic probes. Upon being subjected to these cycles, amphiphiles oscillate between forming lamellae and vesicular structures, which raises an important concern about the encapsulated material that was present originally in the lumen. Thus far, studies have focused mainly on the initial encapsulation event.[7, 23, 26] Consequences of subsequent wet-dry cycles on the encapsulated material is not quite known. Therefore, we also evaluated the encapsulation efficiency of model protocell membranes in these scenarios. The results from this study confirm that the protocell membranes composed of C18 based SCAs readily reassemble into vesicles under multiple wet-dry cycles. Furthermore, in-depth characterization of the self-assembled structures reveal changes in the composition and the physicochemical properties of these model membrane systems. Multiple wet-dry cycles were found to influence properties such as vesicle size and percentage encapsulation. Moreover, the effect of multiple wet-dry cycles on the different properties of the membranes also seem to depend on the membrane composition itself. Our study also provides prefatory proof on how multiple wet-dry cycles, a prebiotically relevant geological phenomenon, would have played an important role in shaping the molecular evolution of protocellular membranes.

3.2 Materials

All amphiphiles used in this study, namely oleic acid (cis-9, $C_{18}H_{34}O_2$, 282.47 g/mol), oleyl alcohol (cis-9, $C_{18}H_{36}O$, 268.478 g/mol) and glycerol 1-monooleate (cis-9, $C_{11}H_{40}O_4$, 356.547 g/mol), were purchased from Nu-Chek-Prep (Elysian, MN, USA) and used without further purification. All other chemicals used in this study were purchased from Sigma Aldrich (Bangalore, India) and used without further purification. For all the experiments Nanopure (18 MΩ-cm) water was used.

3.3 Methods

3.3.1 Vesicle suspension preparation:

The vesicle suspensions were prepared by rehydrating thin dry film of amphiphiles with 200 mM bicine buffer whose pH was 8.6. The thin film was prepared by dissolving the desired amount of OA, OOH and GMO in chloroform, at a concentration of 10 mg/ml, followed by drying them under nitrogen gas flow. The thin film was kept under vacuum for six hours to get rid of any trace amount of chloroform. After rehydration with bicine buffer, the suspension was heated for 45 minutes at 50 °C and vortexed occasionally to suspend the thin film properly. The final concentration of the amphiphile(s) was kept at 6 mM for all the systems.

3.3.2 OA micellar suspension preparation

The OA micellar suspension was prepared by rehydrating a thin dry film OA with 200 mM NaOH solution. Following this, the suspension was heated for 45 minutes at 50 °C and vortexed occasionally to suspend the thin film properly. The final pH was set at 10 and the concentration of the OA was kept at 6 mM.

3.3.3 OA droplet suspension preparation

OA droplet suspension was prepared by decreasing the pH of the OA micellar suspension to pH 5 using HCl. The final concentration of the OA was kept at 6 mM.

3.3.4 POPC membrane preparation

The POPC membrane suspension was prepared by rehydrating a thin dry film POPC with 200 mM bicine buffer of pH 8.6. Following this, the suspension was heated for 45 minutes at 50 °C and vortexed occasionally to suspend the thin film properly. The final concentration of POPC was kept at 2 mM.

3.3.5 Epifluorescence Microscopy

To visualize the self-assembled structures, amphiphile suspensions were stained with nile red in a molar ratio of 1:1000 (nile red: amphiphile). Following this, the suspension was visualized at 40X magnification (NA=0.75) using epifluorescence microscopy (Axio Imager Z1, Carl Zeiss) and the filter for DsRed ((Ex: 558 ± 20 nm, Em: 583 ± 50 nm). Typically, 8-10 µL of the amphiphile suspension was spread on a glass slide, which was covered by an 18 × 18 mm glass coverslip. The sides of the coverslip were then sealed with paraffin after which the slide was imaged immediately.

3.3.6 Wet-Dry cycle reactions

A typical reaction was set-up by adding definite volume of the preformed 6 mM amphiphile suspension in a glass vial. Following this, the amphiphile suspension was dried under a continuous mild flow of N_2 to maintain anoxic condition on a heating block set at 90°C (RCT basic, IKA). The amphiphile suspension was dried at 90°C for one hour followed by rehydration using nanopure water which was at room temperature. After rehydration the suspension was vortexed briefly to mix it properly. This protocol was followed for multiple wet-dry cycles (as need be). At the end of different cycles, a pre-determined volume was taken out for the designated time points and subjected to further analysis. The volume of nanopure water used for rehydration was adjusted in a way to keep the amphiphile concentration constant after different cycles so as to compensate for the volume of the time points taken out.

3.3.7 Vesicle size estimation

To track changes in the average vesicle sizes resulting from the model protocell membrane systems under multiple wet-dry cycles, samples taken after different timepoints were subjected to DLS using a 633 nm red laser from Malvern instruments. In a typical reaction, 1 ml of the amphiphile suspension was taken in a polycarbonate cuvette after different wet-dry cycles (time points) and analyzed, which was followed by vesicle size estimation on a Zetasizer Nano ZS90, (Malvern Panalytical Ltd., Malvern, UK). The data reproducibility was checked by performing at least three independent measurements. The average size of the vesicle

population (Z, in nm) was then plotted against the wet-dry cycle number for the different systems.

3.3.8 Turbidity estimation

The turbidity of the amphiphile suspension was measured by taking the optical density of the suspension at 400 nm. In order to check the effect of multiple wet-dry cycles on the turbidity of the amphiphile suspension, samples after different time points were taken in a quartz cuvette and analyzed, following which the readout was taken using a UV-1800 UV-Vis Spectrophotometer (Shimadzu Scientific Instruments Inc., Columbia, USA). To follow the change in turbidity as a function of wet-dry cycles, the turbidity values obtained after different cycles was normalized to the 0th cycle and plotted against the wet-dry cycle number.

3.3.9 Steady-state fluorescence analysis using nile red, laurdan and pyrene

To discern the influence of multiple wet-dry cycles on the self-assembly of the protocellular membrane systems, different solvatochromic dyes i.e., nile red, pyrene and laurdan were used. After different cycles, the samples were collected and methanol-solution of the dye was added to them. In a typical reaction, 1.4 µl of 300 µM dye solution was added to 70 µl of the sample, to reach a final concentration of 6 µM (to maintain the dye to amphiphile molar ratio at 1:1000). This was followed by incubation for 15 minutes at room temperature to let the fluorophores get embedded in the hydrophobic environment. The fluorescence readouts were taken at 90° angle on a FluoroMax 4 (HORIBA JOBIN VYON fluorescence spectrophotometer) with 150W CW Ozone-free xenon arc lamp. The excitation and emission slit width was kept at 1 nm. Lamp intensity variations were checked and corrected if required. To avoid any contribution coming from the scattering of the self-assembled structures within the fluorescence spectrum, the emission spectra was obtained without any dye and this value was subtracted from the spectra of the test sample.

Nile red: After addition of nile red and the requisite incubation period, the test suspensions were excited at 530 nm, and the emission spectra were collected from 550 nm to 750 nm. The intensity ratio at 610 and 660 nm was used to calculate the I_{610}/I_{660} ratio.

Pyrene: After addition of pyrene and incubation, the test suspensions were excited at 335 nm, and the emission spectra were collected between 350 to 550 nm. The ratio of peak 1 at 372 nm and peak 3 at 383 nm was used to calculate the I_1/I_3 ratio. To discern if there was excimerization, the intensity ratio of 470 nm (I_{Ex}) and peak 1 at 372 nm was used.

Laurdan: In case of laurdan, after the incubation period, the test suspensions were excited at 370 nm, and the emission spectra were collected from 400 to 600 nm. The generalized polarization (GP) was calculated by using the following equation:

$$GP = \frac{(I430 - I500)}{(I430 + I500)}$$

Where, I430 and I500 represent fluorescence intensity at 430 and 500 nm, respectively,

3.3.10 Bilayer estimation using DPH

DPH partitions into the hydrophobic core of the membrane, upon which its fluorescence increases and is directly proportional to the bilayer content. In a typical reaction, 50 µl (of 6 mM) amphiphile suspensions, collected after different wet-dry cycles, were diluted by adding 100 µl of bicine buffer pH 8.6 to keep the total amphiphile concentration at 2 mM. It is pertinent to note that this is way above the critical bilayer concentration for OA (C18)-based membrane systems. 2 µl of 150 µM DPH methanol solution was added to 150 µl of the amphiphile suspension, to finally give 2 µM DPH concentration. After addition of DPH, the suspension was mixed and incubated for 20 min at room temperature to allow the partition of DPH into the membrane. After incubation, the test suspensions were transferred to a 96-well black plate and the fluorescence was measured using a plate reader (TECAN Infinite M200PRO) by exciting the samples at 350 nm and measuring the emission at 452 nm (at 50% gain).

3.3.11 Encapsulation efficiency (EF)

Calcein was used to determine the EF of the protocellular membrane systems over different wet-dry cycles. A previously published protocol was followed to determine the EF using calcein[50].In the reaction, calcein (prepared in bicine buffer, pH 8) was added to the amphiphile suspension to reach a concentration of 20 µM (way below

its self-quenching concentration). The suspension was then subjected to wet-dry cycles and samples were collected after different time points. Typically, 2 µl of 20 mM CoCl$_2$ solution was added to 100 µl of the sample, to reach a final concentration of CoCl$_2$ at 400 µM. The concentration of Co^{2+} ion was set at 400 µM as at this concentration, the Co^{2+} ion cannot induce vesicle aggregation or disruption, but is also at a much higher concentration than calcein (20 times). Calcein has a striking affinity for Co^{2+} ion. Upon binding to Co^{2+} ion, the fluorescence of calcein gets quenched. Co^{2+} ions cannot cross the membrane and go into the lumen of the vesicle. On the other hand calcein can permeate very slowly through the membrane (less than 2% of the encapsulated calcein gets released over a period of 24 hours for pure OA and OA:GMO mixed system)[51]. Addition of CoCl$_2$ to the suspensions (collected after different wet dry cycles), makes sure that only the calcein molecules which did not get encapsulated in the wet phase and are present outside the vesicles will get quenched by Co^{2+} ion. This allows one to evaluate the fluorescence signal of the (encapsulated) calcein molecules and derive the percentage EF for the various samples. The fluorescence readouts were obtained using a FluoroMax 4 instrument (HORIBA JOBIN VYON fluorescence spectrophotometer) with a 150W CW Ozone-free xenon arc lamp, by exciting the samples at 495 nm and measuring the emitted light at 515 nm. The excitation and emission slit widths were taken as 2 and 1 nm, respectively.

The encapsulation efficiency was calculated by using the following equation:

Encapsulation efficiency (%) $= 100 * \left(\frac{Fi - Fb}{Ft - Fb}\right)$

Where Ft represents the total fluorescence of the sample before adding CoCl$_2$. Fi represents the fluorescence after addition of CoCl$_2$. Fb represents the fluorescence in the absence of calcein, which also accounts for the scattering of the incident light by the vesicles. The EF at 0th cycle was subtracted from the EF of all other cycles for all the four systems for baseline correction.

3.3.12 Thin layer chromatography (TLC) analysis:

Qualitative analysis of the chemical stability of the different amphiphiles after multiple wet-dry cycles in the various reactions was carried out by running the collected samples on a normal phase silica plate (Merck). A mobile phase of Toluene:

Chloroform: Methanol, in 50:40:10 v/v, was used to separate the amphiphiles based on the difference in their polarity. After this, the TLC plates were stained using 0.05% primulin prepared in acetone: water (8:2 v/v) and visualized by using iBright FL1500 Imaging System (Invitrogen, ThermoFisher Scientific) (2X2 binning, 480 nm illumination).

3.3.13 Statistical analysis:

All statistical analysis was performed using Microsoft Excel 2016. Two-tailed t-test was used to check the significance of difference between the values within a system and also to compare between values of particular time points across systems. Values were considered statistically significant for values with $P < 0.05$.

3.4 Results

In this study, model protocellular membrane systems were constructed using oleic acid (OA), oleyl alcohol (OOH) and glycerol 1- monooleate (GMO); whose chemical structures are shown in Figure 3.1. A total of four different model membrane systems were concocted with varying composition and complexity. Only OA was used to construct the pure OA system. The two binary mixed systems were prepared by mixing OA either with GMO or OOH in 2:1 ratio. The tertiary mixed system was prepared by mixing all the three components together (OA:OOH:GMO system) in 4:1:1 ratio. Vesicle suspension for all the four mixed systems was prepared using 0.2 M bicine buffer of pH 8.6. Wet-dry cycles were carried out till 12 cycles (see methods section). Samples were collected after different time points (i.e., after the following cycles: 0th, 1st, 2nd, 4th, 8th, and 12th) and subjected to further analysis. After each cycle the pH of all the suspension was measured and was found to be unaffected throughout.

3.4.1 Self-assembly of model protocellular membrane systems under multiple wet-dry cycles

The self-assembly behavior of the four different model protocellular membrane systems, with varying compositions, was investigated under multiple wet-dry cycles, using steady state fluorescence spectroscopy. To have a comprehensive understanding of the self-assembled structures, three solvatochromic dyes i.e., nile

red, laurdan and pyrene were used . Nile red is a polarity-sensitive, hydrophobic fluorophore commonly used to stain hydrophobic environments and study self-assembly of amphiphiles[32-33]. In water, the overall fluorescence intensity of nile red is lower compared to when nile red is encapsulated in hydrophobic environment such as vesicle, micelle, droplet etc. In water its emission maximum was found at 660 nm when excited at 530 nm (Figure 3.2). In the presence of hydrophobic environment such as in OA vesicles, a blue shift was observed in its emission spectrum with a maximum at 626 nm. In the presence of OA oil droplets, the emission maximum was found to be further blue shifted to 600 nm (Figure 3.3). It was observed that for all the four systems under study, the pattern of emission spectra of nile red with its emission maximum at 626 nm did not change over multiple wet-dry cycles when compared with their respective 0th cycle (i.e., before being subjected to wet-dry condition) as shown in Figure 3.4. This suggested that all the four systems were able to reassemble into vesicular structures over multiple cycles. Furthermore, the intensity ratio of 610 nm and 660 nm (I_{610}/I_{660}) was plotted to look at the self-assembled structures in more detail as the I_{610}/I_{660} ratio reflects the micropolarity of the assembly. The I_{610}/I_{660} ratio for OA micelles and droplets was found to be 1.17±0.2 and 3±0.8, respectively (Figure 3.5). As the emission of nile red is polarity sensitive, when present inside the micelle, nile red molecules would experience more water molecules because of the dynamic nature of micelles, which will lower the I_{610}/I_{660} ratio. When present in a droplet like structure, it would be buried deep in the hydrophobic region, experiencing lesser water molecules and this is reflected in its high I_{610}/I_{660} ratio. Therefore, I_{610}/I_{660} ratio can help to distinguish between different self-assembled structures such as micelles, bilayers and droplets. In the presence of all the four model membrane systems, the emission maximum of nile red was found to be at 626 nm. Moreover, the I_{610}/I_{660} ratio for all the four membrane systems was between 1.4 to 1.5 (Figure 3.5), indicating the presence of bilayer structures. For the OA, OA:GMO and OA:GMO:OOH systems, the difference between the I_{610}/I_{660} ratio after different cycles with respect to their 0th cycle, was found to be insignificant based on a two-tailed t-test.. This further confirmed that the self-assembly process of these amphiphiles had not been affected by multiple wet-dry cycles (Figure 3.6 Panel a, c and d). However, in the case of OA:OOH binary system, the I_{610}/I_{660} ratio was found to have significantly increased (p-value < 0.05) from cycle 2 onwards with respect to its 0th cycle (see Table 3.1 and Figure 3.6 Panel b). Interestingly, from

cycle 2 onwards, the nile red I_{610}/I_{660} ratio of OA:OOH system was found to be similar to that of pure OA system based on a two-tailed t-test (see Table 3.2). This indicated a change in the micropolarity of the OA:OOH binary membrane system from cycle 2 onwards. Along with nile red, laurdan was also used to characterize the self-assembled structures over multiple wet-dry cycles. As shown in Figure 3.7, in the presence of OA droplet, laurdan's emission maximum was found to be around 450 nm, which indicates the presence of non-polar (or less water-accessible) environment. In the presence of oleic acid vesicles, the emission spectrum shows a maximum at 490 nm indicating the presence of a water-accessible micro environment[34]. In the case of all the four systems, the emission maximum was found to be at 490 nm over multiple wet-dry cycles. This further confirmed the bilayer (vesicular) nature of the self-assembled structures, which remained unaffected even after multiple cycles. After different cycles, the nature of the self-assembled structures in all the four model membrane systems was also evaluated using microscopy. Nile red was used to dope the samples for better visualization (see method section). As shown in Figure 3.8, in all the four systems, vesicular structures (MLVs) were observed from 0th to 12th cycle. This validated the results and conclusions drawn from the nile red and laurdan studies.

Oleic acid (OA)

Oleyl alcohol (OOH)

Glycerol 1-monooleate (GMO)
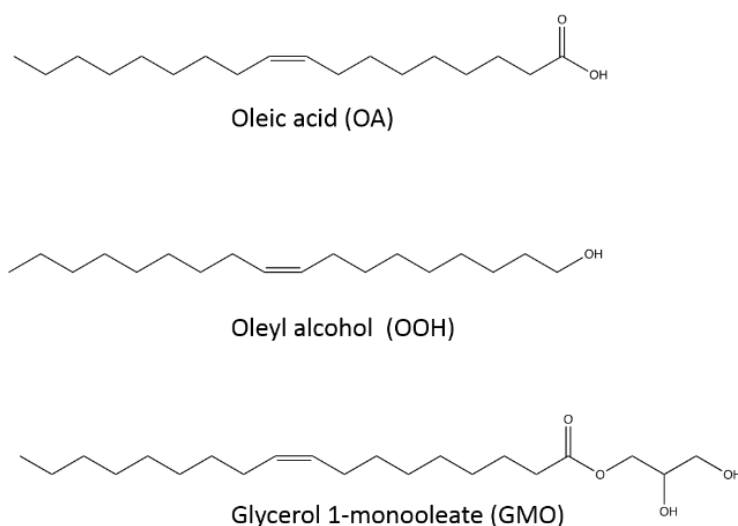
Figure 3.1: *Chemical structures of the amphiphiles OA, GMO and OOH used this study. The structures were drawn using ChemDraw professional (PerkinElmer) 20.0.*
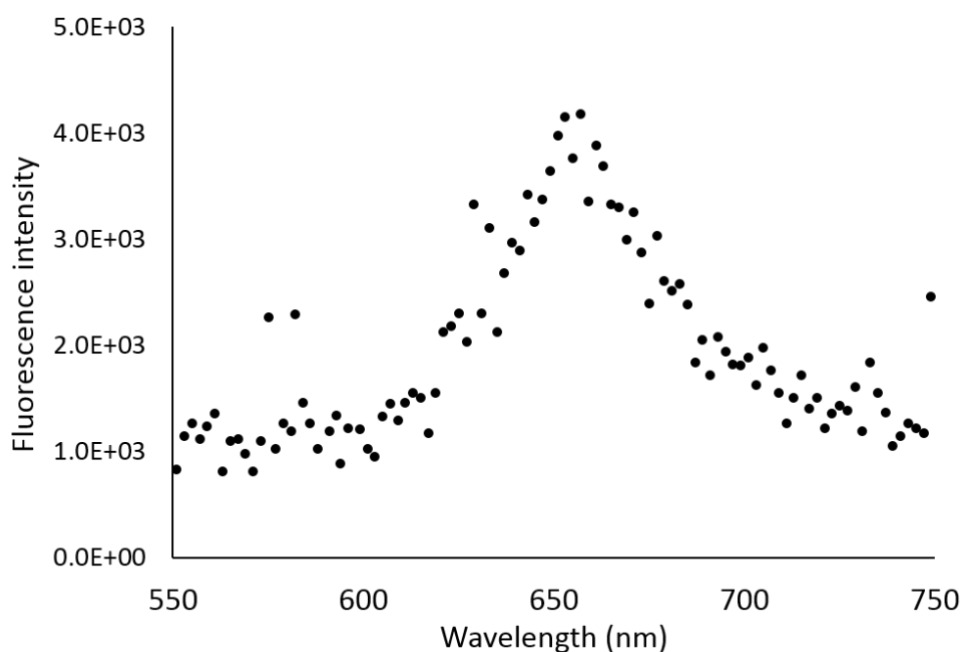
Figure 3.2: *Emission spectrum of nile red in water when excited at 530 nm (N = 4).*
Emission maximum was observed at 660 nm.

Figure 3.3: *Emission spectra of nile red in the presence of different OA-based self-*
assembled structures such as micelles, oil droplets and vesicles.
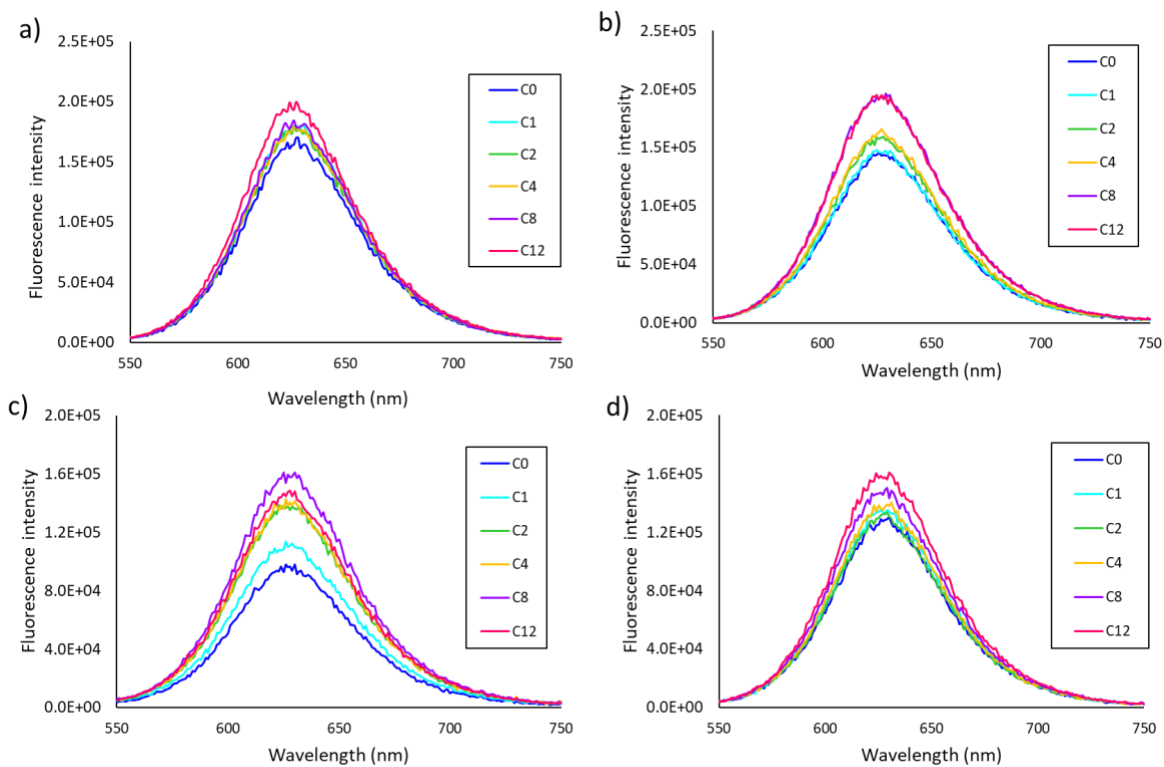
Figure 3.4: *Emission spectrum of nile red in four different membrane systems over multiple wet-dry cycles when excited at 530 nm. a, b, c and d represents only OA membrane, OA:OOH binary mixed membrane, OA:GMO mixed membrane and OA:GMO:OOH mixed membrane system. (N = 4). Emission maximum of nile red was found near 626 nm which remained unaltered over cycles.*
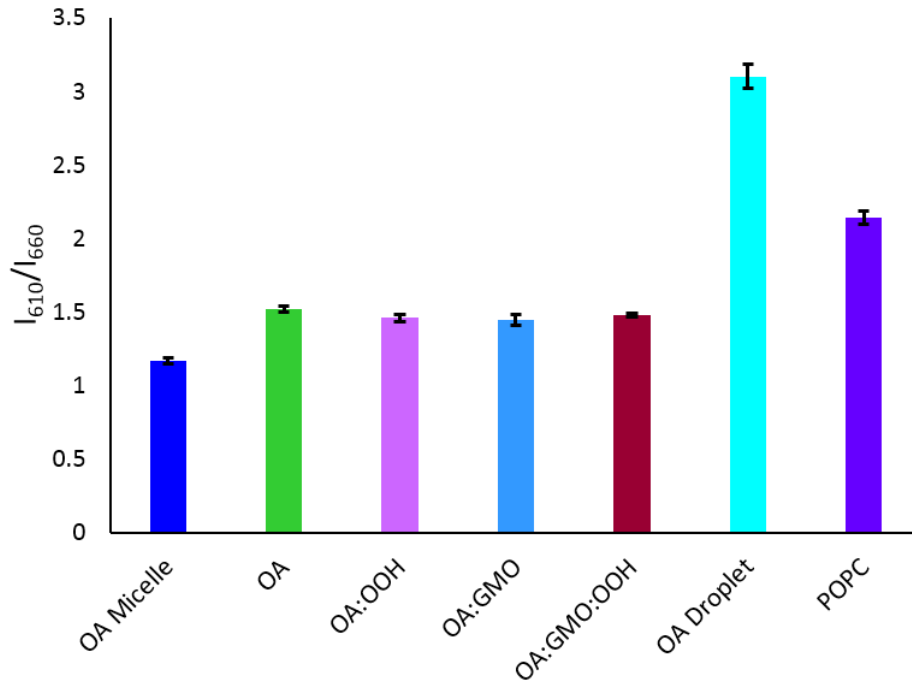
Figure 3.5: I_{610}/I_{660} ratio of nile red in presence of control samples i.e. OA micelles, OA droplets, the four model protocellular membrane systems (before subjecting to cycling conditions) and POPC membrane when excited at 530 nm. The I_{610}/I_{610} ratio was found to be significantly highest in presence of OA droplet followed by in POPC membrane and lowest in presence of OA micelles (based on a two-tailed t-test). In comparison between four model membrane system the I_{610}/I_{610} ratio value was lowest for the OA:GMO system with a p-value of <0.05 based on a two-tailed t-test. N = 4, error bar = S.D.
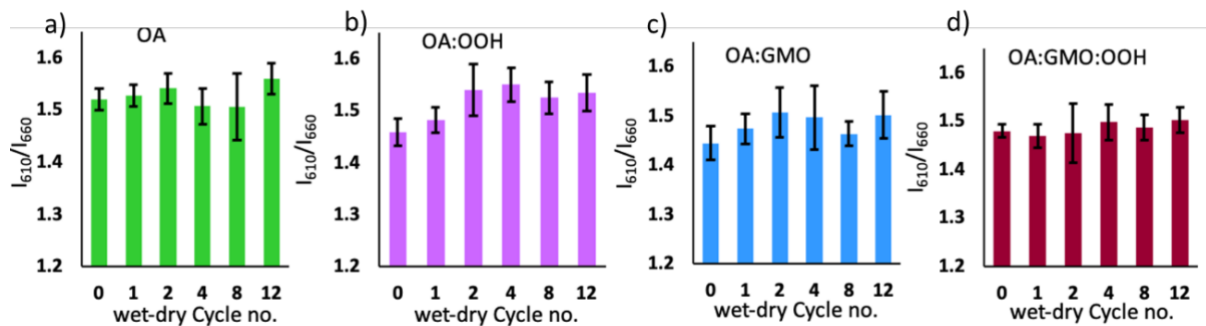
Figure 3.6: a to d represents I_{610}/I_{660} ratio of nile red in the presence of four different mixed amphiphile systems over multiple wet-dry cycles, N=4, error bar =S.D.
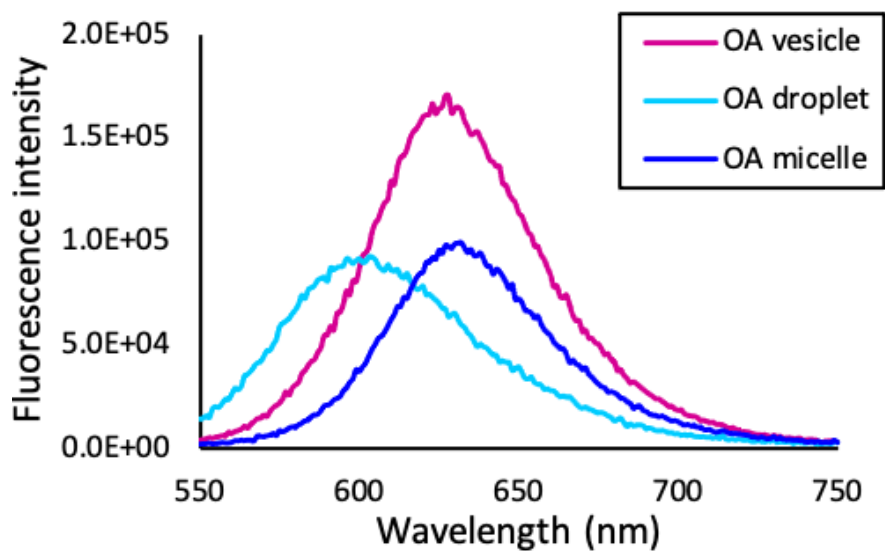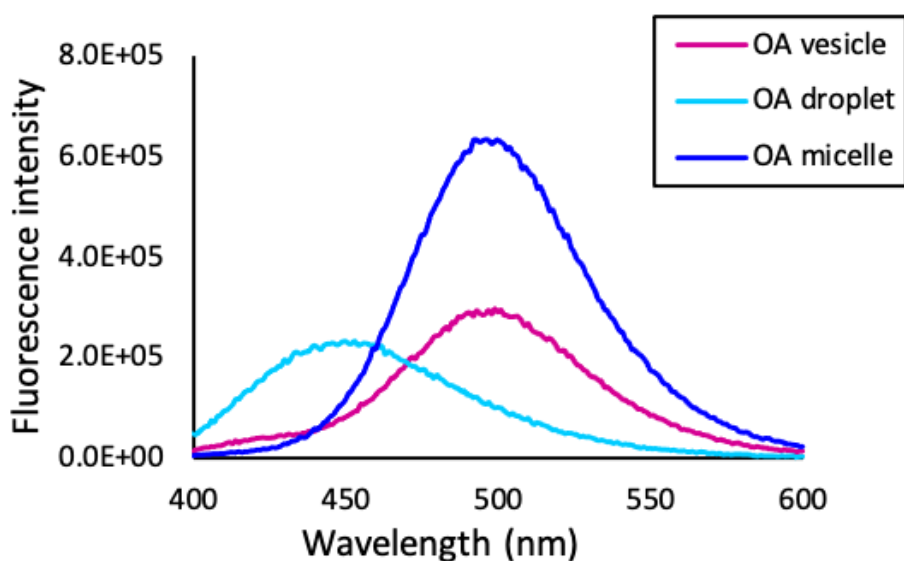
Figure 3.7: *Emission spectra of laurdan in presence of different OA-based self-assembled structures such as micelles, oil droplets and vesicles.*

Table 3.1: *Comparison of the nile red I_{610}/I_{610} ratio of different wet-dry cycles with 0th cycle using two-tailed t-test for OA:OOH mixed membrane system. N = 4.*

t-test	Nile red I_{610}/I_{660} ratio comparison over wet-dry cycles				
	OA:OOH				
	Cy0 vs Cy1	Cy0 vs Cy2	Cy0 vs Cy4	Cy0 vs Cy8	Cy0 vs Cy12
p-Value	0.243	0.027	0.004	0.017	0.013

Table 3.2: *Comparison of the nile red I_{610}/I_{610} ratio of different wet-dry cycles between OA only and OA:OOH mixed membrane systems using two-tailed t-test. N = 4.*

t-test	Nile red I_{610}/I_{660} ratio comparison between wet-dry cycles					
	OA vs OA:OOH					
	Cy0 of OA vs OA:OOH	**Cy1** of OA vs OA:OOH	**Cy2** of OA vs OA:OOH	**Cy4** of OA vs OA:OOH	**Cy8** of OA vs OA:OOH	**Cy12** of OA vs OA:OOH
p-Value	0.010	0.028	0.998	0.112	0.588	0.330
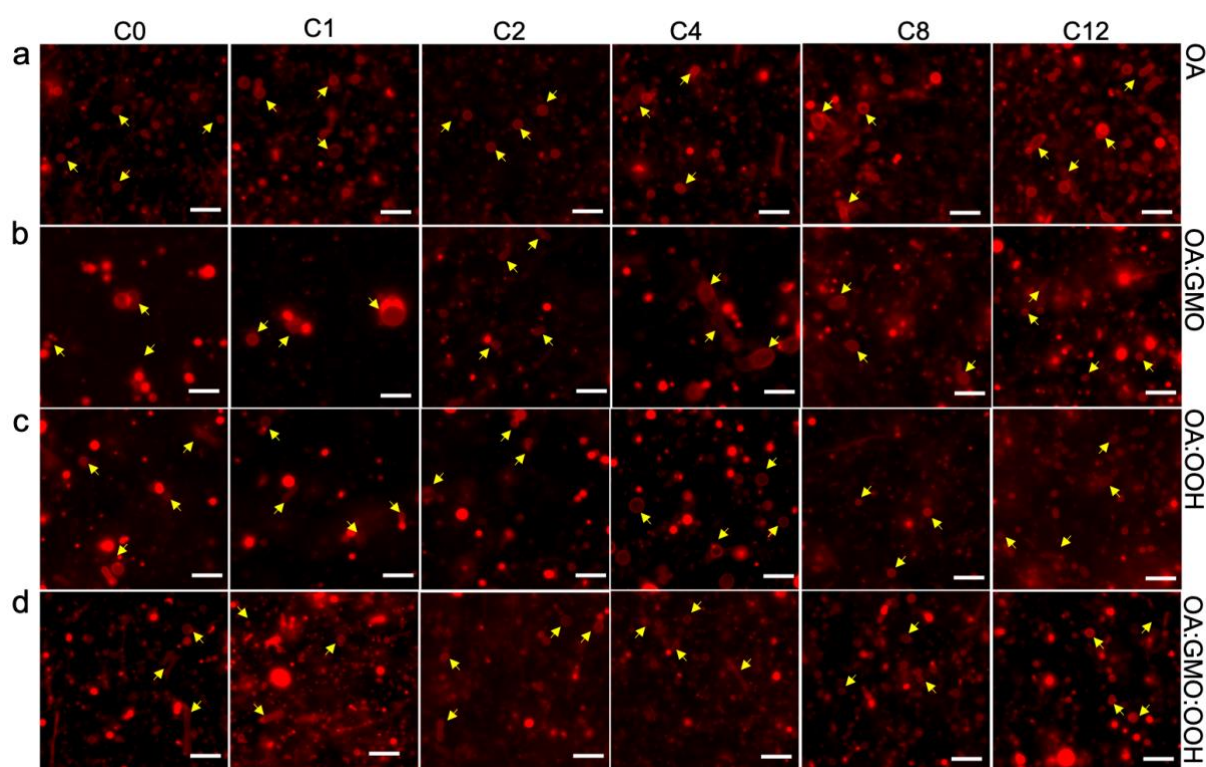
Figure 3.8. *Epifluorescence microscopy images of the four different mixed membrane systems over multiple wet-dry cycles (from cycle 0 to cycle 12) stained with nile red. Panels (a) to (d) show the four different systems, i.e., a) Pure OA system, b) OA:GMO mixed binary system, c) OA:OOH mixed binary system and d) OA:GMO:OOH mixed tertiary system. Yellow arrows indicate vesicles. N=4, Scale bar is 10 μm in all images. The self-assembled structures are pseudo-colored in red for better visualization.*

To gain a more nuanced understanding of the membrane micropolarity in the four systems, pyrene was used. When excited with a light of 350 nm, pyrene shows five characteristic emission peaks between 370 nm to 400 nm.[32, 35] While comparing the pyrene emission spectra after different cycles with their respective 0th cycle, it was found that, for pure OA, OA:GMO and OA:GMO:OOH systems, the overall pattern of emission did not change over time as shown in Figure 3.9 Panel a to c. However for OA:OOH system, an increase in the emission intensity was observed around 470 nm (Figure 3.10). The ratio of the intensities of the 1st peak (I_1) to the 3rd peak (I_3) is reflective of the polarity of pyrene's microenvironment.[32,35] The ratio is maximal when the environment is polar and this ratio decreases upon decreasing the polarity of the

environment (i.e., when pyrene gets partitioned into a hydrophobic interface). The I_1/I_3 ratio of pyrene was found to be highest in water at 1.7±0.2.. For OA based droplet and micellar systems, the I_1/I_3 was found to be 0.88±0.1 and 0.92±0.09, respectively (Figure 3.11). Therefore, we monitored the I_1/I_3 ratio of pyrene for all the four membrane systems post wet-dry cycling, and compared this for a given cycle in each system with its respective 0th cycle, to look at changes in the membrane micropolarity. For all the four model membrane systems, the I_1/I_3 was found to be between 0.86 to 0.91 (Figure 3.11). In the case of pure OA system, upon comparing the I_1/I_3 ratio of the 0th cycle with the I_1/I_3 ratio of other cycles, the difference was found to be insignificant based on a two-tailed t-test (Figure 3.12). This indicates that the membrane micropolarity did not change with increasing cycles. In the case of OA:OOH system, the I_1/I_3 ratio was found to decrease significantly from the 4th cycle onwards (Figure 3.12 and Table 3.3). For OA:GMO and OA:GMO:OOOH mixed membrane systems, the I_1/I_3 ratio remained overall unaffected over wet-dry cycling (Figure 3.12, blue and maroon trace, respectively). Interestingly, the I_1/I_3 ratio of pure OA and binary OA:OOH mixed system was found to be similar, and lower than that of the I_1/I_3 ratio of binary OA:GMO and the mixed tertiary OA:GMO:OOH systems. The higher I_1/I_3 ratio in case of OA:GMO and OA:GMO:OOH mixed membrane systems indicates a higher propensity for the water molecules to interact with the membrane in the presence of the GMO. This could stem from conical shape of GMO, which can result in packing defects on the membrane. Conversely, in the pure OA and binary OA:OOH system, the membrane is comparatively less accessible to water as reflected in the I_1/I_3 ratio. Therefore, we observed segregation of these two clusters in the plot based on the water accessibility difference in the four different membrane systems.

As the different amphiphiles used in this study vary in their head group charge, polarity and shape, upon admixing, this can potentially give rise to complex properties such as phase behavior and different water mobility on the membrane surface. This was further evaluated by calculating the laurdan generalized polarization (GP) value[34, 36, 37] to investigate the effect of wet-dry cycling on the phase properties of the membranes. Mobility of water molecules in the membrane also depends on the mobility of amphiphiles itself of the membrane.[36] As observed from the results, the binary OA:OOH mixed system possesses the lowest GP values

among all four systems (see Figure 3d). The GP value was highest for the binary OA:GMO mixed system followed by the tertiary OA:GMO:OOH mixed system (Figure 3.13). This indicates that the presence of GMO potentially hinders the movement of the neighboring lipid molecules, thus increasing the relative order in the membrane. On the other hand, in the presence of OOH, the lateral mobility of the neighboring lipid molecules increases. The probable reason behind might stem from the difference in the melting temperatures of the amphiphiles. The melting temperature of OA is 13.4°C and 16.3°C for its alpha and beta isomorphic forms In case of OOH and GMO their melting temperatures are 6°C and 35°C respectively. As all the steady-state fluorescence readouts were taken at room temperature (25°C), it is fair to assume that the presence of GMO would result in a more ordered phase, hindering the movement of the neighboring lipid molecules. When GP values after different cycles were compared with their respective 0th cycle for all the membrane systems, it was observed that for OA and OA:OOH and OA:GMO mixed systems, the GP value did not change after 12 wet-dry cycles (based on two-tailed t-test) as shown in Figure 3.13. However, for OA:GMO:OOH mixed system, the GP value significantly increased after the 8th cycle (Figure 3.13). These results allude to the possibility that with increasing wet-dry cycles in case of the OA:GMO:OOH mixed systems, the mobility of water molecules on the membrane decreases and membrane order increases. Altogether, the nile red and laurdan emission spectra, along with the microscopy analysis, demonstrates that the four systems under study are able to reassemble into bilayer (vesicles) even after multiple wet-dry cycles. However, the detailed analysis and comparison of I_{610}/I_{660} ratio of nile red indicated change in membrane micropolarity of the OA:OOH mixed system over wet-dry cycles. I_1/I_3 of pyrene further suggested segregation of membrane systems based on their micropolarity. The laurdan GP value indicated that the membrane order of the OA:GMO:OOH mixed membrane increased over cycles.
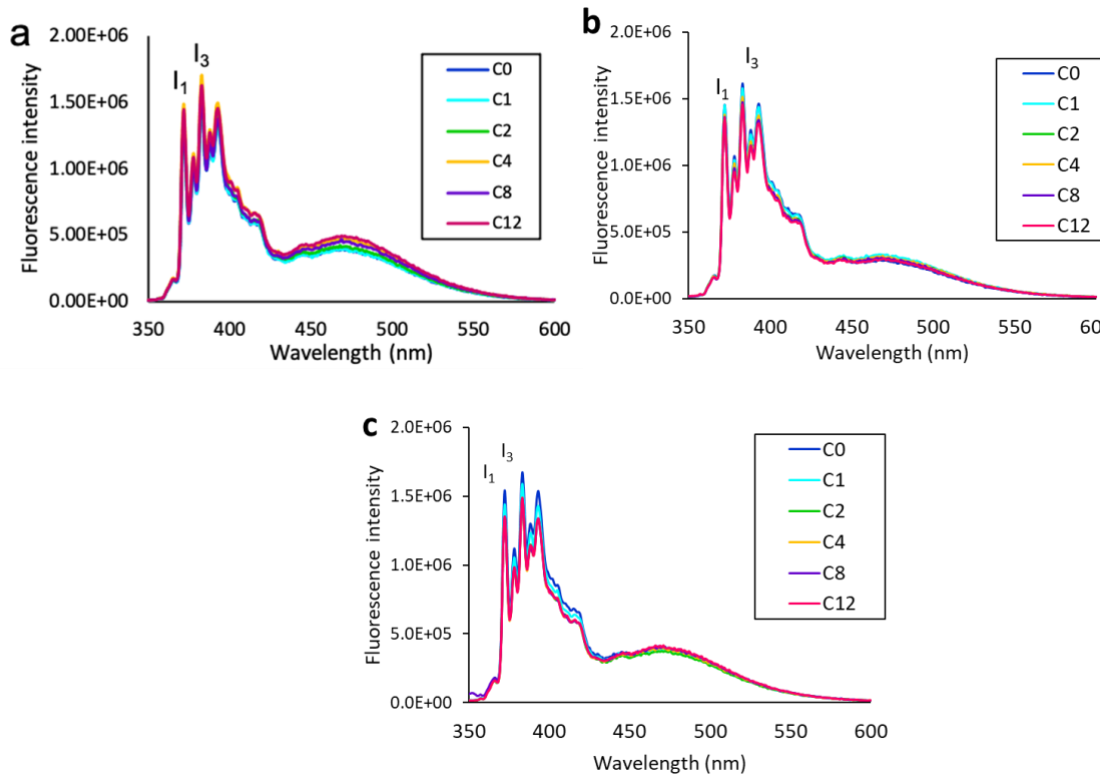
Figure 3.9: *Emission spectra of pyrene in in different membrane systems over multiple wet-dry cycles, from cycle 0 (C0) to cycle 12 (C12). I_1 and I_3 indicate peak 1 and peak 3 of pyrene emission. a) Pure OA system, b) OA:GMO mixed binary system, and c) OA:GMO:OOH mixed tertiary system. N=4, error bar =SD.*
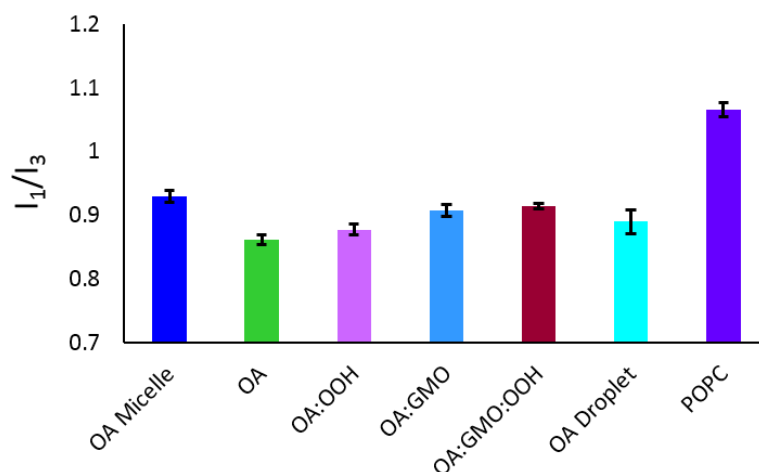
Figure 3.11: *Pyrene I_1/I_3 ratio in the presence of control samples i.e. OA micelles, OA droplets and the four model protocellular membrane systems (before subjecting to cycling conditions) when excited at 335 nm. The I_1/I_3 ratio was found to be significantly highest in presence of OA micelles (based on a two-tailed t-test). In comparison between four model membrane system the I_1/I_3 ratio was highest for the OA:GMO and OA:GMO:OOH system with a p-value of <0.05 based on a two-tailed t-test. The difference I_1/I_3 ratio between OA:GMO and OA:GMO:OOH system was found to be insignificant based on a two-tailed t-test. N = 4, error bar = S.D.*
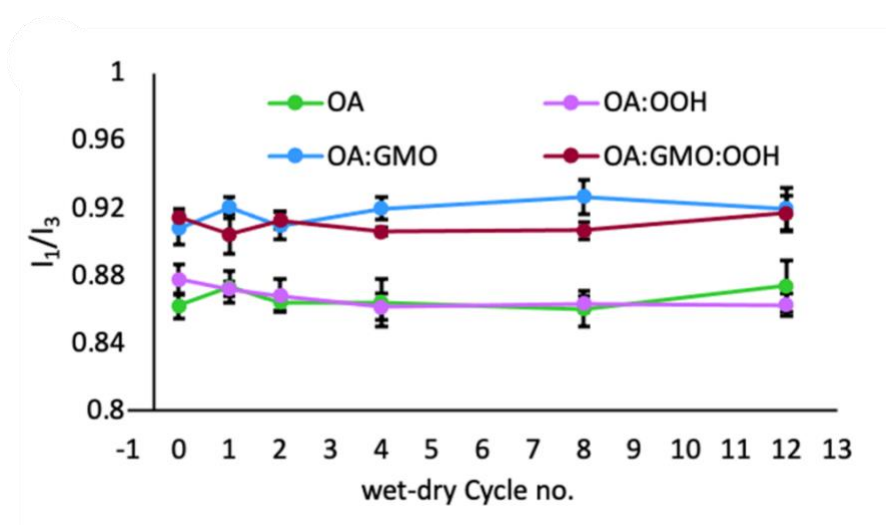
Figure 3.12: *Pyrene I_1/I_3 ratio in the presence of four different mixed amphiphile systems over multiple wet-dry cycles, N=4, error bar =SD.*
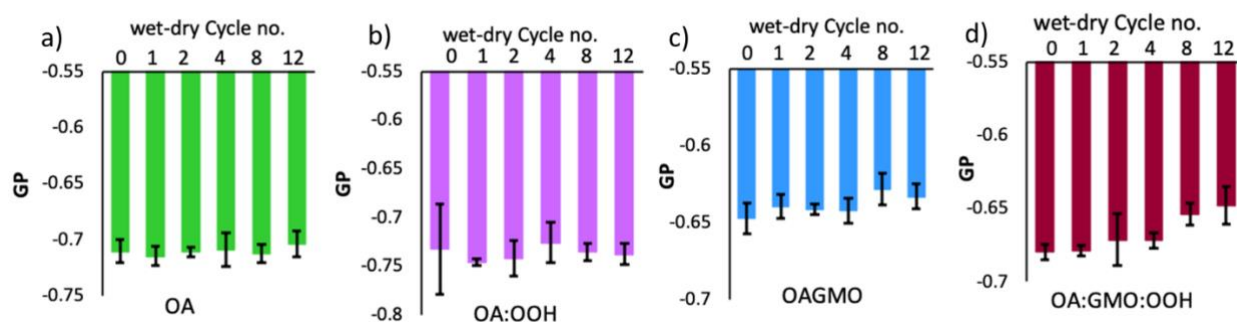
Figure 3.13: *a to d represents Laurdan GP values of four different mixed amphiphile systems over multiple wet-dry cycles, N=4, error bar =SD. a) Pure OA system, b) OA:OOH mixed binary system, c) OA:GMO mixed binary system, and d) OA:GMO:OOH mixed tertiary system. N=4, error bar =SD.*

Table 3.3 *Comparison of the pyrene I_1/I_3 ratio of different wet-dry cycles with 0th cycle using two-tailed t-test for OA:OOH mixed membrane system. N = 4.*

| t-test	Pyrene I_1/I_3 ratio comparison over wet-dry cycles				
	OA:OOH				
	Cy0 vs Cy1	Cy0 vs Cy2	Cy0 vs Cy4	Cy0 vs Cy8	Cy0 vs Cy12
p-Value	0.293	0.193	0.033	0.028	0.033

3.4.2 Stability of the amphiphiles under multiple wet-dry cycles

To characterize the potential basis of the aforementioned changes in the membrane physicochemical properties under wet-dry cycles, the chemical stability of the three amphiphiles used in the study was systematically evaluated. This is because instability of a particular amphiphile can have a net effect on the composition and, thereby, the physicochemical properties of the membrane. Towards this end, we characterized the emission spectra of pyrene in detail, as only in case of the OA:OOH mixed system we observed a drastic increase in intensity at around 470 nm over wet-dry cycling (Figure 3.10). In addition to the previously mentioned five sharp monomer vibronic peaks that occur between 370 nm and 400 nm, the emission

spectra of pyrene shows a broad peak for excimer (I_{Ex}) around 470 nm.[32, 38] To quantify excimer formation, we looked at the intensity ratio of 470 and 372 nm (I_{EX}/I_1), which reflects relative excimerization.[38, 39] Despite several existing studies pertaining to pyrene excimer formation in the membrane, detailed understanding of this process is still lacking.[38-43] Different studies have proposed different models of pyrene excimerization. Few models suggest that excimerization occurs by collision between ground-state pyrene monomer (P) and excited state pyrene (P*) monomer, and this is essentially a diffusion controlled process.[38, 41-42] Other models suggest excimer formation by pyrene aggregation in the hydrophobic core results from the static interaction between P and P* monomers when present in close proximity.[40, 43] Nonetheless, in all of the proposed models, excimerization results from interaction (close proximity) between P and P*. Steady-state pyrene fluorescence fails to provide enough evidence to comment on the mechanism of pyrene excimerization. However, from our control experiments, it was observed that the I_{EX}/I_1 ratio increased with increasing pyrene concentration when the OA (membrane) concentration was fixed (Figure 3.14). This suggested that excimerization (interaction between P and P*) increases with increasing pyrene concentration. On the other hand, when OA membrane concentration was varied while keeping the pyrene concentration fixed, the I_{EX}/I_1 ratio increased with decreasing OA concentration (Figure 3.15). Interestingly in both of the scenarios, the I_1/I_3 ratio of pyrene did not change (Figure 3.16). This further underscores that upon increasing the relative density of pyrene in the bilayer, either by increasing pyrene concentration in the suspension or by decreasing bilayer content, there is resultant excimer formation. Given this, we looked at the excimer formation (I_{EX}/I_1) for all the four membrane systems over cycles. In case of OA only and OA:GMO:OOH mixed systems, the I_{EX}/I_1 ratio (excimerization) was found to increase after 8th and 4th cycles, respectively (based on two-tailed t-test) indicating significant decrease in bilayer content occurring after these respective cycles (Figure 3.17 green and maroon trace). For OA:GMO system, no change in the I_{EX}/I_1 ratio was observed over cycles indicating no change in the bilayer content (see Figure 3.17 blue trace). However, in the case of OA:OOH system, the bilayer content decreased with increasing cycles as the I_{EX}/I_1 increased significantly just after 1st wet-dry cycle (see Figure 3.17 purple trace and Table 3.4).

To validate this observation, diphenyl hexatriene (DPH) was used (see methods section). DPH has been used in previous studies as a reporter of bilayer formation and to quantify bilayer content.[7, 44] Therefore, we used DPH to carefully monitor the change in bilayer content for all the four membrane systems over multiple cycles. In OA only membranes, the DPH fluorescence remained constant till 8th cycle but by 12th cycle the fluorescence intensity decreased. This confirms that the bilayer content reduced after 8th cycle, which supports the pyrene excimerization data (Figure 3.18). For OA:OOH system, the DPH fluorescence started to decrease drastically just after the 2nd cycle till about the 8th cycle. This indicated that the bilayer content decreased with increasing cycles, corroborating with the amount of excimer formation. In case of the OA:GMO mixed membrane system, the DPH fluorescence remained unchanged throughout confirming that the total bilayer content remained unchanged for this system over the cycling period. DPH fluorescence for the OA:GMO:OOH mixed system decreased by 8th cycle, corroborating pyrene excimerization data . This suggested that these three amphiphiles are not equally stable under wet-dry cycles. Between OA, GMO and OOH, GMO seemed stable but OOH seemed comparatively unstable under multiple wet-dry cycles. The instability under such regimes could stem from chemical degradation and/or evaporation of the amphiphile.
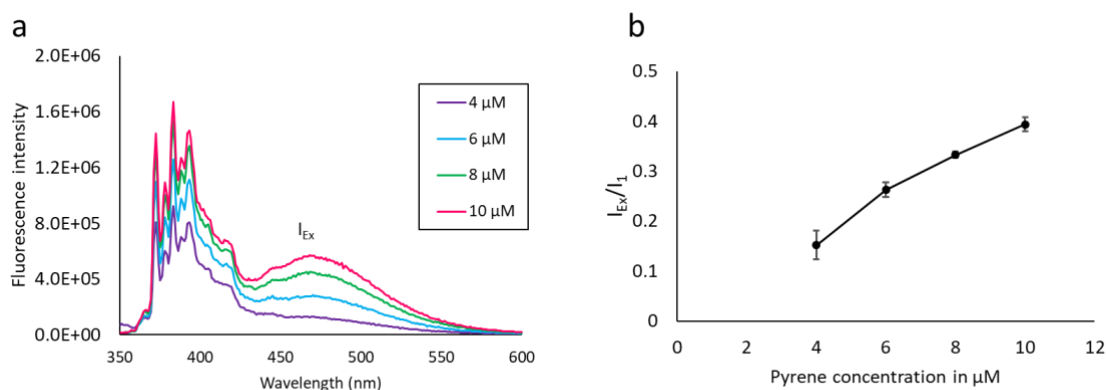
Figure 3.14: *(a) Emission spectrum of pyrene in the presence of 6 mM pure OA membrane system over varying pyrene concentration (4 µM to 10 µM) as shown in the legend. (N = 4). (b) Pyrene I_{Ex}/I_1 ratio (extent of excimarization) in 6 mM pure OA membrane system over varying pyrene concentration (4 µM to 10 µM). The I_{Ex}/I_1 ratio increases significantly with increasing pyrene concentration (based on two-tailed t-test). N = 4, error bar = S.D.*
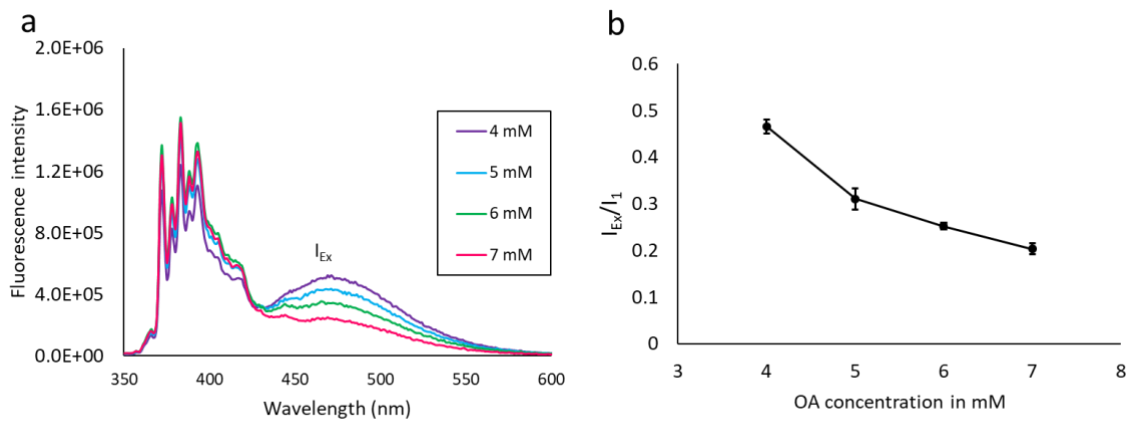
Figure 3.15: *(a) Emission spectrum of pyrene in the presence of varying concentration (4 mM to 7 mM) of OA only membrane system with fixed pyrene concentration is at 6 µM. (N = 4). (b) Pyrene I_{Ex}/I_1 ratio (extent of excimarization) over varying OA only membrane system at constant (6 µM) pyrene concentration. The I_{Ex}/I_1 ratio decreases significantly with increasing OA concentration (based on two-tailed t-test). N = 4, error bar = S.D.*
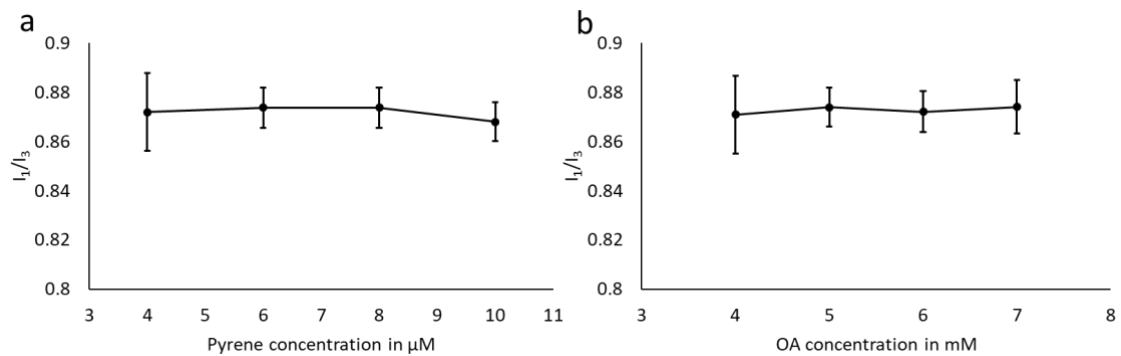
Figure 3.16: *(a) Pyrene I_1/I_3 ratio in 6 mM OA only membrane system over varying pyrene concentration (4 µM to 10 µM). The I_1/I_3 ratio remained unaltered with varying pyrene concentration (based on two-tailed t-test). (b) Pyrene I_1/I_3 ratio (extent of excimerization) over varying concentration of OA only membrane system and at a constant (6 µM) pyrene concentration. The I_1/I_3 ratio remained unaltered with varying OA concentration (based on two-tailed t-test). N = 4, error bar = S.D.*
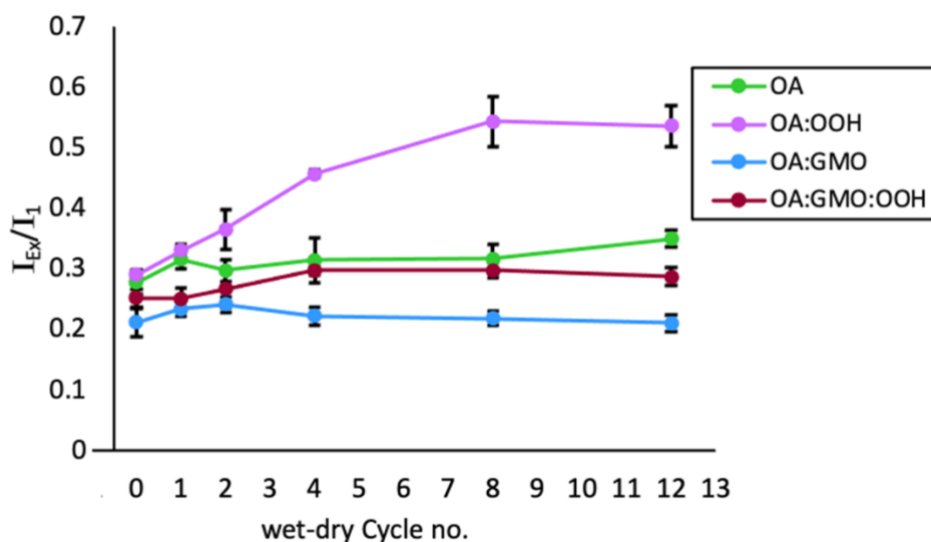
Figure 3.17: *Pyrene I_{EX}/I_1 ratio in the presence of four different mixed amphiphile systems over multiple wet-dry cycles, N=4, error bar =S.D.*

Table 3.4: *Comparison of the pyrene I_{Ex}/I_1 ratio (excimerization) of different wet-dry cycles with 0th cycle using two-tailed t-test of OA:OOH mixed membrane system. N = 4.*

t-test	Pyrene I_{EX}/I_1 ratio comparison over wet-dry cycles				
	OA:OOH				
	Cy0 vs Cy1	Cy0 vs Cy2	Cy0 vs Cy4	Cy0 vs Cy8	Cy0 vs Cy12
p-Value	4.63E-04	3.94E-03	4.06E-08	1.95E-05	7.49E-06
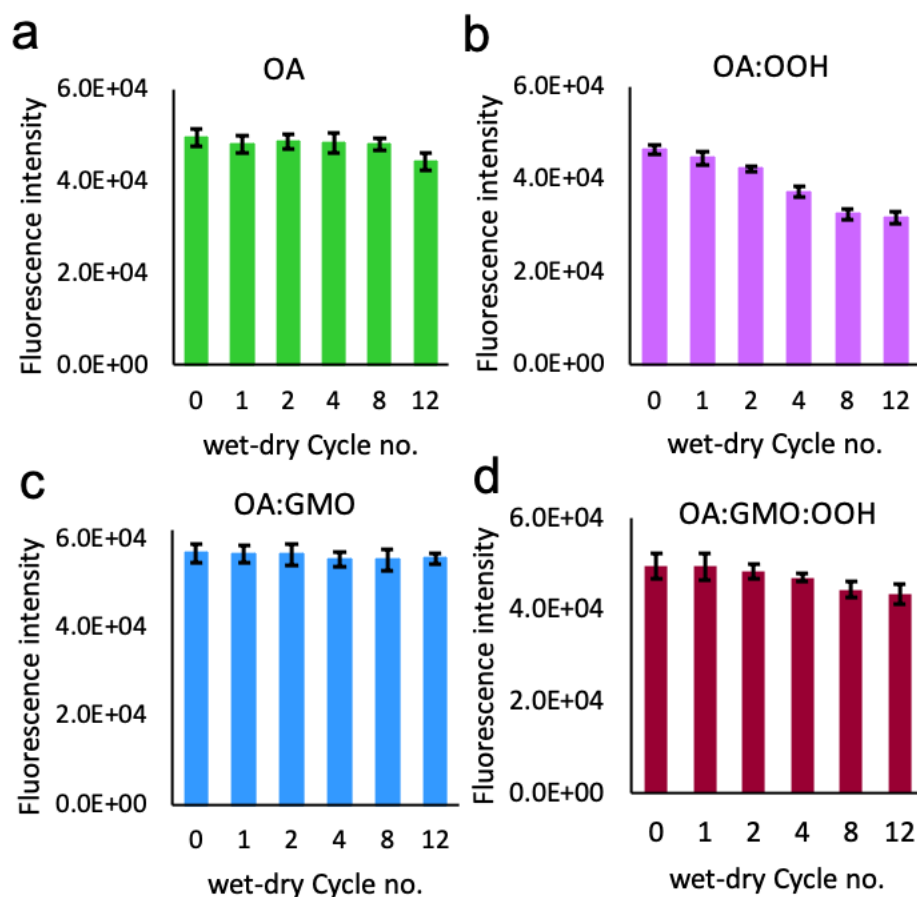
Figure 3.18. *Panels a to d show the DPH fluorescence intensity in the presence of the four mixed membrane systems over multiple wet-dry cycles, N=4, error bar =SD. a) Pure OA system, b) OA:OOH mixed binary system, c) OA:GMO mixed binary system, and d) OA:GMO:OOH mixed tertiary system.*

In order to examine the molecular stability of the SCAs, we used thin layer chromatography (TLC) . After different wet-dry cycles, amphiphile suspensions were run on a TLC plate. It was observed that in the case of the pure OA system, only one band corresponding to OA was observed throughout all cycles. The retention factor (R_f) of OA from the reaction samples matched with that obtained for OA control, and no degradation bands were observed (Figure 3.19). In the case of the OA:GMO mixed system, two bands corresponding to OA and GMO were observed. The R_f of the OA and GMO from the reaction timepoints was same as that of the OA and GMO controls, respectively. Apart from the two bands for OA and GMO, no degradation band was observed on the TLC plate (Figure 3.20). In the case of the OA:OOH system, as suspected, it was observed that the intensity of the band corresponding

to OOH reduced with increasing wet-dry cycles and diminished by the 8th cycle (Figure 3.21). Similar observations were confirmed even for the OA:GMO:OOH system as the band corresponding to OOH disappeared by the 8th cycle but the band corresponding to OA and GMO remained persistent throughout (Figure 3.22). However, no degradation bands were observed even after 12 cycles . The wet-dry cycles were carried out at 90°C and the system was under continuous flow of N_2. In a previous study by Claramonte et al. reported the chemical degradation of OOH to occur above 200°C.[45] Given this, it is fair to assume that OOH evaporated out of the system under cycling conditions. Moreover, oxidative degradation of the unsaturation that is present in all of the three amphiphiles is known to occur at high temperature in the presence of O_2 .[46, 47] As the wet-dry cycle condition used in this present study involves a temperature of 90°C and anoxic conditions, we conclude that no oxidative degradation of the amphiphiles occurred over the course of our reaction time period.

Figure 3.19: *TLC analysis of OA only membrane system over multiple wet-dry cycles, N=3. From left to right, lanes 1 to 4 represent time points obtained after different wet-dry cycles, from cycle 0 (C0) to cycle 12 (C12). Lane 5 represents OA control spot.*
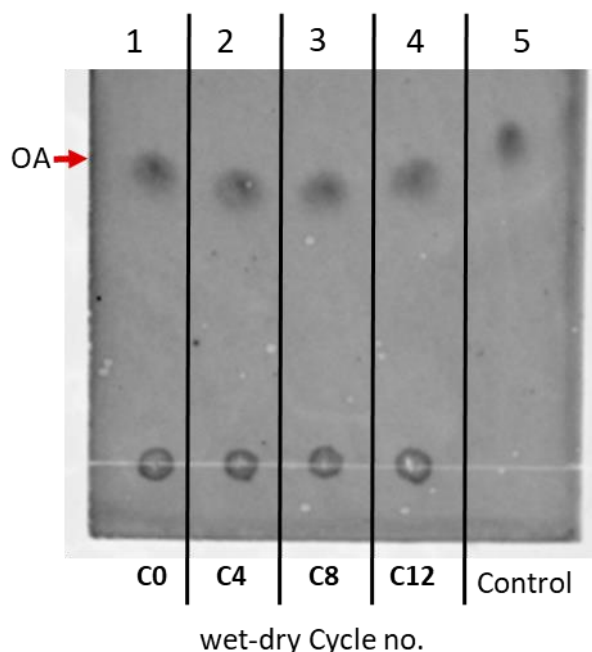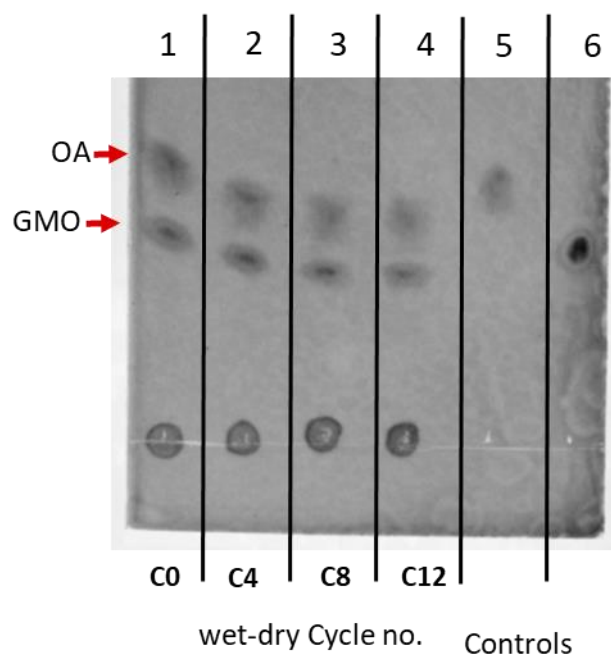
Figure 3.20: TLC analysis of OA:GMO mixed membrane system over multiple wet-dry cycles, N=3. From left to right, lanes 1 to 4 represent time points obtained after different wet-dry cycles, from cycle 0 (C0) to cycle 12 (C12). Lanes 5 and 6 represent OA control (5) and GMO control (6), respectively.
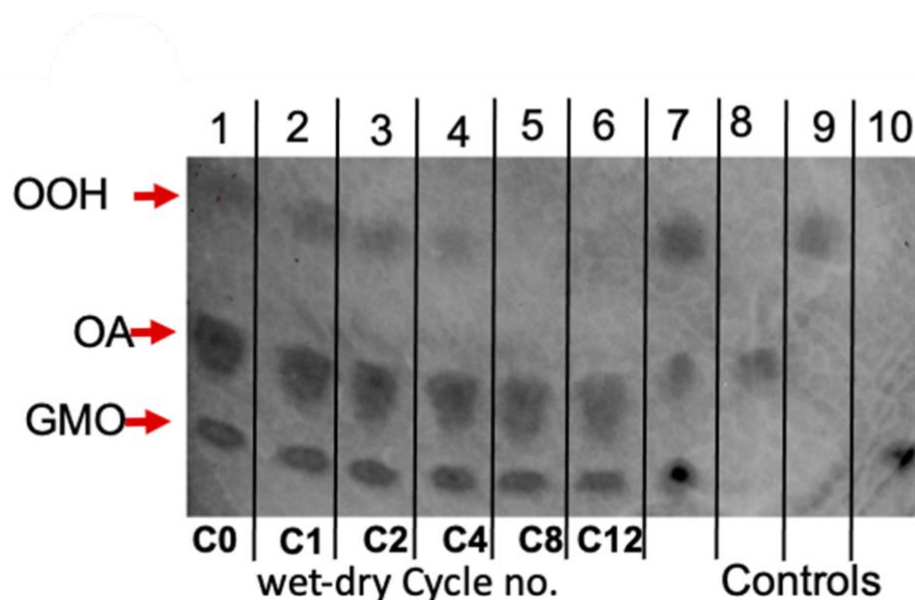
Figure 3.22: TLC analysis of OA:GMO:OOH system over multiple wet-dry cycles, N=3. (Figure S27 contains the uncropped and contrast non-adjusted version of the same TLC image). From left to right, lanes 1 to 6 represent timepoints obtained after different wet-dry cycles, from cycle 0 (C0) to cycle 12 (C12). Lanes 7 to10 represent different controls, 7) co-spot of OA, GMO and OOH, 8) OA control, 9) OOH control, 10) GMO control.

3.4.3 Influence of multiple wet-dry cycles on the physical properties of model protocell membrane systems

We aimed to understand the influence of wet-dry cycling on the physical property of the four vesicular systems by monitoring the change in turbidity. The turbidity was measured at 400 nm and normalized to the 0th cycle. In the case of pure OA and the binary mixed system of OA:OOH, the turbidity initially increased drastically and reached a steady value by the 2nd cycle as shown in Figure 3.23). For the OA:GMO:OOH mixed system, the turbidity increased faintly with increasing wet-dry cycles (Figure 3.23). However, for the OA:GMO binary system, with increasing cycles the turbidity slightly decreased (Figure 3.23). In a recent study, Wang et al. showed that the turbidity of OA suspension increases linearly with increasing vesicular lamellarity and concentration, and roughly with the logarithm of vesicle

size.[48] By using multiple approaches, we confirmed that no structural transition (such as vesicle to droplet or micelle) occurred during multiple wet-dry cycles, which might have resulted in the increase in turbidity. Moreover, no amphiphiles were added externally in between the cycles. On the other hand, the bilayer content was found to reduce in the pure OA, and the OA:GMO:OOH and OA:OOH mixed systems, under wet-dry cycling. This potentially indicates that there is a change in either membrane lamellarity and/or vesicle size, which might be affecting the turbidity of the suspension.

Towards this, we measured the change in vesicle size over multiple wet-dry cycles using dynamic light scattering (DLS) . We examined how the average size (Z) of the vesicle population changed with multiple wet-dry cycles (this was followed up to 8th cycle). When the average size (Z) was plotted for the different membrane systems against the number of wet-dry cycles, it was observed that for the pure OA system the Z value started to decrease just after the 1st cycle and remained constant from 2nd cycle onwards (Figure 3.24). For the OA:GMO and OA:GMO:OOH mixed systems, a rapid decline in the Z value was observed just after the 1st wet-dry cycle, subsequent to which it remained unaffected (Figure 3.24). However, for the OA:OOH binary system, the Z value was found to decrease after the 2nd wet-dry cycle followed by an increase in the 4th cycle and this further increased in 8th cycle (Figure 3.24). The observations indicate that, when subjected to wet-dry cycles, bigger vesicles break down into comparatively smaller vesicles in case of pure OA, OA:GMO and OA:GMO:OOH mixed systems. In case of OA:OOH system, the Z was comparatively lower even to begin with (0th cycle).

To check if wet-dry cycles always decrease the average vesicle size, we ran a control experiment using sonicated OA membrane suspension of the same concentration. Sonication is a well-known process that helps breakdown large vesicles into smaller sized ones.[49] Sonicated OA suspension was subjected to multiple wet-dry cycles and was found to show an increase in Z till the 2nd cycle, followed by a decrease soon thereafter (Figure 3.25). Overall, the findings indicate that wet-dry cycles push the average size of the vesicle population to a certain regime that depends on the size of the population to begin with. Here, the increase in turbidity in case of the OA and OA:OOH systems, with increasing wet-dry cycles, does not correlate with the change in vesicle size as the average vesicle size

decreased under wet-dry cycles. Thereby, it is reasonable to assume that the contributing factor behind the increase in turbidity observed could be because of the increase in vesicle lamellarity. It is crucial to mention here that the vesicle suspension is polydisperse and the average size estimation (Z) overlooks the presence of vesicles that are large (10 microns and above); an inherent limitation of the instrument.
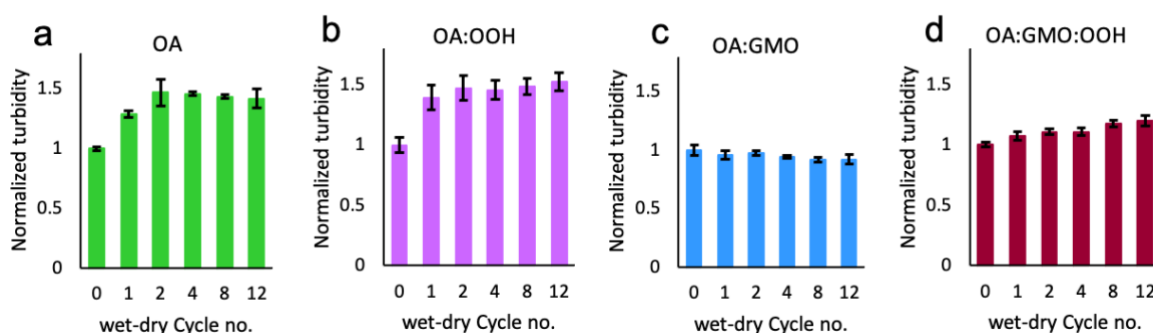
Figure 3.23. *Panels a to d show the turbidity measurements of the four mixed membrane systems under multiple wet-dry cycles at 400 nm, N=4, error bar =SD. a) Pure OA system, b) OA:OOH mixed binary system, c) OA:GMO mixed binary system, and d) OA:GMO:OOH mixed tertiary system.*
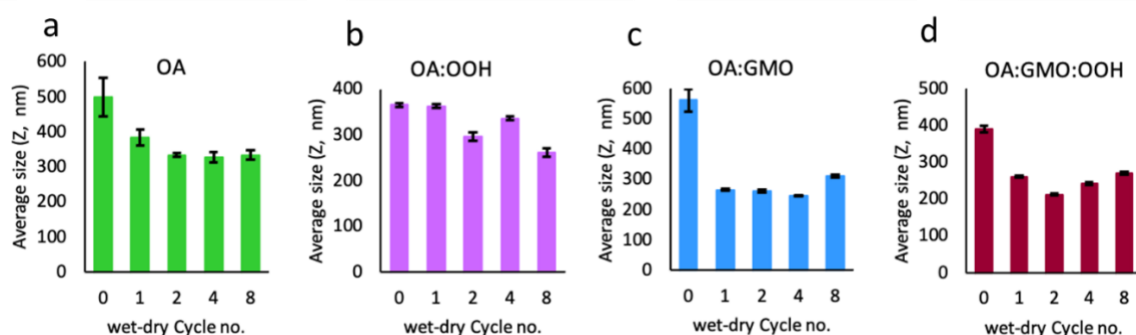
Figure 3.24: *Panels a to d shown average size of the population of four different mixed amphiphile systems plotted over different wet-dry cycles, N=3, error bar =SD. a) Pure OA system, b) OA:OOH mixed binary system, c) OA:GMO mixed binary system, and d) OA:GMO:OOH mixed tertiary system.*
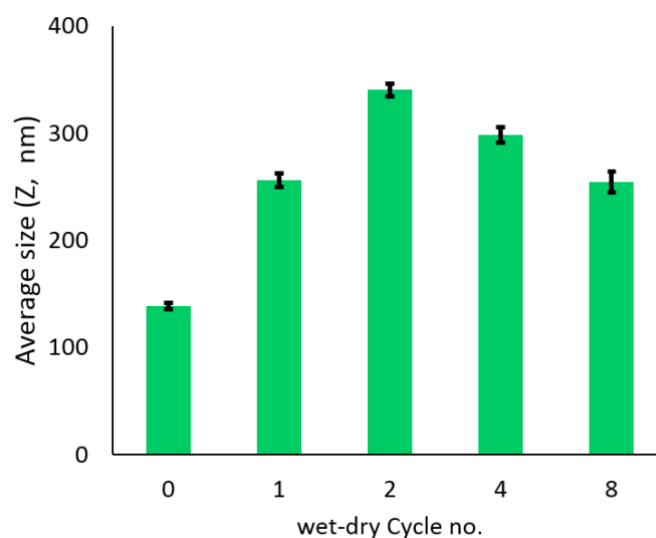
Figure 3.25: *Average size of the population of sonicated OA only membrane system plotted over different wet-dry cycles, N=3, error bar =SD.*

3.4.4 Encapsulation efficiency of model protocell membrane systems under multiple wet-dry cycles

As discussed previously, upon dehydration, the vesicles form multilamellar structures, organizing the solute molecules within a two-dimensional matrix (in-between lipid layers). Upon rehydration, when vesicles are reformed, the solutes can get encapsulated in the lumen of vesicles and in between the layers of multilamellar vesicles.[8, 9] This has implications for concentrating small molecules and redispersing them, thereby facilitating otherwise energetically uphill concentration-dependent reactions. In the present study, we looked at the influence of multiple wet-dry cycles on the encapsulation of calcein in the four different membrane systems. It was observed that in all the four systems, the encapsulation efficiency (EF) increased with increasing wet-dry cycles. For OA and OA:OOH systems, the EF was found to increase gradually with increasing cycle number (Figure 3.26). In both these cases, the EF percentage reached a steady value by the 8th cycle and remained unchanged thereafter. The EF of OA:OOH system was found to be higher than that of the OA system after the 1st cycle. As is evident from the previous results, OOH evaporated out of the system, thereby resulting in a similar EF pattern for both the OA and OA:OOH. In the case of the OA:GMO and OA:GMO:OOH mixed systems, a similar pattern was observed where a sudden increase in percentage EF was

observed by cycle 2, followed by gradual increment thereafter (Figure 3.26). This indicates that the presence of GMO helps in better encapsulation. Overall, the observations show that the EF increases with increasing cycle number when vesicles are subjected to multiple wet-dry cycles, similar to what was observed in the freeze-thaw cycles. This has direct implications for the formation of protocellular systems as this can facilitate concentrating molecular building blocks of life (nucleotides, amino acids etc.) inside the vesicular entities.
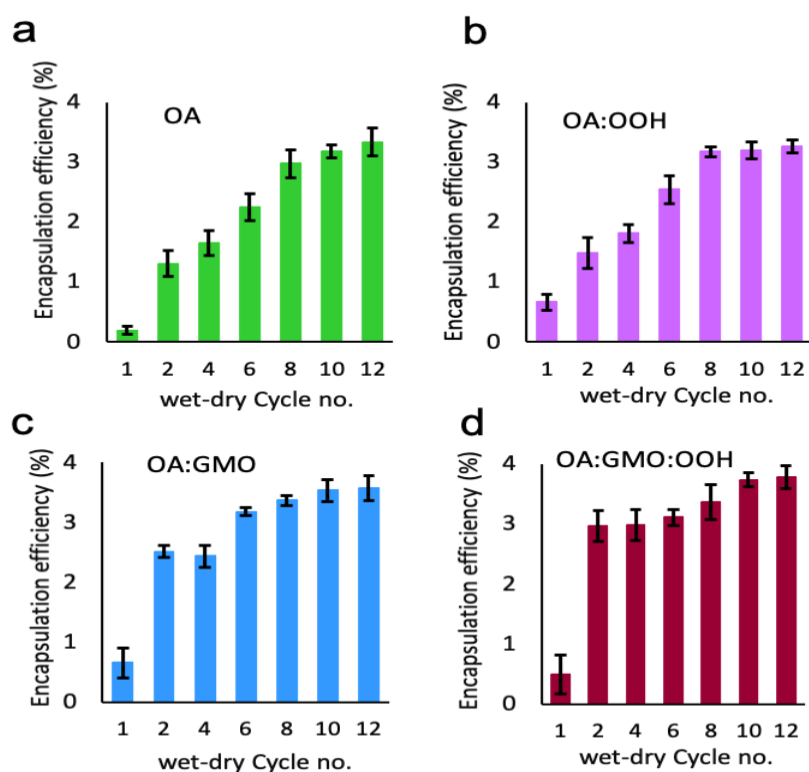
Figure 3.26: Panels a to d represent the percentage encapsulation efficiency of all the mixed membrane systems plotted over wet-dry cycles, N=4, error bar = SD. a) Pure OA system, b) OA:OOH mixed binary system, c) OA:GMO mixed binary system, and d) OA:GMO:OOH mixed tertiary system.

3.5 Conclusions and Discussions

Wet-dry cycles are thought to be common recurring events on the early Earth with fundamental implications for protocell formation.[9] In this regard, a crucial aspect of our present study was to evaluate the ability of model protocellular membrane

systems to retain their structural and compositional integrity under wet-dry cycling. We constructed model protocell membrane systems of varying compositions to understand how compositionally different systems would behave under such conditions. Towards this end, we found that the four compositionally different C18 chain length-based membrane systems of OA, OA:OOH, OA:GMO and OA:GMO:OOH, were all able to reassemble into vesicular structures under multiple wet-dry cycles. Using various solvatochromic fluorescent probes (nile red, pyrene and laurdan), we characterized the self-assembled structures to monitor changes that might result because of the wet-dry cycling process. It is reasonable to assume that the composition and physicochemical properties of protocellular membranes would have largely been governed and influenced by their environment, and the complex interactions that they would have facilitated. Previous studies from our lab and other groups, have evaluated the stability of model protocell membranes under pertinent environmental conditions. These include varying pH and dilution regimes, presence of cations, and varying temperatures; parameters that would have acted as early Earth environmental conditions that would have selected for process that survived these constraints.[5-7, 21] In the absence of such conditions, different protocellular membranes with varying compositions could coexist without undergoing much change over time. In this study, we showed how common geological events prevalent on the early Earth, such as wet-dry cycles, can govern the composition and properties of model protocellular membranes. Our results highlight the ability of wet-dry cycles to impinge on the membrane composition, thereby bringing changes in a membrane's physiochemical properties such as membrane micropolarity and phase behavior. We demonstrated that OOH gets evaporated out of the membrane system under multiple wet-dry cycles. This changes the overall membrane composition, and over multiple cycles, the OA: OOH and OA:GMO:OOH mixed systems actually change their composition to convert to pure OA and OA:GMO mixed systems, respectively. This highlights an important point, which is that model protocellular membrane systems can chemically evolve under wet-dry cycling conditions.

Our results also demonstrate that multiple wet-dry cycles can affect vesicle size distribution and turbidity of the suspension. When starting with a polydisperse population, the average vesicle size decreases with wet-dry cycles. Nonetheless, the composition of the membrane and the initial vesicle size can influence these results.

From turbidity estimation, it was observed that the change in turbidity under wet-dry cycles is largely dependent on the membrane composition. As seen in the case of OA and OA:OOH systems, the turbidity increases with increasing cycles, while in the case of OA:GMO mixed system the turbidity decreases. The change in turbidity highlights a potential change in vesicle size and lamellarity. Therefore, in future studies, it would be important to look at changes in membrane lamellarity as a function of wet-dry cycles. Previous studies have demonstrated that multiple wet-dry cycles result in the oligomerization of monomers such as nucleotides and amino acids[10-18]. When vesicles reform, the oligomers can get encapsulated within these vesicles forming protocellular entities. While characterizing the percentage encapsulation efficiency of compartments under multiple wet-dry cycles, we found that in all the four different systems, the encapsulation efficiency increases with increasing number of cycles. In conclusion, this study demonstrates that model protocellular membrane systems can not only sustain wet-dry cycling conditions, these phenomena can also bring about a change in the membrane composition and their physicochemical properties. Overall, the observations provide strong support for how model protocellular membrane systems would have been selected for by prebiotically relevant conditions detailed in here. Notably, these environmental parameters would have directly shaped the amphiphile composition thereby impinging on the emergence and chemical evolution of protocellular entities on the prebiotic Earth.

3.6 References

1. Segré, Daniel, et al. "The lipid world." *Origins of Life and Evolution of the Biosphere* 31.1 (2001): 119-145.
2. Monnard, Pierre-Alain, and Peter Walde. "Current ideas about prebiological compartmentalization." *Life* 5.2 (2015): 1239-1263.
3. Chen, I. A., and P. Walde. "Cold Spring Harbor Perspect." *Biol* 2 (2010): a002170.
4. Szostak, Jack W., David P. Bartel, and P. Luigi Luisi. "Synthesizing life." *Nature* 409.6818 (2001): 387-390.
5. Thomas, Jacquelyn A., and F. R. Rana. "The influence of environmental conditions, lipid composition, and phase behavior on the origin of cell membranes." *Origins of Life and Evolution of Biospheres* 37.3 (2007): 267-285.
6. Sarkar, Susovan, et al. "Prebiological membranes and their role in the emergence of early cellular life." *The Journal of Membrane Biology* 253.6 (2020): 589-608.

7. Sarkar, Susovan, et al. "Compositional heterogeneity confers selective advantage to model protocellular membranes during the origins of cellular life." *Scientific reports* 10.1 (2020): 1-11.

8. Damer, Bruce, and David Deamer. "Coupled phases and combinatorial selection in fluctuating hydrothermal pools: A scenario to guide experimental approaches to the origin of cellular life." *Life* 5.1 (2015): 872-887.

9. Damer, Bruce, and David Deamer. "The hot spring hypothesis for an origin of life." *Astrobiology* 20.4 (2020): 429-452.

10. Forsythe, Jay G., et al. "Ester-mediated amide bond formation driven by wet–dry cycles: A possible path to polypeptides on the prebiotic Earth." *Angewandte Chemie International Edition* 54.34 (2015): 9871-9875.

11. Mamajanov, Irena, et al. "Ester formation and hydrolysis during wet–dry cycles: generation of far-from-equilibrium polymers in a model prebiotic reaction." *Macromolecules* 47.4 (2014): 1334-1343.

12. Rodriguez-Garcia, Marc, et al. "Formation of oligopeptides in high yield under simple programmable conditions." *Nature communications* 6.1 (2015): 1-7.

13. Joshi, Manesh Prakash, Anupam A. Sawant, and Sudha Rajamani. "Spontaneous emergence of membrane-forming protoamphiphiles from a lipid–amino acid mixture under wet–dry cycles." *Chemical science* 12.8 (2021): 2970-2978.

14. Becker, Sidney, et al. "Wet-dry cycles enable the parallel origin of canonical and non-canonical nucleosides by continuous synthesis." *Nature communications* 9.1 (2018): 1-9.

15. Mungi, Chaitanya V., et al. "Synthesis of barbituric acid containing nucleotides and their implications for the origin of primitive informational polymers." *Physical Chemistry Chemical Physics* 18.30 (2016): 20144-20152.

16. Rajamani, Sudha, et al. "Lipid-assisted synthesis of RNA-like polymers from mononucleotides." *Origins of Life and Evolution of Biospheres* 38.1 (2008): 57-74.

17. Mungi, Chaitanya V., and Sudha Rajamani. "Characterization of RNA-like oligomers from lipid-assisted nonenzymatic synthesis: implications for origin of informational molecules on early earth." *Life* 5.1 (2015): 65-84.

18. Dagar, Shikha, Susovan Sarkar, and Sudha Rajamani. "Geochemical influences on nonenzymatic oligomerization of prebiotically relevant cyclic nucleotides." *RNA* 26.6 (2020): 756-769.

19. Ross, David S., and David Deamer. "Dry/wet cycling and the thermodynamics and kinetics of prebiotic polymer synthesis." *Life* 6.3 (2016): 28.

20. Higgs, Paul G. "The effect of limited diffusion and wet–dry cycling on reversible polymerization reactions: implications for prebiotic synthesis of nucleic acids." *Life* 6.2 (2016): 24.

21. Mansy, Sheref S. "Model protocells from single-chain lipids." *International journal of molecular sciences* 10.3 (2009): 835-843.

22. Apel, Charles L., David W. Deamer, and Michael N. Mautner. "Self-assembled vesicles of monocarboxylic acids and alcohols: conditions for stability and for the encapsulation of biopolymers." *Biochimica et Biophysica Acta (BBA)-Biomembranes* 1559.1 (2002): 1-9.

23. Maurer, Sarah Elisabeth, et al. "Chemical evolution of amphiphiles: glycerol monoacyl derivatives stabilize plausible prebiotic membranes." *Astrobiology* 9.10 (2009): 979-987.

24. McCollom, Thomas M., Gilles Ritter, and Bernd RT Simoneit. "Lipid synthesis under hydrothermal conditions by Fischer-Tropsch-type reactions." *Origins of Life and Evolution of the Biosphere* 29.2 (1999): 153-166.

25. Maurer, Sarah. "The impact of salts on single chain amphiphile membranes and implications for the location of the origin of life." *Life* 7.4 (2017): 44.

26. Mansy, Sheref S., et al. "Template-directed synthesis of a genetic polymer in a model protocell." *Nature* 454.7200 (2008): 122-125.

27. Murillo-Sanchez, S., and D. Beau. "ls, JMG Manas, R. Pascal and K. Ruiz-Mirazo." *Chem. Sci* 7 (2016): 3406.

28. O'Flaherty, Derek K., et al. "Copying of mixed-sequence RNA templates inside model protocells." *Journal of the American Chemical Society* 140.15 (2018): 5171-5178.

29. Izgu, Enver Cagri, et al. "N-carboxyanhydride-mediated fatty acylation of amino acids and peptides for functionalization of protocell membranes." *Journal of the American Chemical Society* 138.51 (2016): 16669-16676.

30. Wan, Fang, et al. "Aqueous rechargeable zinc/sodium vanadate batteries with enhanced performance from simultaneous insertion of dual carriers." *Nature communications* 9.1 (2018): 1-11.

31. Joshi, Manesh Prakash, et al. "Formation and stability of prebiotically relevant vesicular systems in terrestrial geothermal environments." *Life* 7.4 (2017): 51.

32. Xu, Huifang, et al. "Spontaneous vesicle formation and vesicle-to-micelle transition of sodium 2-ketooctanate in water." *Journal of colloid and interface science* 509 (2018): 265-274.

33. Molla, Mijanur Rahaman, and Suhrit Ghosh. "Hydrogen-Bonding-Mediated Vesicular Assembly of Functionalized Naphthalene–Diimide-Based Bolaamphiphile and Guest-Induced Gelation in Water." *Chemistry–A European Journal* 18.32 (2012): 9860-9869.

34. Parasassi, Tiziana, and Enrico Gratton. "Membrane lipid domains and dynamics as detected by Laurdan fluorescence." *Journal of fluorescence* 5.1 (1995): 59-69.

35. Kalyanasundaram, K., and J. K. Thomas. "Environmental effects on vibronic band intensities in pyrene monomer fluorescence and their application in studies of micellar systems." *Journal of the American Chemical Society* 99.7 (1977): 2039-2044.

36. Harris, Faith M., Katrina B. Best, and John D. Bell. "Use of laurdan fluorescence intensity and polarization to distinguish between changes in membrane fluidity and phospholipid order." *Biochimica et Biophysica Acta (BBA)-Biomembranes* 1565.1 (2002): 123-128.

37. Puff, Nicolas, et al. "Improved Characterization of Raft-Mimicking Phase-Separation Phenomena in Lipid Bilayers Using Laurdan Fluorescence with Log-Normal Multipeak Analysis." *Langmuir* 36.16 (2020): 4347-4356.

38. Barenholz, Yechezkel, et al. "Lateral Organization of Pyrene-labeled Lipids in Bilayers as Determined from the Deviation from Equilibrium between Pyrene Monomers and Excimers (∗)." *Journal of Biological Chemistry* 271.6 (1996): 3085-3090.

39. Ioffe, Valeriya, and Galyna P. Gorbenko. "Lysozyme effect on structural state of model membranes as revealed by pyrene excimerization studies." *Biophysical chemistry* 114.2-3 (2005): 199-204.

40. Blackwell, Mary F., Kleoniki Gounaris, and James Barber. "Evidence that pyrene excimer formation in membranes is not diffusion-controlled." *Biochimica et Biophysica Acta (BBA)-Biomembranes* 858.2 (1986): 221-234.

41. Birks, J. B., et al. "'Excimer'fluorescence V. Influence of solvent viscosity and temperature." *Proceedings of the Royal Society of London. Series A. Mathematical and Physical Sciences* 280.1381 (1964): 289-297.

42. Galla, Hans-Joachim, and Erich Sackmann. "Lateral diffusion in the hydrophobic region of membranes: use of pyrene excimers as optical probes." *Biochimica et Biophysica Acta (BBA)-Biomembranes* 339.1 (1974): 103-115.

43. Winnik, Francoise M. "Photophysics of preassociated pyrenes in aqueous polymer solutions and in other organized media." *Chemical reviews* 93.2 (1993): 587-614.

44. London, E., and G. W. Feigenson. "A convenient and sensitive fluorescence assay for phospholipid vesicles using diphenylhexatriene." *Analytical biochemistry* 88.1 (1978): 203-211.

45. Claramonte, MD Contreras, F. Girela Vilchez, and A. Parera Vialard. "Thermal behaviour and heat capacity of some high molecular weight alcohols and esters used in pharmaceutical preparations." *Thermochimica acta* 222.2 (1993): 209-218.

46. Abbas Ali, M., et al. "Effect of heating on oxidation stability and fatty acid composition of microwave roasted groundnut seed oil." *Journal of food science and technology* 54.13 (2017): 4335-4343.

47. Malainey, Mary E., Roman Przybylski, and Barbara L. Sherriff. "The effects of thermal and oxidative degradation on the fatty acid composition of food plants and animals of Western Canada: implications for the identification of archaeological vessel residues." *Journal of Archaeological Science* 26.1 (1999): 95-103.

48. Wang, Anna, Christopher Chan Miller, and Jack W. Szostak. "Core-shell modeling of light scattering by vesicles: Effect of size, contents, and lamellarity." *Biophysical journal* 116.4 (2019): 659-669.

49. Tenchov, B. G., et al. "A probability concept about size distributions of sonicated lipid vesicles." *Biochimica et Biophysica Acta (BBA)-Biomembranes* 816.1 (1985): 122-130.

50. Oku, Naoto, Debra A. Kendall, and Robert C. MacDonald. "A simple procedure for the determination of the trapped volume of liposomes." *Biochimica et Biophysica Acta (BBA)-Biomembranes* 691.2 (1982): 332-340.

51. Adamala, Katarzyna P., Aaron E. Engelhart, and Jack W. Szostak. "Collaboration between primitive cell membranes and soluble catalysts." *Nature communications* 7.1 (2016): 1-7.

Chapter 4

pH-responsive self-assembled compartments as tunable model protocellular membrane systems.

(Adapted from, Sarkar et al. 2022; *ChemBioChem*)

4.1 Introduction:

Semipermeable boundaries composed of amphiphiles are considered to be crucial for the emergence of cellular life on the early Earth (protocells).[1–3] Protocellular membranes are assumed to be relatively simpler and composed of SCAs.[2,3] Fatty acids (FA) have been studied extensively in this regard because of their prebiotic relevance, ability to assemble into cell-sized vesicles and the capacity to encapsulate solutes.[2–4] Unlike diacyl phospholipids (PL), FA vesicles, due to their unique dynamic nature, possess properties such as high permeability to solutes and increased fluidity, which are crucial to support the emergence and sustenance of protocells.[3–5] FAs can assemble into different structures under aqueous conditions depending upon the surrounding pH. In acidic and alkaline pH conditions, the FAs are predominantly in their protonated and deprotonated states and thus assemble into oil droplets and micellar structures, respectively.[6] FAs assemble into vesicles within a narrow pH range (approximately 7–8.5), which is close to the apparent pKa of their acid head group (negative logarithm of the acid dissociation constant).[3,6] This ability to form vesicles only in a narrow pH regime results in significant shortfalls and limits the environments that would have been suitable for the emergence of protocells.[4,7,8] Previous studies showed that certain prebiotically pertinent reactions such as RNA polymerization [9,10], nucleotide activation chemistry [11] and nonenzymatic replication [12], are all facilitated in acidic pH regimes. Also, the RNA phosphodiester backbone is most stable in the pH range 4-5.[10] On the other hand, alkaline pH [9,10] can facilitate amino acid oligomerization [13] and formose reaction.[14] This emphasizes the FA-based membranes' disadvantage to support the emergence and sustenance of protocellular life forms.

Towards this, the addition of co-surfactants like fatty alcohols and fatty acid monoglycerides has been shown to stabilize FA-based vesicles in alkaline pH regimes but not in acidic pH.[8,15] Moreover, the archean oceans are proposed to have had acidic pH.[16] This underlines the importance of exploring alternate, prebiotically plausible membrane forming SCAs. Towards this, Powner and Sutherland reported the synthesis of alkylphosphates (aliphatic chains containing phosphate head groups) from fatty alcohols under prebiotic settings.[16] Phosphates is also a major constituent of contemporary plasma membranes and genetic material backbone (DNA and RNA). Traces of short alkylphosphates have also been found in

meteorites.[17] Previous studies have reported the ability of different alkylphosphates to assemble into vesicles in narrow acidic pH (around pH 2).[18,19] Because of the low solubility of alkylphosphates under aqueous and ambient conditions (RT), these assemblies were found to be unstable. Albertsen et al. added co-surfactants with decyl phosphate to overcome this problem and looked at the vesicle forming ability of mixed decyl phosphate (C10) systems.[20] Recently, Gao M et al. investigated the vesicle formation of sodium dodecyl phosphate (C12) in neutral pH in *n*-butanol/water mixed solvent to increase its solubility.[21]

Inspired by these studies, we aimed to systematically characterize the self-assembly behaviour of mono-N-dodecyl phosphate (DDP) and discern its membrane's physicochemical properties. We explored the aggregation behaviour and vesicle formation propensity of DDP from pH 2 to 10 using microscopy, UV-vis spectroscopy and photon correlation spectroscopy. Using steady-state fluorescence spectroscopy, the different properties of DDP membranes, such as micropolarity, order (packing) and fluidity were also determined over varying pH. The effect of the addition of varying ratios of 1-dodecanol (DOH), a prebiotically plausible co-surfactant, on the self-assembly and properties of DDP-DOH membrane systems was also characterized. Our results show that DDP alone can assemble into vesicle over a wide range of pH from 2 to 10. However, the assembly process and the nature of the self-assembled structures are dependent on the surrounding pH. Interestingly, DDP membrane properties were found to be responsive to pH change owing to different protonation states of DDP molecules at a given pH. DDP membrane micropolarity and fluidity increased, with increasing pH, and the membrane packing (order) decreased with increasing pH. DOH was found to modulate the self-assembly behaviour and properties of DDP membranes when doped in varying ratios. DOH decreased the overall membrane packing and stabilized the mixed vesicles under alkaline conditions potentially by providing a H-bonding partner.

Terrestrial hydrothermal hot springs [22] and deep-sea hydrothermal vents [23] have been proposed as potential sites for the emergence of early cellular life on Earth. They both are characterized by elevated temperatures (about 50-90°C). However, the high-temperature behaviour of model protocellular membranes remains understudied as predominant studies have been carried out at ambient conditions (room temperatures).[1–6,15,20] Mansy et. al. reported thermostable membranes

composed of decanoic acid-decanol and decanoic acid-decanol-monocaprin (2:1 and 4:1:1 molar ratio, respectively) that were able to retain encapsulated oligonucleotides up to 70°C for more than 1 hour.[24] Galvanized by this, we studied the high-temperature behaviour of both DDP-based and DDP-DOH mixed membranes, at varying temperature (35°C to 65°C) and in different pH conditions. We also compared these membrane systems with other conventional FA-based membranes. The membrane packing (as indicated by GP value) was found to decrease with an increase in temperature, suggesting an increase in permeability. The degree of change of this packing parameter was dependent on the membrane composition and the surrounding pH. Apart from this change, our results also indicated morphological changes in the self-assembled structures upon an increase in temperature. Importantly, DDP molecules were also found to assemble into stable bilayers more readily at lower concentrations when compared to FA of the same chain length. On comparing the properties of DDP membranes with different PL and FA-based membranes at pH 8, DDP membranes showed similar micropolarity as PL membranes. Nonetheless, DDP membrane packing was similar to that of FA-based membranes indicating their unique dynamic nature. At pH 4, DDP membranes showed compact packing and low fluidity. The crystalline nature of these membranes at pH 4 was confirmed by the presence of sharp peaks in XRD pattern which were absent at pH 8. Pertinently, this highlighted the tunable nature of DDP membranes in response to pH and the ability of these compartments to change their property and adapt in response to changes in the immediate environment. Subsequently, we engineered novel tunable membrane systems by mixing DDP with PL, and also show that this pH-responsive tunable nature of DDP membranes can also be extended to the resultant hybrid membranes. Specifically, the addition of DDP to different PL membranes was found to change the membrane order in response to pH. Such mixed PL-DDP membrane systems with tunable nature can also be useful in synthetic biology applications and for engineering biosensors.

4.2 Materials:

All single chain amphiphiles used in this study, namely, mono-N-Dodecyl phosphate (DDP), Dodecanoic acid (LA), 1-Dodecanol (DOH), Decanoic acid (DA), Myristoleic acid (MOA) and Oleic acid (OA) were procured from Sigma Aldrich (Bangalore, India) and used without further purification. All the phospholipids used in this study,

1-palmitoyl-2-oleoyl-glycero-3-phosphocholine (POPC), 1,2-dipalmitoyl-sn-glycero-3-phosphocholine (DPPC), 1,2-dimyristoyl-sn-glycero-3-phosphocholine (DMPC), 1,2-di-dodecyl-sn-glycero-3-phosphocholine (DLPC), 1,2-di-decanoyl-sn-glycero-3-phosphocholine (DDPC) were purchased from Avanti Polar Lipids, Inc (AL 35007, United States) and used without further purification. All other chemicals used in this study were purchased from Sigma Aldrich (Bangalore, India). For all the experiments, nanopure water (with resistivity 18 MΩ-cm) was used. The chemical structures of all the amphiphiles including DDP is shown in Figure 1 along with their respective melting points.
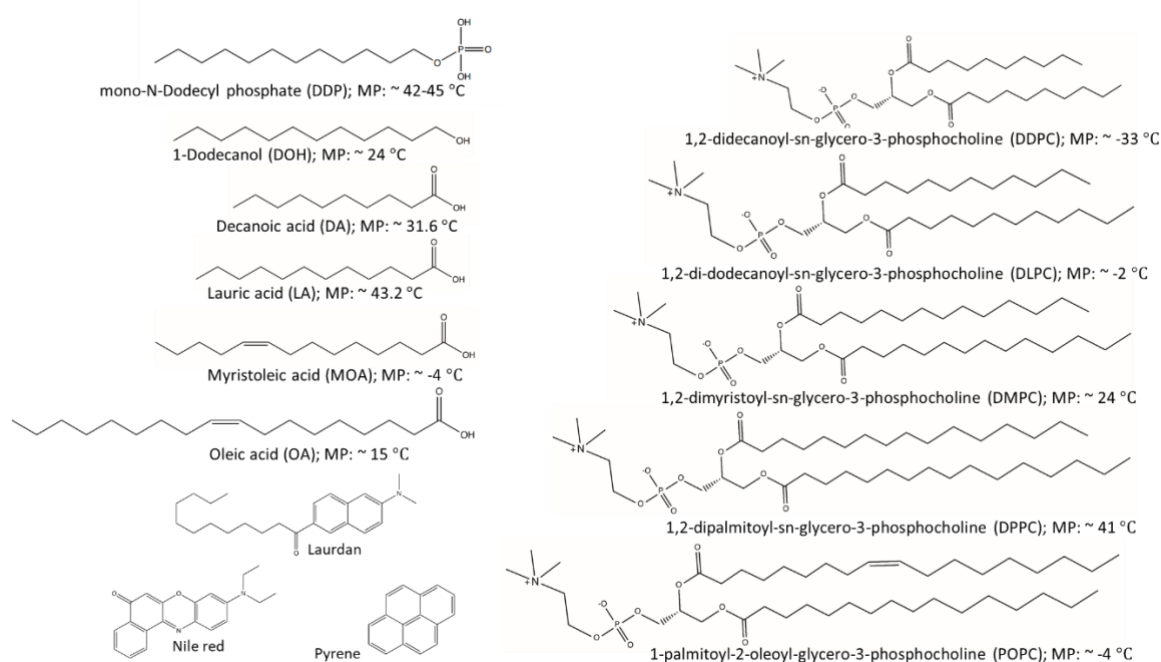

Figure 4.1: *Chemical structures of the fatty acids (DA, LA, MOA and OA), DDP, DOH and phospholipids (DDPC, DLPC, DMPC, DPPC and POPC) along with their melting points (MP), and the fluorophores (laurdan, nile red and pyrene) used in this study. The structures were drawn using ChemDraw professional (PerkinElmer) 20.0. The melting temperatures were obtained from ChemSpider.*

Pence, Harry E., and Antony Williams. "ChemSpider: an online chemical information resource." (2010): 1123-1124.

4.3 Methods:

4.3.1 Vesicle suspension preparation:

The lipid suspensions (DDP, DDP:DOH, FA and PL) were prepared by rehydrating the thin lipid dry film with a buffer of the desired pH. The lipid film was prepared by drying the desired volume of chloroform solution of the lipids under nitrogen gas flow. Any trace amount of chloroform was removed by keeping the thin film under vacuum for another six hours. After rehydration with buffer, the suspension was heated for 1 hour at 45°C and vortexed occasionally to suspend the thin film properly. For pH 2 and 3, 100 mM Glycine-HCl buffer, for pH 4 and 5 100 mM Na-acetate buffer, for pH 6, 7 and 8, 100 mM K-phosphate buffer, for pH 9 and 10, 100 mM Glycine-NaOH buffer was used, respectively, to rehydrate the lipid dry film.

4.3.2 Microscopy:

Lipid samples were observed under 40X magnification using a Differential Interference Contrast (DIC) microscope AxioImager Z1 (Carl Zeiss, Germany), (NA = 0.75) to observe the presence of various higher-order aggregates. Typically ~10 μL of the lipid suspension was spread on a glass slide, covered and sealed with a glass coverslip and observed immediately at room temperature (25°C).

4.3.3 Dynamic light scattering (DLS)

To characterize the size distribution of the self-assembled structures (vesicle), 5 mM lipid suspension (DDP and DDP:DOH) was subjected to DLS using a 633 nm red laser from Malvern instruments. In a typical reaction, 1 ml of the lipid suspension was taken in a polycarbonate cuvette and analysed by vesicle size estimation on a Zetasizer Nano ZS90, (Malvern Panalytical Ltd., Malvern, UK) at 45°C. The data reproducibility was checked by performing at least three independent measurements. The correlation function (g) was plotted over time and the data was fitted into 1st and 2nd order exponential decay graphs. The decay constants were calculated from the graphs. The size distribution was plotted as a function of % intensity of the scattered light. The average size of the vesicle population (Z) was also plotted for different pH.

4.3.4 Turbidity estimation

The turbidity of the lipid suspension was measured by taking the optical density of the suspension at 600 nm. Samples were loaded into a quartz cuvette and the turbidity was measured at 45°C using a UV-1800 UV-Vis Spectrophotometer (Shimadzu Scientific Instruments Inc., Columbia, USA).

4.3.5 Powder X-ray Diffraction

10 mM of aqueous vesicle suspension of DDP at pH 4 and pH 8, was drop-casted repeatedly on a glass slide to make a thick film. It was then air-dried, followed by vacuum drying for 24 hours at room temperature. Data was recorded on the Bruker D8 Advance X-ray diffractometer for these samples from 2° to 80°. The parameters for the same were as follows: scan speed = 0.5 second/step, increment: 0.2, rotation: 15.

4.3.6 Foamability and foam stability assay:

Glass vials (of diameter 1.2 cm and height 5 cm) containing 1 mL of DDP suspension of different pH (pH 2, 4, 6, 8 and 10) were kept in a cardboard box and the box was shaken vigorously by hand for 2 mins to generate foam. To look at the foamability of each suspension, the foam volume was measured right after the foaming process. Foam stability was characterized by measuring the volume of foam volume after different time points (2, 4 and 8 hours).

4.3.7 Steady-state fluorescence analysis using nile red, laurdan and pyrene:

The self-assembly behavior and physicochemical properties of the membranes were evaluated using solvatochromic dyes. In a typical reaction, 2 µl of 200 µM dye solution was added to 80 µl of the sample, to reach a final concentration of 5 µM (to maintain the dye to amphiphile molar ratio at 1:2000). This was followed by incubation of the suspension for 20 minutes at 45°C with shaking at 1000 rpm to let the fluorophores incorporate into the hydrophobic environment. The fluorescence readouts were taken at 90° angle on a FluoroMax 4 (HORIBA JOBIN VYON fluorescence spectrophotometer) with 150 W CW Ozone-free xenon arc lamp. The excitation and emission slit width were kept at 2 nm. For laurdan anisotropy measurements, excitation and emission slit width were kept at 4 nm. Lamp intensity variations were checked and corrected if required. To avoid any contribution coming

from the scattering of the self-assembled structures within the fluorescence spectrum, the emission spectrum of a control sample was obtained without any added dye and this value was subtracted from the spectrum of the test sample.

Nile red: After the addition of nile red and incubation for the requisite period, the test suspensions were excited at 530 nm, and the emission spectra were collected from 550 nm to 750 nm. The intensity ratio at 610 and 660 nm was used to calculate the I_{610}/I_{660} ratio.

Pyrene: After the addition of pyrene and incubation, the test suspensions were excited at 335 nm, and the emission spectra were collected between 350 to 550 nm. The ratio of peak 1 (I_1) at 372 nm and peak 3 (I_3) at 383 nm was used to calculate the I_1/I_3 ratio. To discern if there was excimerization, the intensity ratio of 470 nm (I_{Ex}) and peak 1 at 372 nm was used.

Laurdan: In the case of laurdan, after the incubation period, the test suspensions were excited at 370 nm and the emission spectra were collected from 400 to 600 nm. The generalized polarization (GP) was calculated by using the following equation:

$$GP = \frac{(I430 - I500)}{(I430 + I500)}$$

where, I430 and I500 represent fluorescence intensity at 430 and 500 nm, respectively.

For the laurdan anisotropy measurements, after the addition of laurdan and the incubation period, the test suspensions were excited at 370 nm, and the emission intensity was collected at 450 nm. The anisotropy was calculated by using the following equation:

$$\text{Anisotropy} = \frac{(I_{VV} - GI_{VH})}{(I_{VV} + 2GI_{VH})}$$

Where, I_{VV} denotes intensity with vertical excitation and vertical emission. I_{VH} denotes intensity with vertical excitation and horizontal emission. The instrument calculated the correction factor (G) for each measurement.

4.3.8 Statistical analysis:

All statistical analysis was performed using Microsoft Excel 2016. Two-tailed t-test was used to check the significance of the difference between the values within a system and also to compare between values of particular time points across systems. Values were considered statistically significant for values with $P < 0.05$.

4.4 Results

4.4.1 Self-assembly of DDP and physicochemical properties of DDP self-assembled structures at varying pH.

4.4.1.1 pH dependent self-assembly behaviour of DDP.

To understand the pH dependent self-assembly behaviour of DDP, the suspension's turbidity was measured at 600 nm from pH 2 to 10. Aggregates such as vesicles, droplets and crystalline structures would scatter more light than monomers and micellar aggregates because of their large size, leading to an increase in turbidity [15,25]. As shown in Figure 4.2 the highest turbidity (1.2±0.08) was observed in pH 2 indicating the formation of large aggregates. The turbidity then decreased moderately in a non-linear manner with increasing pH till pH 8. A sudden decrease in turbidity was observed in the alkaline pH between 9 to 10 (~0.29) indicating a structural transition and potential presence of smaller aggregates such as micelles and monomers. To understand this further we used pyrene, a solvatochromic fluorophore. Upon excitation at 335 nm, the pyrene monomer shows five vibronic peaks in the range of 370-400 nm. The intensity ratio for the first and third peak (I_1/I_3) is known to indicate the polarity of the pyrene microenvironment [26,27]. The ratio is highest in water (1.68±0.08) and it decreases upon partitioning of pyrene into hydrophobic regions. In DDP suspension, the I_1/I_3 ratio was observed to be in between 0.89 - 0.85 from pH 2 to 10, denoting the presence of hydrophobic aggregates (Figure 4.3). The ratio was highest at pH 2 (0.89) and gradually decreased with increasing pH (till pH 8) indicating a decrease in polarity. The ratio again increased significantly at pH 9 and 10, indicating structural transition corroborating with the observed decrease in turbidity.

Next, to investigate the nature of the DDP self-assembled structures at different pH, the suspensions were examined under the microscope. Large vesicles were observed from pH 2 to 10 as shown in Figure 4.4. However, at pH 2, large crystalline aggregates were also observed along with vesicles, explaining the high turbidity. From pH 3 to 10, only large micron-size oligovesicular vesicles (MLVs) were observed. At pH 8, aggregation of vesicular structures was observed that resulted in rosette-like structures (Figure 4.5). To determine the nature of the self-assembled structures in the suspension, foamability and foam stability assay were carried out at different pH (pH 2, 4, 6, 8 and 10). Foam formation and its stability in a surfactant suspension depend upon gas transfer between bubbles, the flow of liquid in the foam, and film rupture between bubbles [28]. Large assemblies such as vesicles and lamellar structures increase the local viscosity of the suspension hence, decreasing the drainage of liquid from the foam and preventing the transfer of gases between bubbles thereby, stabilizing foam [28,29]. As a result, the foam produced by suspensions containing vesicles is typically larger in volume as compared to micellar suspension [29]. This is because the smaller size of the micelles fails to increase the local viscosity of the suspension and prevent the drainage of the liquid. Further, the repulsion between deprotonated surfactants also prevents the formation of a rigid barrier at the air/water interface. In our experiments, the highest foam volume of 3.1±0.2 ml was observed at pH 6, followed by 1.6±0.3 ml of foam at pH 8, indicating that a higher amount of vesicular structures was potentially present in the suspension at pH 6 (Figure 4.6). No foam was observed at pH 10, confirming the predominance of micelles and monomers in the suspension. Low volumes of foam of 0.2±0.05 ml and 0.6±0.1 ml, were observed in pH 2 and pH 4, respectively. The foam was completely diminished at pH 2, 4 and 8 after 2 hours (Figure 4.7). At pH 6, the foam was found to be stable even after 8 hours of incubation suggesting the extent of vesicular self-assembly that was facilitated at this pH (Figure 4.8).

This behaviour of self-assembly over varying pH can be explained by factoring in the protonation state and the solubility of DDP in water. Previous studies report the pKa values of DDP to be 2.85 (pKa1) and 7.35 (pKa2) as it possesses two proton donating sites [30]. At pH 2, 87.5% of DDP molecules remain in a doubly protonated state [$C_{12}H_{25}OPO(OH)_2$] resulting in low solubility in water. With increasing pH, DDP gets gradually deprotonated hence its solubility increases. The mono-protonated

species $C_{12}H_{25}OP(OH)O_2^-$ can H-bond by themselves or with the doubly-protonated species ($C_{12}H_{25}OPO_3^{2-}$). This can result in the formation of acid-soap complex and thereby facilitating membrane formation as has been observed in the case of FAs too [6,31]. With increasing pH, the amount of mono and di-deprotonated species increases as summarized in Table 4.1. At pH 4, 93.45% and 6.5% of DDP are in the mono-protonated and doubly protonated state, respectively. 95% of DDP remains in the mono-protonated state with 5% of the di-deprotonated species at pH 6, which results in efficient H-bonding and vesicle formation. At pH 8, the mono-protonated and di-deprotonated species are present in 81% and 19% respectively, reflecting a comparatively more negative charge on the vesicle surface. More than 99% of DDP remains in the di-deprotonated state at pH 10. The presence of two negative charges on the head group would bring about repulsion between the DDP molecules hence, resulting in predominant micelle formation at pH 10.

To investigate the size of the vesicular structures at different pH, dynamic light scattering (DLS) was used. The autocorrelation functions data (g) was found to fit the double exponential model for pH 4, 6, 8 and 10 (Figure 4.9) because of the varying sizes in the suspension [32, 33]. However, the presence of large precipitating crystalline aggregates observed at pH 2, hindered the DLS measurement of this sample, hence was not considered. Upon plotting the scattering intensity as a function of particle size, we observed a bimodal distribution, with a smaller size distribution around 50 to 150 nm and a larger size distribution around 250 to 1000 nm of the self-assembled structures for pH 4, 6, 8 and 10 (Figure 4.10 Panel a). The particles with bigger size contribute more to scattering light compared to smaller size ones. In the case of pH 4 and 8, the scattering intensity contribution from the larger size population was higher as compared to the scattering intensity from that of the smaller size population, with an average size of 356±73 and 337±22 nm, respectively (Figure 4.10 Panel b). At pH 10, the average size of the population was found to be lowest at 183±17 nm, potentially because of the presence of micellar structures.
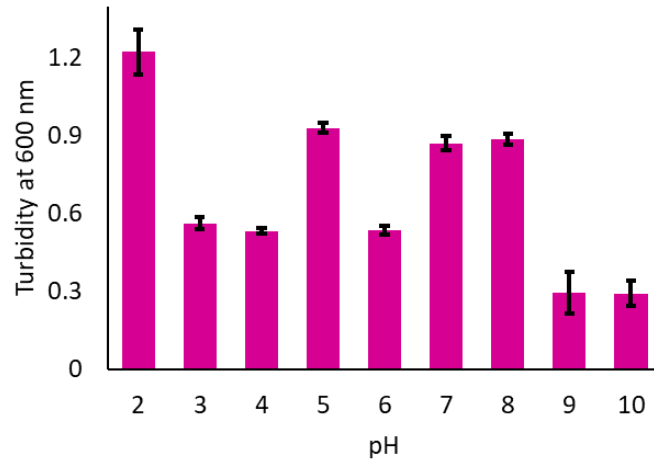
Figure 4.2: *The bar plot shows the turbidity measurements obtained at 600 nm (y-axis) for the 10 mM DDP suspension at different pH (x-axis) and 45°C, N = 3, error bar = SD*
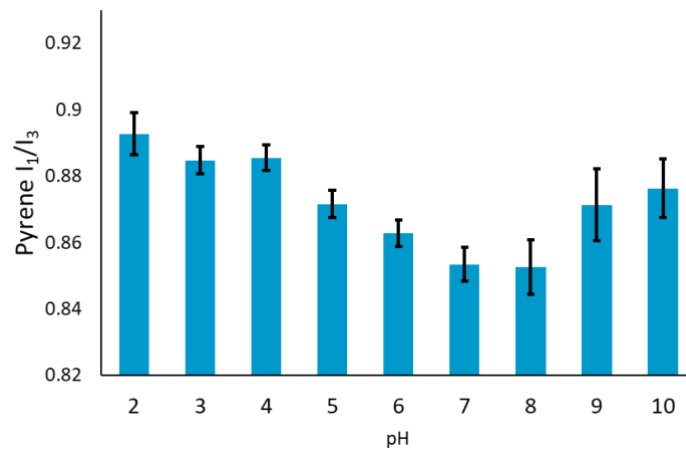

Figure 4.3: *Pyrene I_1/I_3 ratio of 10 mM DDP suspension at different pH (x-axis) at 45°C, N = 4, error bar = SD. The I_1/I_3 ratio was found to be highest at pH 2, indicating less hydrophobicity of the environment.*
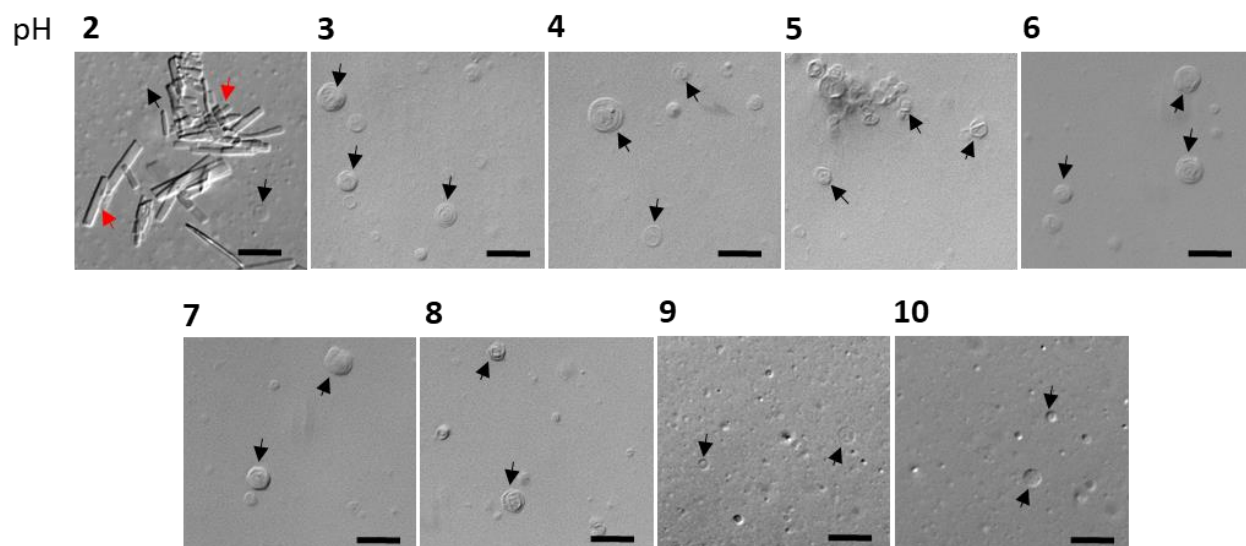
Figure 4.4: *DIC microscopy images of DDP suspension at different pH. Black and red arrows indicate vesicles and crystalline aggregates, respectively. N = 3, Scale bar = 10 μm.*
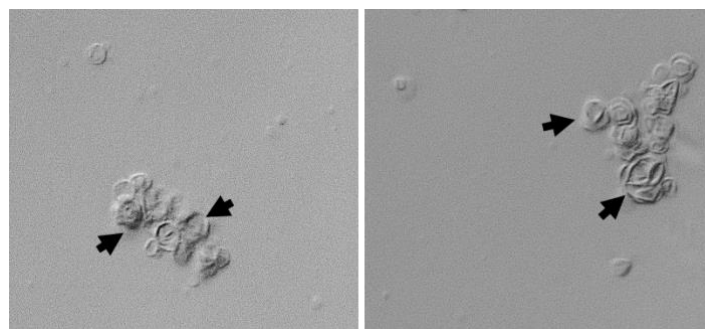
Figure 4.5: *DIC microscopy images of DDP suspension at pH 8. Black arrows indicate clumped vesicles. N = 3, Scale bar = 10 μm.*
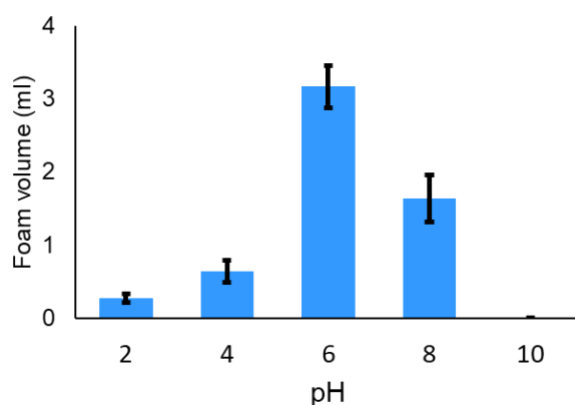
Figure 4.6: *Foam stability assay of DDP suspensions at different pH. The bar graphs show the volume (ml) of foam formed in 5 mM DDP suspension (y-axis) at different pH (x-axis). N = 3, error bar = SD.*
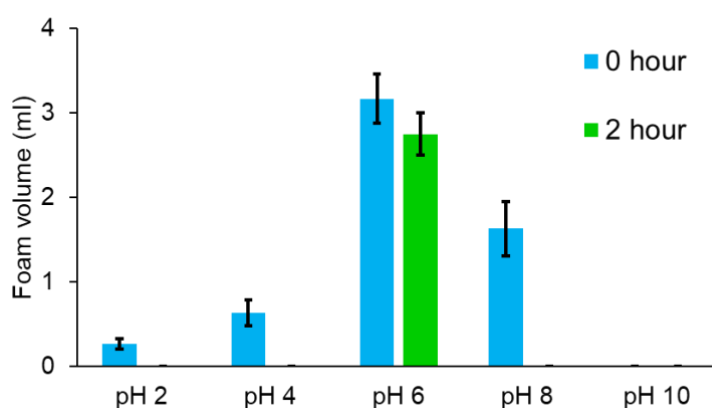
Figure 4.7: *Foam stability assay of DDP suspensions. The bar graphs show the volume (ml) of foam formed in 5 mM DDP suspension (y-axis) at different pH (x-axis) at the initiation and after two hours of incubation at room temperature. N = 3, error bar = SD.*
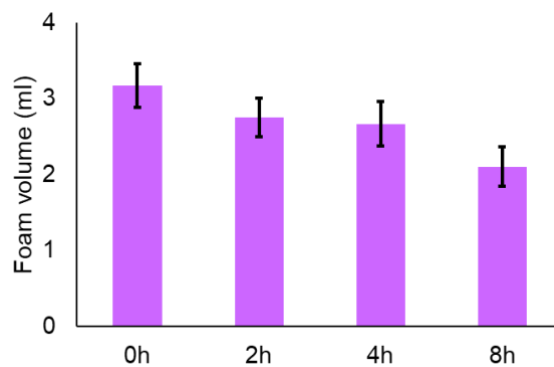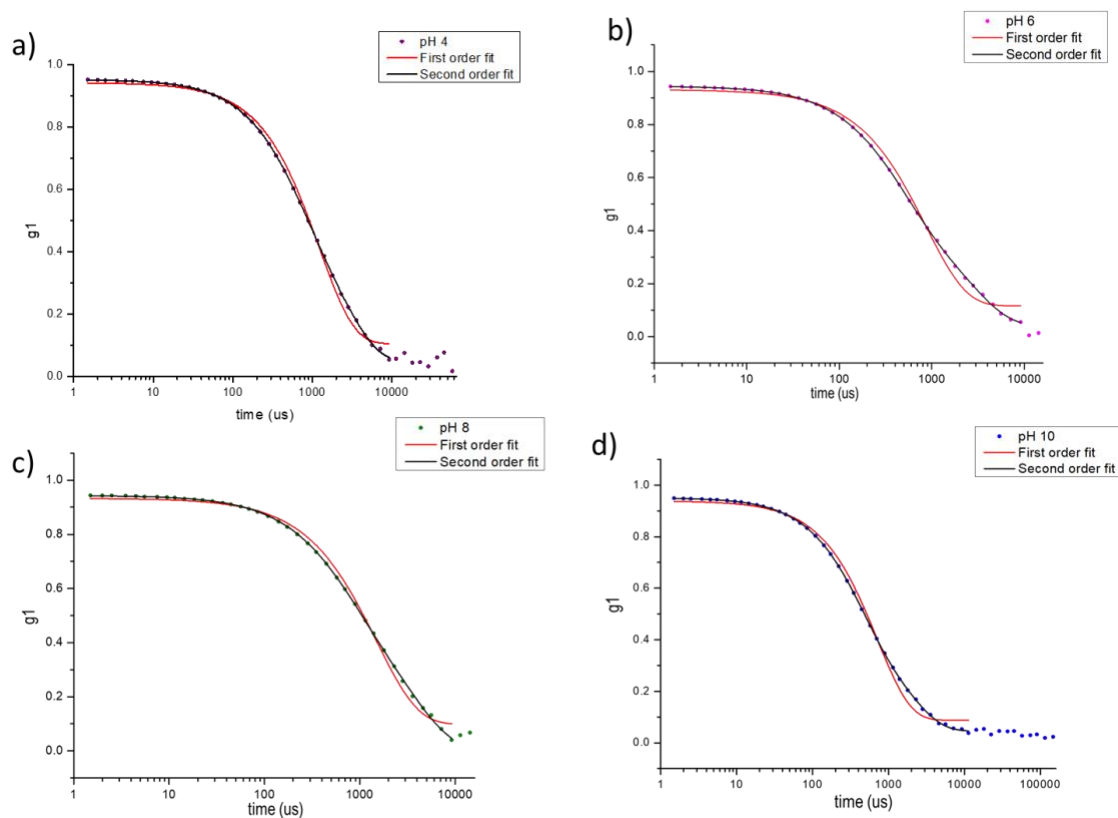
Figure 4.9: The DLS correlation function at different pH. a, b c, and d represents pH 2, 4, 8 and 10 respectively. The DLS data was fitted using both first-order exponential decay curve (red) as well as second-order exponential decay curve (black). As observed, the correlation data perfectly fit the second-order exponential decay curve for all four pH, indicating the heterogeneity in the size of self-assembled structures. N = 4.
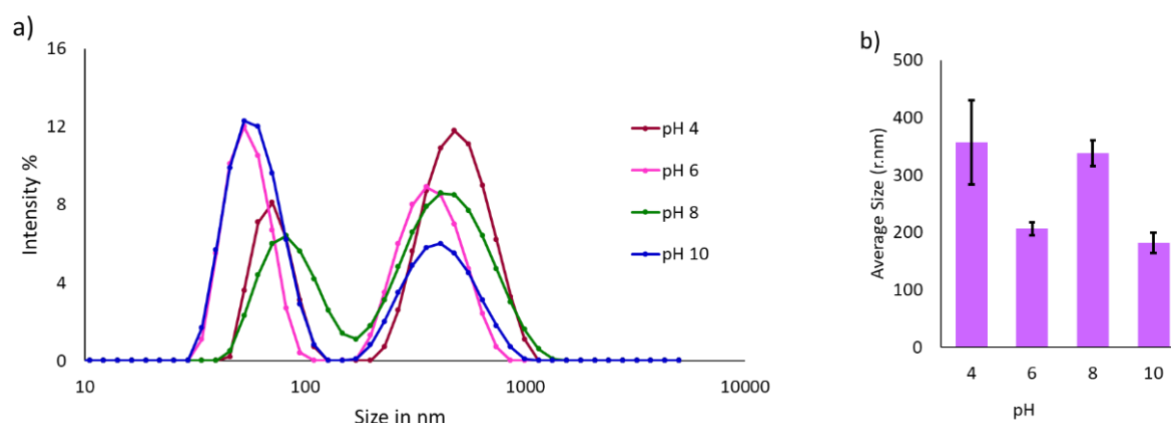
Figure 4.10: a) The scatter plot shows the size distribution of the self-assembled structures of DDP suspension at different pH plotted as a function of % intensity of scattered light at 45°C, N = 4. b) Average size (nm) of the population of DDP suspension plotted over different pH, N = 4, error bar = SD.

4.4.1.2 Physicochemical properties of DDP membrane as a function of pH

To better understand the physicochemical properties of DDP membranes, and the effect of surrounding pH on membrane properties, we used different solvatochromic probes. DDP membrane micropolarity at different pHs was measured using nile red (NR), a hydrophobic fluorophore. NR shows an emission maximum at 660 nm in bulk water (Figure 4.11). Upon incorporation into a hydrophobic environment, a blue shift is observed in its emission spectrum indicating less water accessibility [27,34]. Studies using PL membranes show that NR localizes in the interfacial region of the membranes [35]. The NR emission intensity ratio of 610 nm to 660 nm (I_{610}/I_{660}) was measured to gauge the micropolarity of the DDP membrane. Higher the ratio, lesser is the water accessibility on the membrane, thereby, indicating a decrease in micropolarity [27,34]. NR I_{610}/I_{660} was found to be lowest (0.2±0.03) in water. NR showed an emission maximum at 590 nm upon incorporation in the DDP membrane at pH 4 with the I_{610}/I_{660} ratio of 2.4±06, indicating the low micropolarity of the membrane (Figure 4.12 Panel a and b). From pH 4 to 6, the ratio decreased to 2.2±0.03 with a new emission maximum at 620 nm, indicating increased micropolarity. From pH 6 to 10, micropolarity remained unaltered with an emission maximum at 620 nm (Figure 4.12 Panel a and b). This showed that upon increasing the pH from 4 to 6, the water accessibility on the membrane increases and remains

unchanged above pH 6. However, for PL membranes (POPC), the I_{610}/I_{660} ratio was found to be constant over a range of pH (4 to 10), owing to no observable change in the POPC membrane micropolarity at different pHs (Figure 4.13 Panel a and b).

Next, laurdan was employed to investigate the order of DDP membranes at different pHs. Laurdan generalized polarization (GP) value provides a quantitative measure of the mobility of amphiphiles within a leaflet [31]. Upon incorporation into membrane containing water accessible liquid-disordered phase, laurdan shows an emission maximum near 500 nm. In contrast, when incorporated into a solid-ordered phase, laurdan shows an emission maximum near 430 nm due to the reduced accessibility of water [27,36]. Upon incorporation into DDP membranes at pH 4, laurdan emission maximum was found to be at 430 nm with a GP value of 0.69±0.01, alluding towards highly ordered membrane due to tightly packed DDP molecules (Figure 4.14 Panel a and b). At pH 6, laurdan showed two peaks, one at 430 nm corresponding to the ordered phase and the second one at 490 nm corresponding to the liquid-disordered phase with a GP value of -0.3±0.01. Upon increasing the pH to 8 and 10, the peak intensity corresponding to the ordered phase (at 430 nm) decreased, with GP values of -0.5±0.08 and -0.45±0.02, respectively. This shows that upon increasing the pH, the order (packing) of the DDP membrane decreases. The decrease in membrane order with increasing pH corroborates with increased membrane micropolarity.

To confirm that this change in membrane order with varying pH is unique to DDP, we measured the GP of two different PL membrane systems at different pHs, including POPC (melting temperature, -19°C) and DPPC (melting temperature, 42°C) (Figure 4.1), which form highly disordered and ordered membranes, respectively, at room temperature (25°C). We observed that in the case of both the PL membranes, the GP value remained unchanged at different pH, indicating no change in the membrane order over the course of the pH studied (Figure 4.15). To characterize DDP membrane fluidity as a function of pH, we then evaluated the anisotropy of laurdan. An increase in membrane fluidity will allow free tumbling of laurdan in the membrane, which would be reflected as a decrease in its anisotropy [37]. At pH 4, laurdan anisotropy in the DDP membrane was found to be 0.18±0.02 (Figure 4.16). Upon increasing the pH to 6 and 8, the anisotropy decreased to 0.12±0.02 and 0.10±0.02, respectively, after which it remained unchanged (Figure 4.16). Therefore, with increasing pH, DDP membrane fluidity increased as one would expect based on

the decrease observed in the GP values. This feature of the DDP membrane further highlights the tunable nature of these membranes as a function of pH, and this property stems from the different protonation states. This pH-responsive changes in the DDP membrane's properties underscores its adaptive nature to different environments. This has a potential functional aspect as membrane permeability is directly proportional to membrane lipid packing. Therefore, modulation in membrane properties in response to a change in pH would regulate membrane permeability thereby, the capacity for exchange of matter across the membrane boundary.
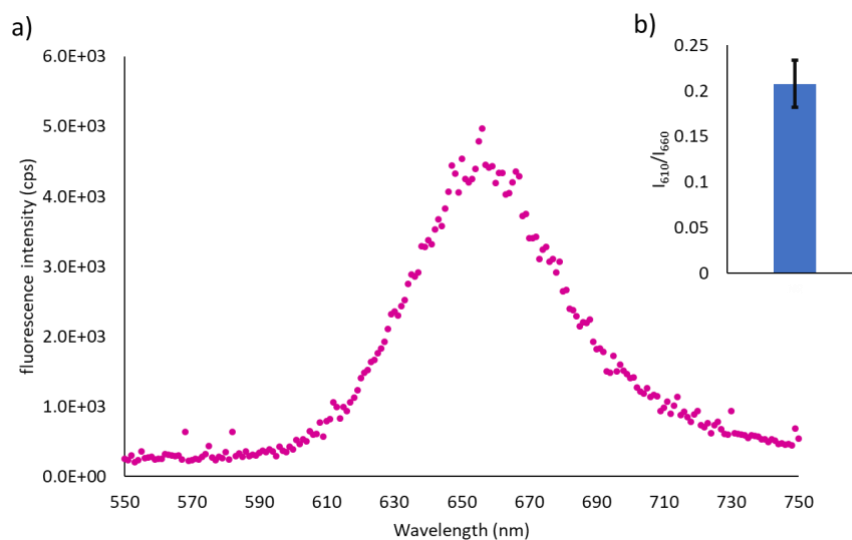
Figure 4.11: *a) Emission spectrum of nile red in water when excited at 530 nm (N = 4). Emission maximum was observed at 660 nm. b) I_{610}/I_{660} emission intensity ratio (0.2±0.02) of nile red in presence of water. N = 3, error bar = SD.*
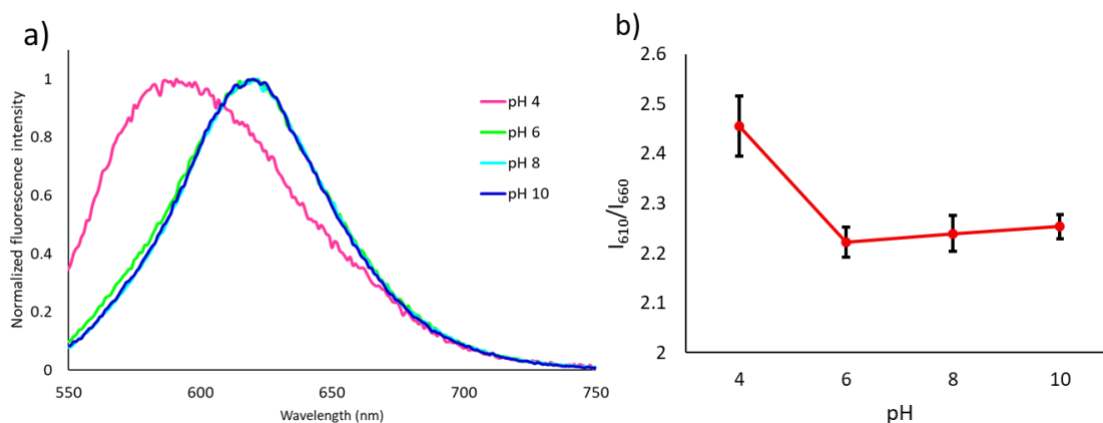
Figure 4.12: *a) Normalized emission spectra of nile red in DDP suspension over varying pH at 45°C, when excited at 530 nm. N = 4. At pH 4, the emission maximum of nile red was found to be near 590 nm, whereas at pH 6, 8 and 10, the emission maximum was near 620 nm. b) The scatter plot shows nile red I_{610}/I_{660} ratio of the DDP suspension over varying pH at 45°C, N = 4, error bar = SD.*
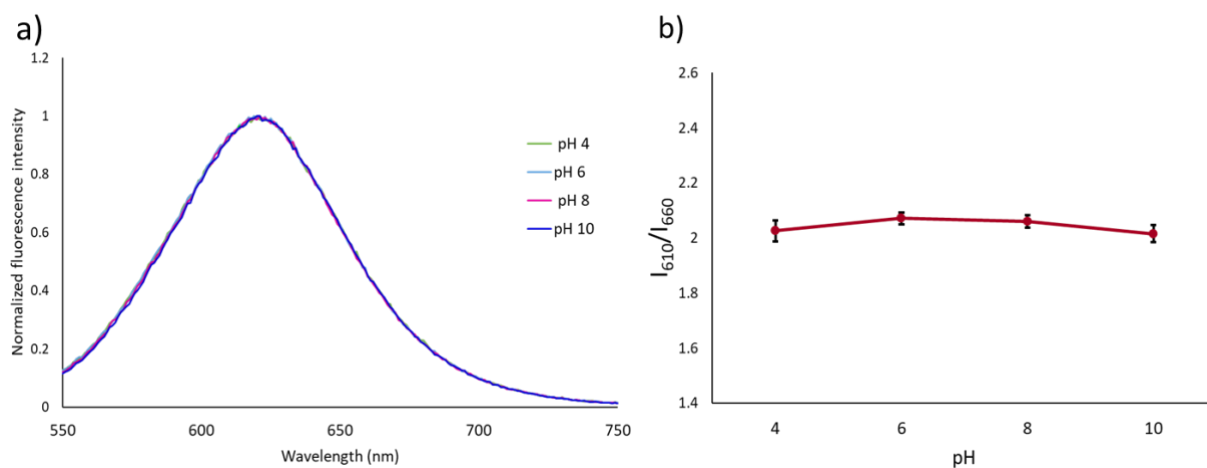

Figure 4.13: *a) Normalized emission spectra of nile red in POPC (phospholipid) vesicle suspension over varying pH at 45°C when excited at 530 nm. N = 4. At all pH, the emission maximum of nile red was found to be near 626 nm. This showed that in POPC membranes, nile red emission maximum doesn't change with a change in pH. b) The scatter plot showing nile red I_{610}/I_{660} intensity ratio of the POPC (phospholipid) vesicle suspension over varying pH at 45°C when excited at 530 nm. N = 4, error bar = SD. The I_{610}/I_{660} remained unaltered (based on a two-tailed t-test) over varying pH.*
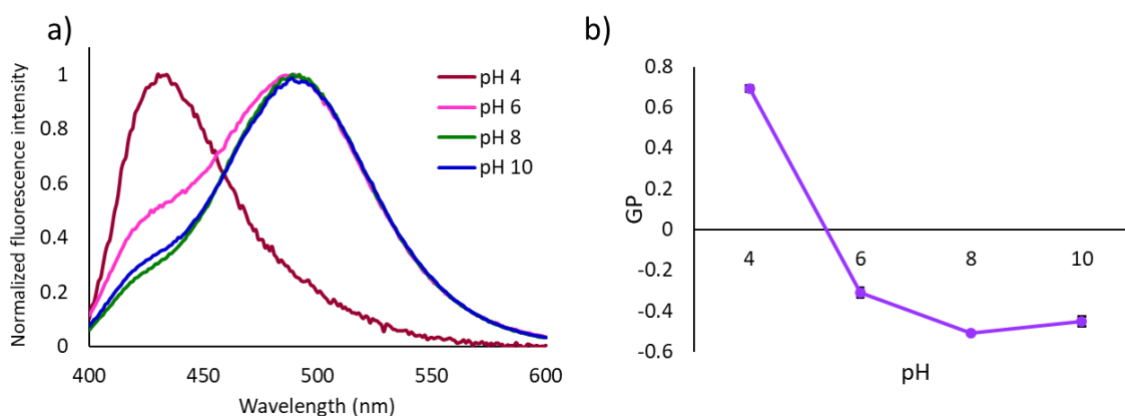

Figure 4.14: *a) Normalized emission spectra of laurdan in DDP suspension over varying pH at 45°C. At pH 4, the emission maximum of laurdan was found to be near 430 nm, whereas at pH 6, 8 and 10, the emission maximum was near 500 nm. N = 4, error bar = SD. b) The*

scatter plot shows laurdan GP values of the DDP suspension over multiple pH at 45°C , N = 4, error bar = SD.
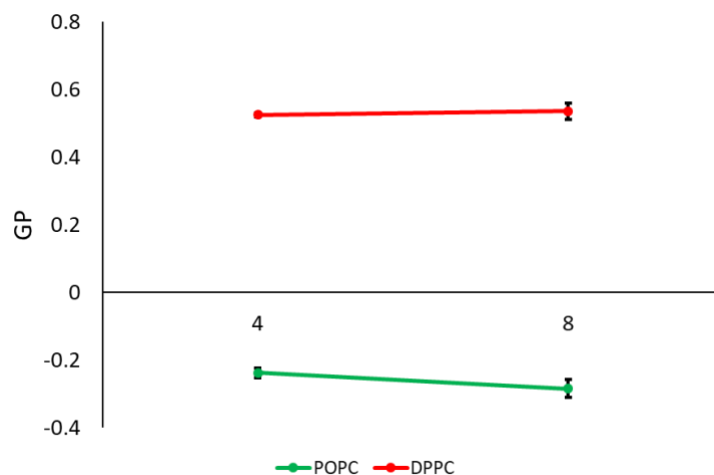

Figure 4.15: *The scatter plot showing laurdan GP values of POPC and DPPC (phospholipids) vesicle suspensions over varying pH at 45°C when excited at 530 nm. N = 4, error bar = SD. The GP value remained unaltered (based on a two-tailed t-test) between the two pHs.*
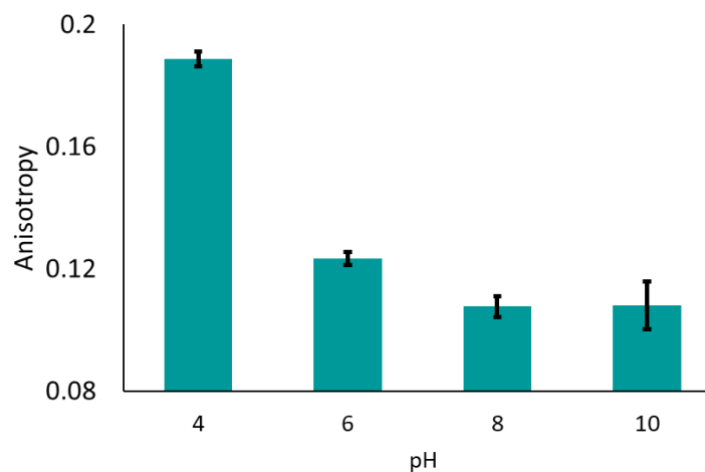

Figure 4.16: *Laurdan anisotropy values of the DDP over varying pH at 45°C, N = 4, error bar = SD. The anisotropy was found highest at pH 4.*

Table 4.1: *The percentage of different protonated species (double protonated, mono protonated and deprotonated) of DDP (pka1 at 2.85 and pKa2 at 7.35) at different pH calculated using the Henderson-Hasselbalch equation.*

	Species percentage		
pH	Double protonated $C_{12}H_{25}OPO(OH)_2$	Mono protonated $C_{12}H_{25}OP(OH)O_2^-$	Deprotonated $C_{12}H_{25}OPO_3^{2-}$
2	87.5	12.49	6.25E-05
4	6.5	93.45	0.04
6	0.07	94.93	4.99
8	0.00	80.99	18.99
10	0.00	0.199	99.79

4.4.1.3 CBC (Critical Bilayer Concentration) estimation of DDP membranes at different pH

To further investigate the pH-dependent self-assembly process of DDP, its CBC was determined using NR and pyrene at pH 4 and 8. The NR I_{610}/I_{660} ratio was plotted as a function of DDP concentration. As mentioned earlier, NR emission undergoes a blue-shift upon partitioning into hydrophobic regions. Thus, an increase in the I_{610}/I_{660} ratio reflects the formation of self-assembled structures [34]. A steady value of this ratio that continues to remain unaltered even when there is a further increase in DDP concentration, indicates stable membrane formation. A sharp increase in the I_{610}/I_{660} ratio was observed in pH 8 at 0.1 mM DDP concentration (Figure 4.17 and Figure 4.19). At pH 8, blue-shift of the emission light and the I_{610}/I_{660} ratio reached a steady value at a relatively lower concentration when compared to pH 4 (Figure 4.18 and Figure 4.19). In all, the CBC at pH 4 and 8 were found to be 0.9±0.1 and 0.7±0.1 mM, respectively, indicating that DDP assembles more readily at pH 8 (Figure 4.19). To compare the CBC of pure DDP membrane with a FA system, we determined the CBC of lauric acid, which is a FA with the same aliphatic chain length as DDP (C12; Figure 4.1). The CBC of lauric acid was found to be much higher at ~6 mM at pH 8 (Figure 4.20), highlighting the influence of the phosphate head-group on the self-

assembly process. Possessing such a low CBC as DDP is of extreme advantage in the prebiotic context as the presence of high concentrations of solutes in a dilute prebiotic pool would have been challenging, which poses difficulty for compartment formation[3–5].

Next, we plotted the pyrene I_1/I_3 ratio as a function of DDP concentration to crosscheck the CBC values obtained with NR [34]. We observed a sharp decrease in the I_1/I_3 ratio with increasing DDP concentration, which reached a steady value similar to the NR I_{610}/I_{660} ratio, indicating the formation of stable vesicles. The CBC at pH 4 and 8 were found to be 1±0.1 and 0.9±0.1 mM, respectively, when using the pyrene I_1/I_3 ratio (Figure 4.21 Panel a and b). In addition to the five monomer vibronic peaks between 370 to 400 nm, pyrene also shows a broad emission peak near 460 to 500 nm because of excimer formation [26,27]. Pyrene excimerization is considered to occur due to the formation of excited-state dimer by the interaction between the ground-state and excited-state pyrene monomers owing to their close proximity [27,38]. Thus, excimerization points toward the self-assembly process itself and the nature of aggregation too. To quantify the excimer formation, the intensity ratio of 470 nm (I_{Ex}) and 372 nm (I_1) was plotted as a function of DDP concentration. In pH 8, high intensity emission corresponding to excimerization was observed at 0.1 mM DDP, which gradually decreased with increasing DDP concentration (Figure 4.22). Literature suggests that excimer formation at low surfactant concentration reflects premicellar aggregation [39,40]. The continuous decrease in I_1/I_3 ratio at such low DDP concentration suggested the progressive increase in the self-assembled structures. With increasing DDP concentration, pyrene excimerization decreased as pyrene molecules get distributed in the DDP assemblies and the probability to find more than one pyrene in an assembly decreased at pH 8 [40]. However, at pH 4, pyrene excimerization was found to be absent and unaffected by changing DDP concentration. The absence of a strong excimer emission peak at low (below CBC) DDP concentration at pH 4, suggests that pyrene monomers are unable to form excimers inside the aggregates (Figure 4.22). Models suggest that pyrene excimerization is diffusion-limited in 2D space [38]. The 2D model of diffusion-controlled pyrene excimerization was also validated for pyrene labelled phospholipid membrane (py10-PC/POPC and py10-PC/DMPC) and with free pyrene incorporated in DMPC membrane [41]. Therefore, we hypothesize that the low I_{Ex}/I_1 ratio in pH 4

over varying DDP concentrations could reflect the limited diffusion of pyrene monomers in the DDP membranes. Additionally, higher anisotropy and GP value of DDP membrane at pH 4, reflect the rigid nature of the membrane that could prevent the diffusion of pyrene monomers.

To confirm the aforesaid, the crystalline nature of the DDP membranes at pH 4 was investigated by analysing the dried film of a DDP membrane suspension using Powder X-ray Diffraction (PXRD). Multiple sharp peaks were observed in the XRD pattern at pH 4 (Figure 4.23). Such peaks and patterns were absent in the XRD pattern of DDP suspension at pH 8. The appearance of sharp multiple peaks in periodic order at pH 4, denoted the crystalline nature of the membrane [42]. To confirm that the sharp peaks at pH 4 were indeed coming from the DDP membrane, we extracted the DDP molecules from the pH 4 vesicle suspension in chloroform:methanol::2:1 and analysed its dried film XRD pattern. The absence of any peaks in the extracted samples confirmed that the sharp XRD peaks were indeed a characteristic of DDP membranes at pH 4 under aqueous conditions as DDP cannot assemble into vesicles in chloroform:methanol::2:1.
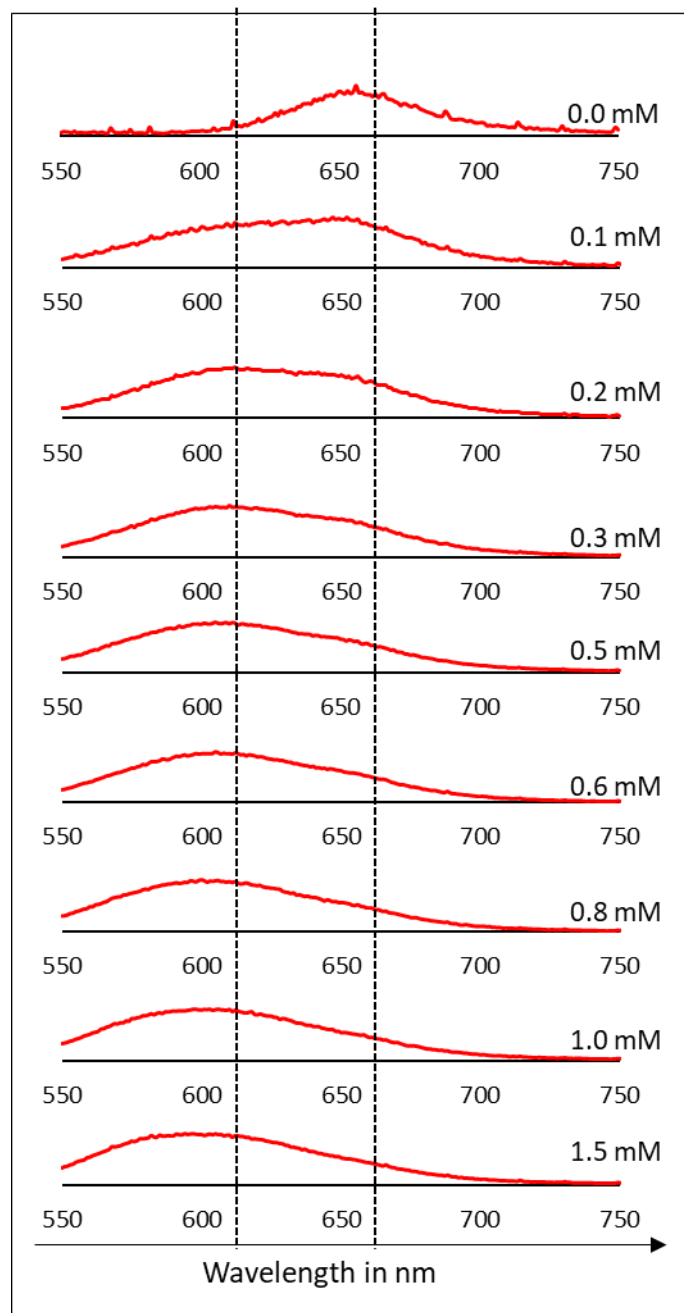
Figure 4.17: *Normalized emission spectra of nile red in DDP suspension at pH 4 when plotted as the function of DDP concentration at 45°C. The black dotted lines indicate the emission at 610 and 660 nm; there is a blue-shift that occurred as a function of DDP concentration indicating an increase in hydrophobicity with increasing DDP concentration. N = 3.*
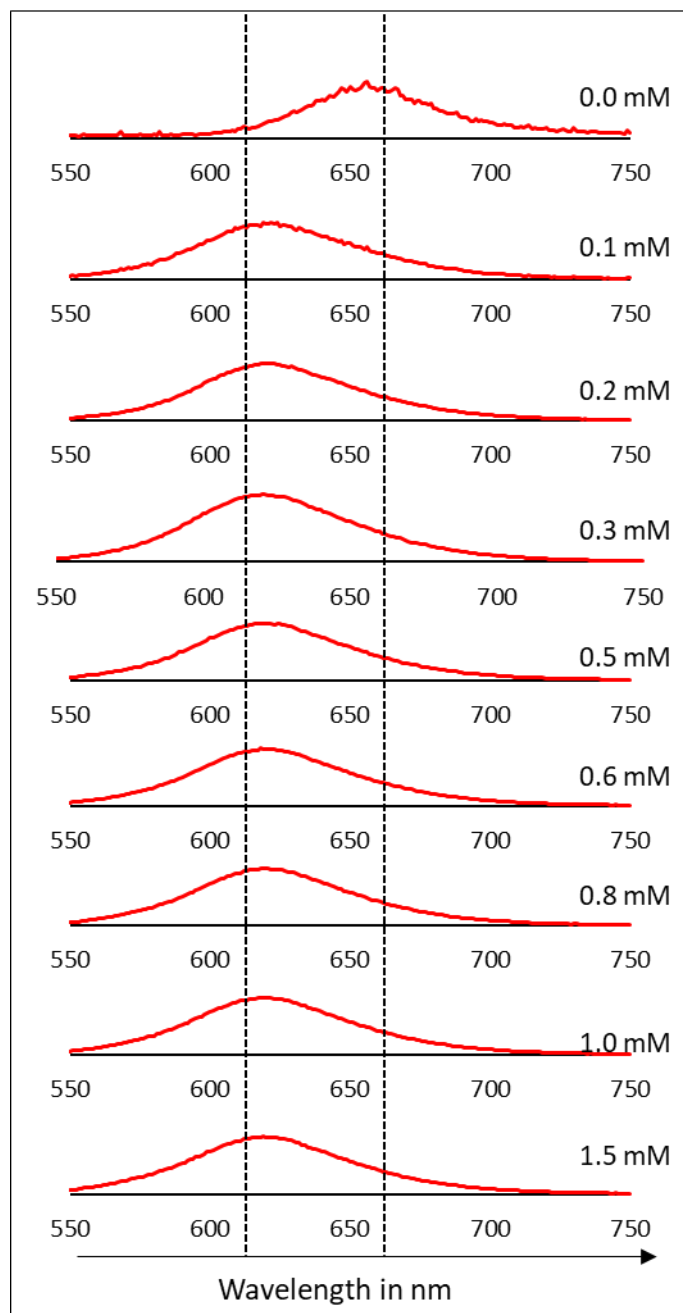
Figure 4.18: *Normalized emission spectra of nile red in DDP suspension at pH 8 when plotted as the function of DDP concentration at 45°C. The black dotted lines indicate the emission at 610 and 660 nm, there is a drastic blue-shift upon addition of DDP (0.1 mM) with a maximum at 620 nm which remained same with further increasing DDP concentration. N = 3.*
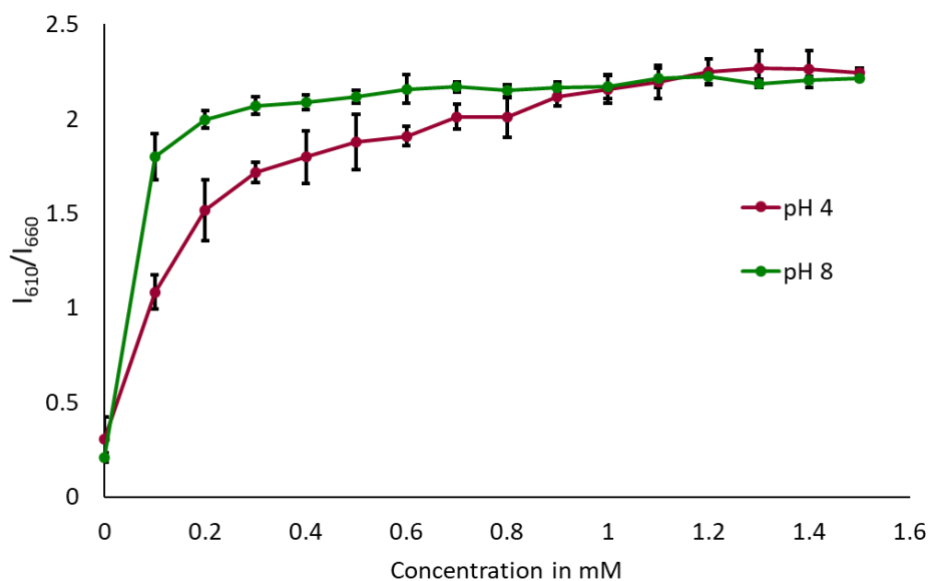
Figure 4.19: *The scatter plot shows nile red I_{610}/I_{660} ratio of DDP suspension at pH 4 and 8, plotted as the function of DDP concentration. N = 3, error bar = SD.*
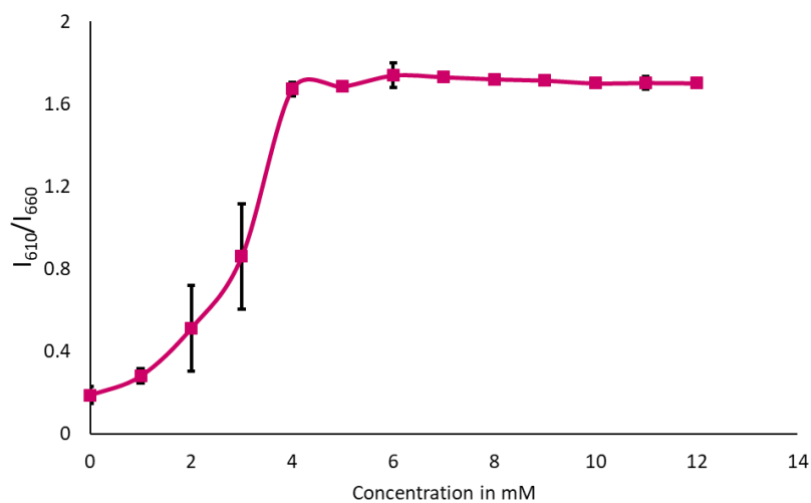
Figure 4.20: *The scatter plot showing nile red I_{610}/I_{660} intensity ratio of LA suspension at pH 8 when plotted as a function of DDP concentration. N = 3, error bar = SD.*
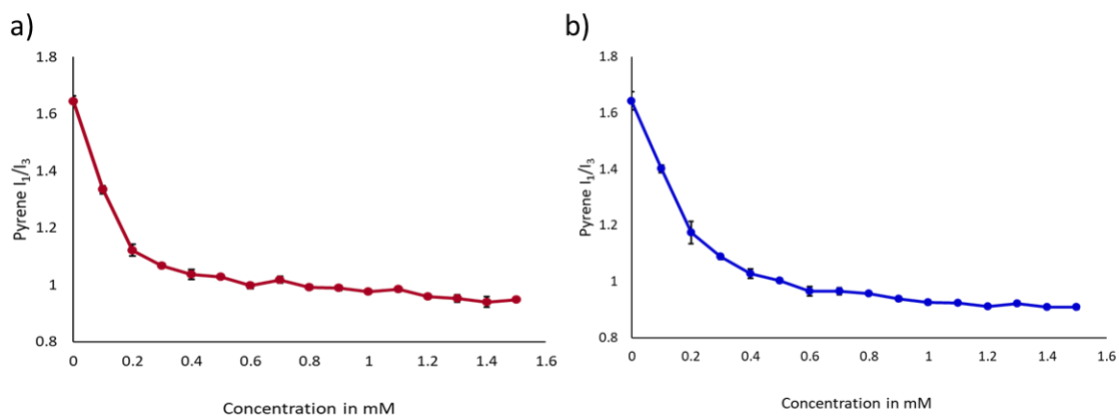
Figure 4.21: *The scatter plot showing the pyrene I_1/I_3 ratio of DDP suspension at pH 4 and 8, plotted as a function of DDP concentration. N = 3, error bar = SD. a and b represents the pyrene I_1/I_3 at pH 4 and 8 respectively.*
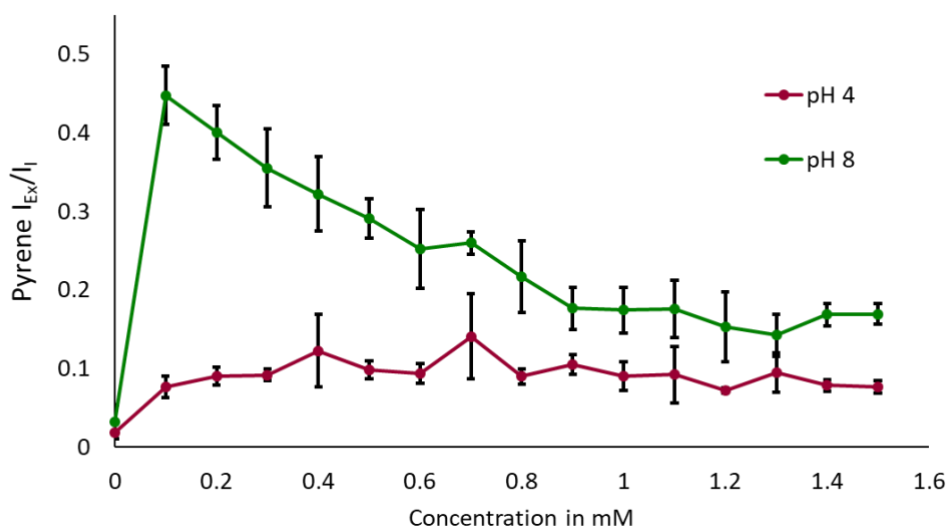

Figure 4.22: *Pyrene I_{Ex}/I_I ratio of DDP suspension at pH 4 and 8, plotted as the function of DDP concentration., N = 3, error bar = SD.*
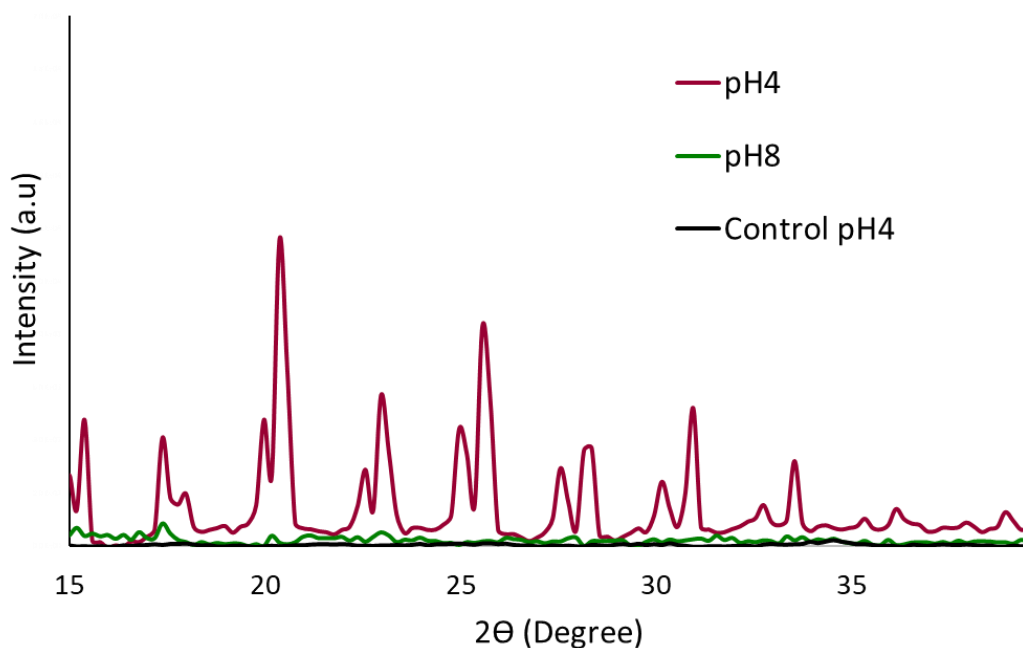
Figure 4.23: PXRD pattern of the dried film generated by repeatedly drop-casting and dried aqueous vesicle suspension of 10 mM DDP at pH 4 (magenta) and pH 8 (green), respectively. The black trace (control at pH 4) shows the XRD pattern of the dried film of extracted DDP molecules from suspension at pH 4 in

4.4.2 Effect of dodecanol (DOH) on the self-assembly and properties of DDP membrane

The addition of fatty alcohols has been shown to stabilize FA vesicles in alkaline pH and increase membrane thermostability [8,15,24]. Contrarily, fatty alcohols are also known to induce FA vesicle destabilization and oil-droplet formation when added in a high molar ratio [8,15]. Given these observations, we aimed to discern the effect of the presence of fatty alcohols when added in conjunction with DDP to result in membranes. Towards this, we mixed DOH with DDP to prepare DDP-DOH mixed membrane systems in different molar ratios i.e. DDP:DOH::1:1, DDP:DOH::2:1 and DDP:DOH::4:1. The turbidity measurements indicated the formation of higher-order aggregates in all three mixed systems over varying pH. Unlike in the pure DDP system, low turbidity of DDP:DOH::1:1 and DDP:DOH::2:1 mixed systems at pH 2, indicated the absence of large crystalline aggregates in the respective suspensions (Figure 4.24 to Figure 4.26). Upon further decreasing the ratio of DOH to DDP in DDP:DOH::4:1, the turbidity at pH 2 increased, similar to what was observed in the

pure DDP system. However, the high turbidity of the three mixed systems at alkaline pH (pH 10), when compared to the pure DDP system, alluded to an increase in vesicle formation in the presence of DOH. Further, the pyrene I_1/I_3 ratio for all the three mixed systems mentioned above, across varying pH, indicated the formation of mixed aggregates with hydrophobic regions (Figure 4.27 to Figure 4.29). The I_1/I_3 ratio of the three mixed systems was significantly lower at pH 10 when compared to the pure DDP system, suggesting better shielding of pyrene molecules from the bulk water (Figure 4.30). Under the microscope, vesicles were observed from pH 3 to 10 in both DDP:DOH::1:1 and DDP:DOH::2:1systems (Figure 4.31 Panel a and b). However, upon decreasing the DOH molar ratio in DDP:DOH::4:1 mixed system, vesicles were observed from pH 2 to 10 similar to what was seen in the only DDP system (Figure 4.31 Panel c). Therefore, the presence of DOH at high concentrations decreased the solubility of DDP molecules in the aqueous phase and thus hamper vesicle formation at pH 2. However, at alkaline pH, DOH can act as H-bond donor and potentially H-bond with the negatively charged phosphate group of DDP, thereby, stabilizing vesicles as is reflected by an increase in the turbidity values (Figure 4.32 Panel a). The average size of the vesicles present in the three mixed systems at pH 10 was found to be significantly higher than the pure DDP system at pH 10 (Figure 4.32 Panel b). This increased vesicle size and turbidity, along with a decrease in pyrene I_1/I_3 ratio, highlights the vesicle stabilizing ability of DOH at alkaline pH, potentially by acting as H-bond donor.

To investigate the physicochemical properties of the DDP:DOH mixed membranes, we used NR and laurdan probes. For all the three mixed systems, i.e. DDP:DOH in 1:1, 2:1 and 4:1 ratios, the change in micropolarity and GP values were evaluated as a function of pH. The trend of change in NR I_{610}/I_{660} ratio with a change in pH was similar to what was seen in the pure DDP membrane system. The I_{610}/I_{660} ratio was high in pH 4 and it decreased with an increase in pH indicating the increase in membrane micropolarity (Figure 4.33). However, the I_{610}/I_{660} ratio in all the mixed systems was overall lower when compared to the pure DDP membrane system (Figure 4.33). The I_{610}/I_{660} ratio was found to be lowest in the DDP:DOH::1:1 system, indicating high micropolarity. This suggested that the presence of DOH increased the membrane water accessibility. The GP values of all three mixed membrane systems decreased with an increase in pH owing to a decrease in membrane packing as

observed in the case of only DDP membrane (Figure 4.34). The GP values of the mixed systems were overall lower in comparison to the pure DDP membrane system, suggesting a decrease in membrane packing in presence of DOH (Figure 4.34). As the melting temperature of DOH (24°C; Figure 4.1) is much lower than that of DDP (42-45°C; Figure 4.1), and the GP values were recorded at 45°C, the presence of DOH potentially impedes DDP membrane packing and increases water accessibility. Similar to the pure DDP membrane, the decrease in laurdan anisotropy showed a decrease in the fluidity of all the mixed membranes upon an increase in pH. The fluidity was highest in pH 4 (with anisotropy value of 0.18) and decreased till pH 8 (with an anisotropy value of 0.1), after which it remained unaltered (Figure 4.35 Panel a to c).
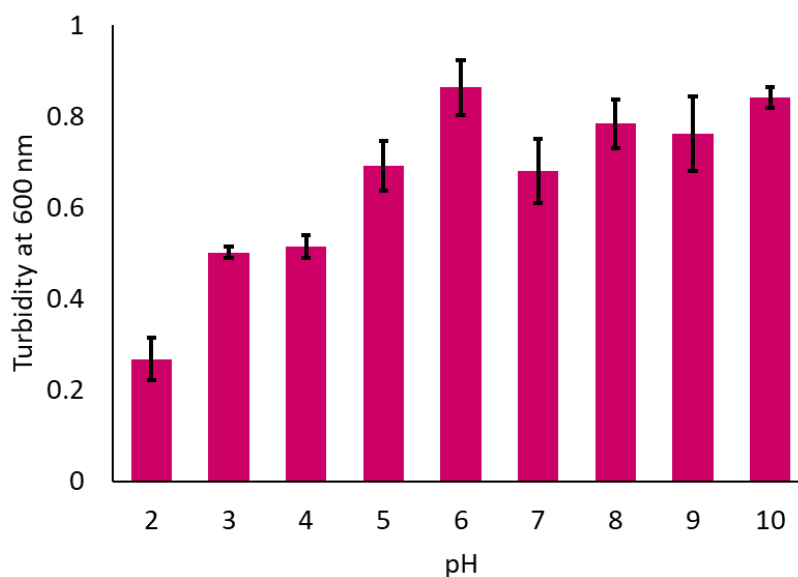

Figure 4.24: *The bar plot shows the turbidity measurements at 600 nm for 10 mM DDP:DOH::1:1 membrane suspension at different pH (x-axis) and 45°C, N = 3, error bar = SD. Lowest turbidity was observed at pH 2 indicating comparatively less amount of higher order structures (vesicles and crystalline aggregates).*
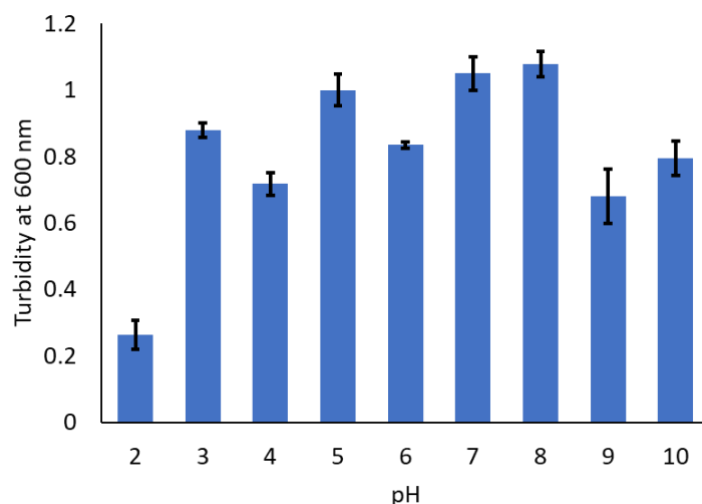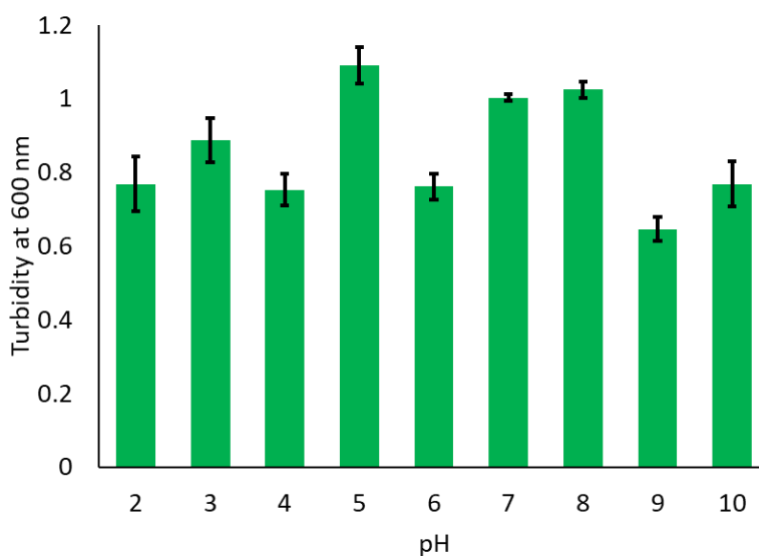
Figure 4.25: *The bar plot shows the turbidity measurements at 600 nm for 10 mM DDP:DOH::2:1 membrane suspension at different pH (x-axis) and 45°C, N = 3, error bar = SD. Lowest turbidity was observed at pH 2 indicating comparatively less amount of higher order structures (vesicles and crystalline aggregates).*

Figure 4.26: *The bar plot shows the turbidity measurements at 600 nm for 10 mM DDP:DOH::4:1 membrane suspension at different pH (x-axis) and 45°C, N = 3, error bar = SD. Lowest turbidity was observed at pH 9 indicating comparatively less amount of higher order structures (vesicles and crystalline aggregates).*
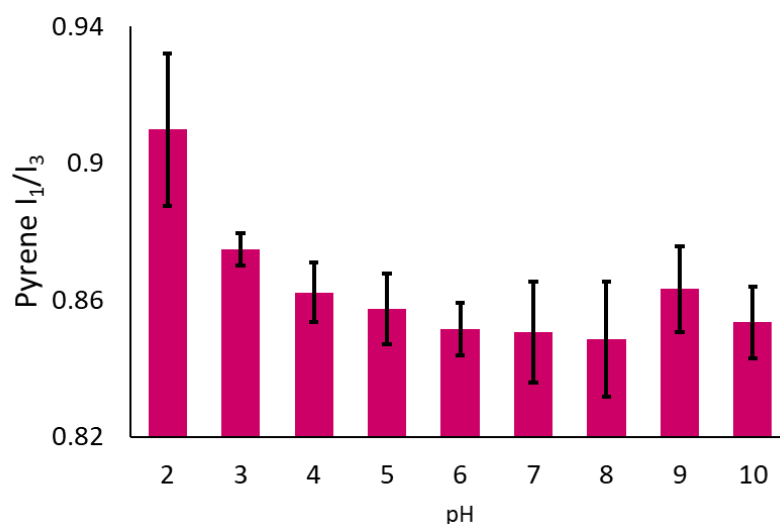
Figure 4.27: *Pyrene I_1/I_3 ratio of 10 mM DDP:DOH::1:1 membrane suspension at different pH (x-axis) at 45°C, N = 4, error bar = SD. Higher ratio indicates less hydrophobicity (more water accessibility). The ratio was observed to be highest at pH 2. From pH 4-10, the ratio remains unchanged based on a two-tailed t-test.*
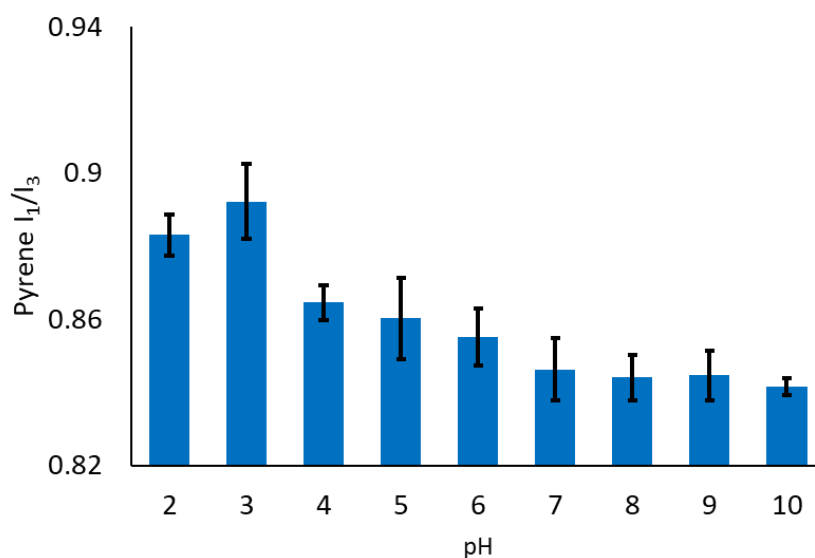

Figure 4.28: *Pyrene I_1/I_3 ratio of 10 mM DDP:DOH::2:1 membrane suspension at different pH (x-axis) at 45°C, N = 4, error bar = SD. Higher ratio indicates less hydrophobicity (more water accessibility). The ratio was observed to be highest at pH 2-3. From pH 6-10, the ratio remains unchanged based on a two-tailed t-test.*
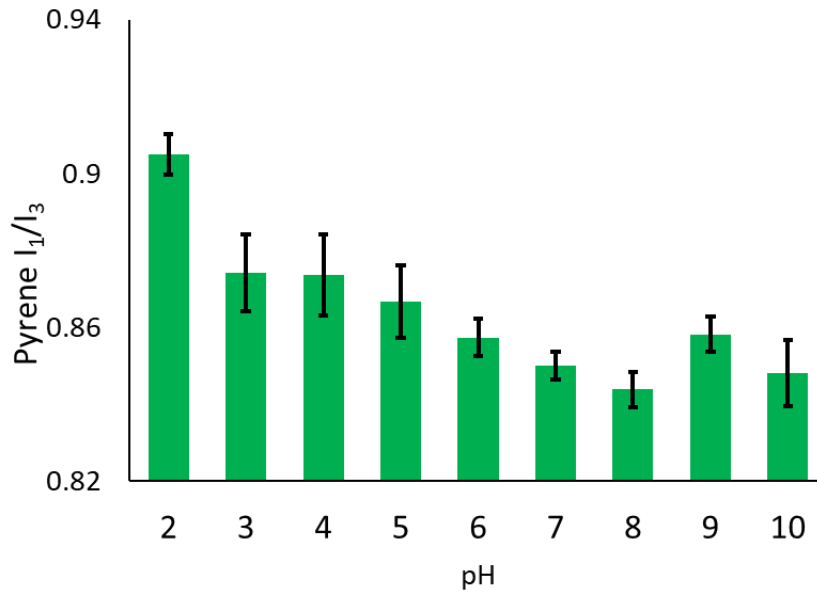
Figure 4.29: *Pyrene I_1/I_3 ratio of 10 mM DDP:DOH::4:1 membrane suspension at different pH (x-axis) at 45°C, N = 4, error bar = SD. Higher ratio indicates less hydrophobicity (more water accessibility). The ratio was observed to be highest at pH 2 and lowest at pH 7-8.*
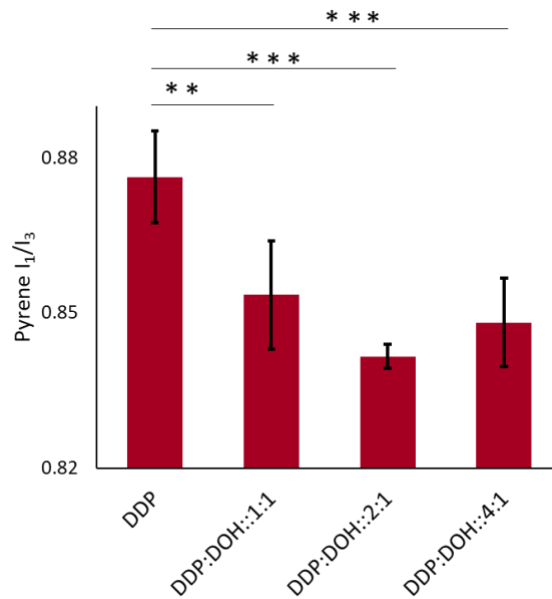

Figure 4.30: *Pyrene I_1/I_3 ratio of 10 mM DDP and different DDP:DOH mixed systems at pH 10 recorded at 45°C, N = 3, error bar = SD. Upon comparison of only DDP membrane with the three DDP:DOH mixed systems, the decrease was found to be significant with a p-value of <0.05 based on a two-tailed t-test.*
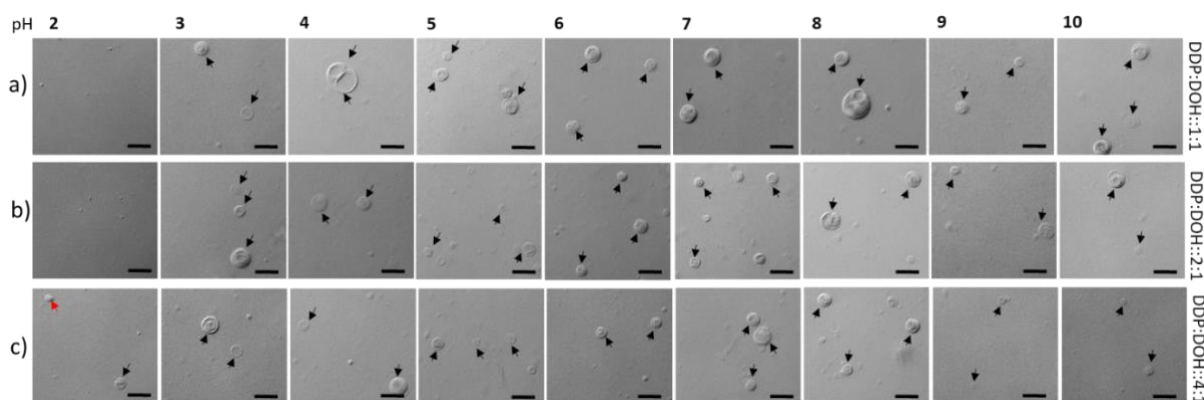
Figure 4.31: *DIC microscopy images of three different DDP:DOH mixed membrane systems over varying pH. Panels (a) to (c) show three different systems, i.e., a) DDP:DOH::1:1, b) DDP:DOH::2:1 and c) DDP:DOH::4:1. Black and red arrows indicate vesicles and crystalline aggregates, respectively. N = 3, Scale bar = 10 µm. Vesicles were seen readily in most of the samples imaged across the varying pH excepting at pH 2 in DDP:DOH::1:1 and DDP:DOH::2:1 systems.*
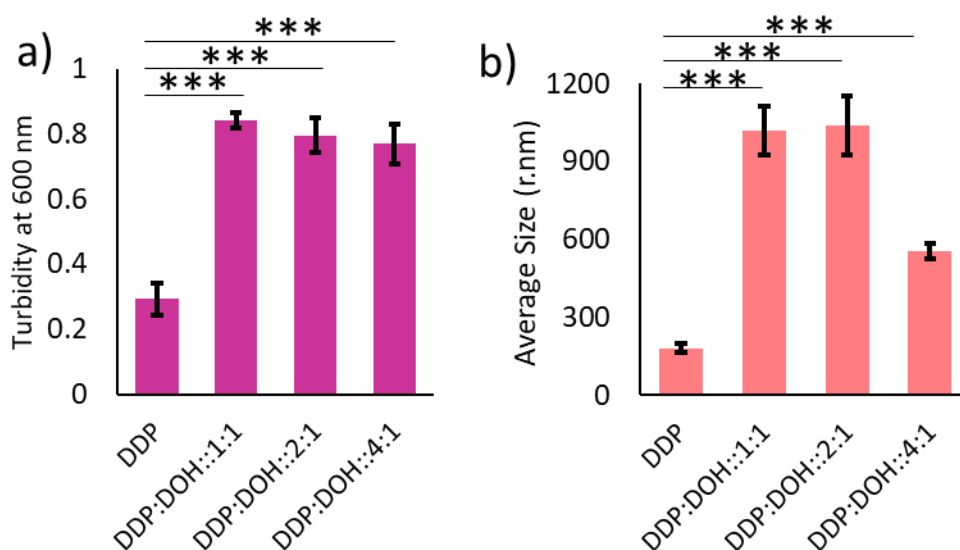

Figure 4.32: *a) Turbidity measurements at 600 nm of 10 mM of DDP and different DDP:DOH mixed membrane systems at pH 10 recorded at 45°C, N = 3, error bar = SD. The comparison between the only DDP with the three DDP-DOH mixed membrane systems showed a difference that was found to be significant with a p-value of < 0.001 based on a two-tailed t-test. b) Average size (nm) of the population of DDP and different DDP:DOH mixed systems at pH 10 recorded at 45°C. N = 4, error bar = SD. The comparison between the only DDP with the three DDP-DOH mixed membrane systems showed a difference that was found to be significant with a p-value of < 0.001 based on a two-tailed t-test.*
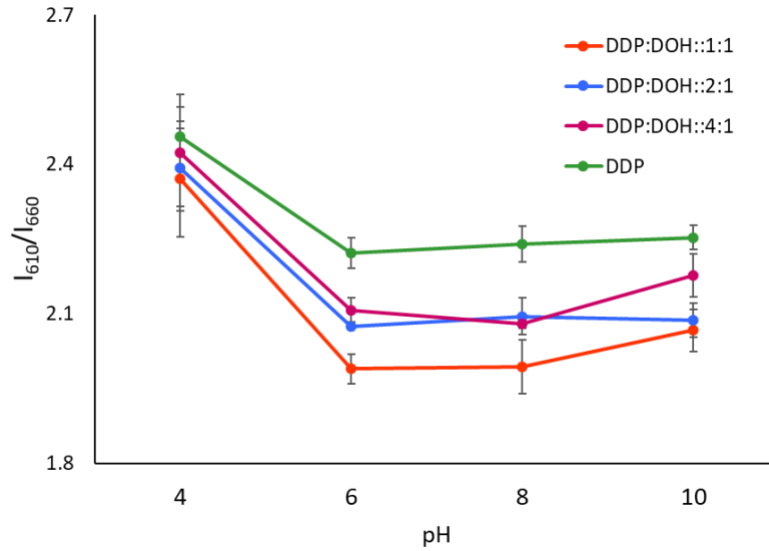
Figure 4.33: *The scatter plot shows nile red I_{610}/I_{660} ratio of the DDP membrane and the different DDP:DOH mixed systems over varying pH at 45°C. N = 4, error bar = SD. Higher I_{610}/I_{660} ratio indicates low micropolarity. With an increase in pH, the ratio decreased showing an increase in micropolarity, for all the systems investigated. The lowest I_{610}/I_{660} ratio was observed for DDP:DOH::1:1 system.*
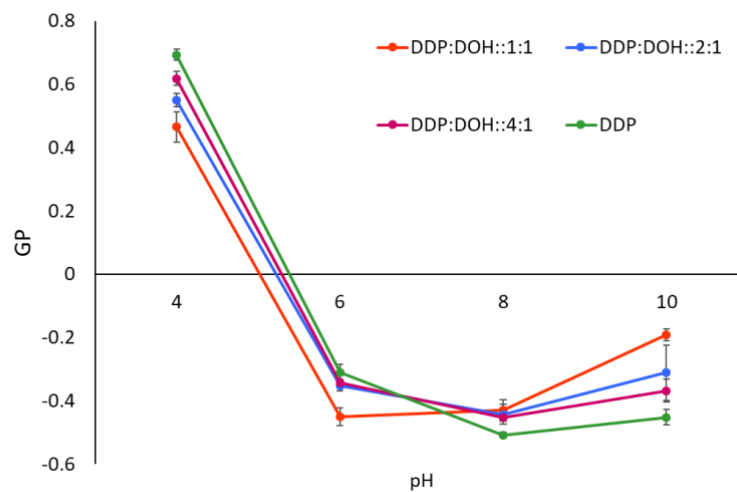

Figure 4.34: *The scatter plot shows laurdan GP values of the DDP membrane and the different DDP:DOH mixed systems over varying pH at 45°C. N = 4, error bar = SD. Higher GP value indicates higher membrane order. With an increase in pH, the GP value decreased showing a decrease in membrane order, for all the systems investigated.*
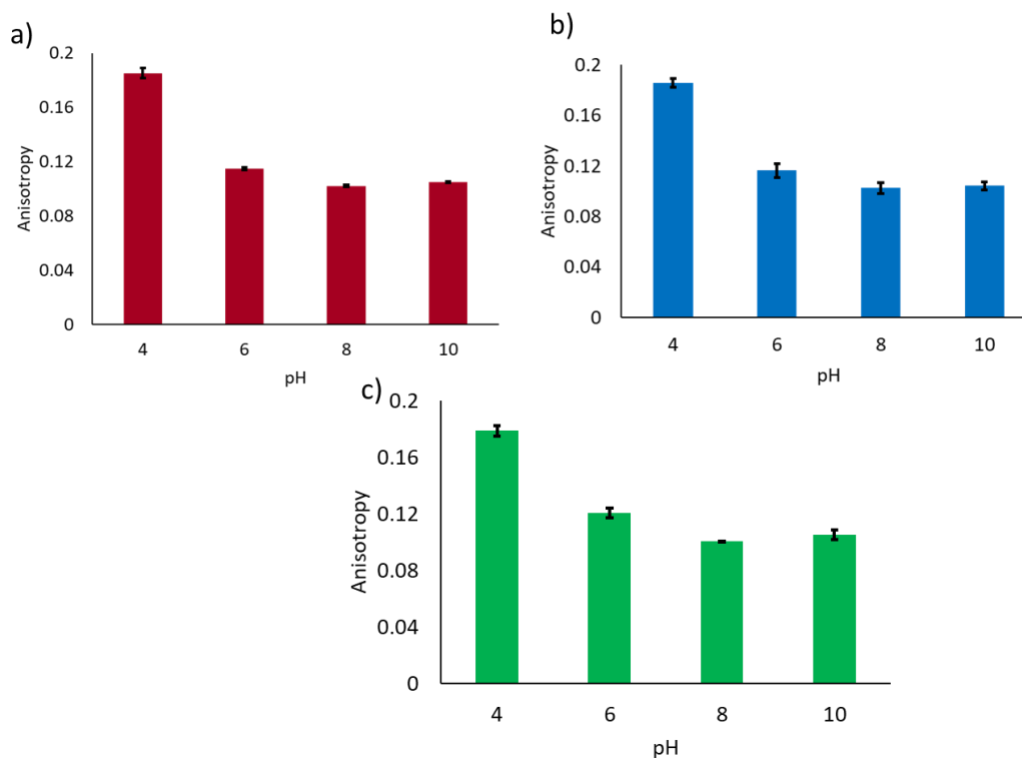
Figure 4.35: *Laurdan anisotropy values of the DDP:DOH mixed membrane systems over varying pH at 45°C. N = 4, error bar = SD. Higher Anisotropy value indicates lower fluidity. a), b) and c) represents DDP:DOH:1:1, DDP:DOH:2:1 and DDP:DOH:4:1 mixed system respectively. With an increase in pH, the :anisotropy value decreased showing an increase in membrane fluidity.*

4.4.3 High-temperature behaviour of DDP and DDP:DOH mixed membranes at different pH.

To understand the temperature-dependent phase behaviour of DDP-based membranes, the GP values were measured from 35°C to 65°C at pH 4 and 8 and were compared with values obtained for LA and myristoleic acid (MOA) membranes at pH 8. For the pure DDP membranes at pH 4, the GP value was 0.71±0.05 at 35°C corresponding to a highly ordered phase. With increasing temperature, it decreased owing to increased thermal motion (Figure 4.36). At 65°C, it decreased to 0.48±0.01 indicating a decrease in membrane packing. For the DDP membranes at pH 8, the GP value at 35°C was -0.32±0.01 reflecting the disordered nature of the membrane (Figure 4.37). With increasing temperature, the GP value further decreased to -0.62±0.05 at 65°C, indicating a highly disordered DDP membrane. This highlighted

the thermostability of the DDP membrane, especially at low pH (pH 4) against high temperature-induced membrane dissolution. To understand the effect of DOH on this, the GP of the DDP:DOH::1:1 mixed system was also monitored from 35°C to 65°C as the presence of fatty alcohol is shown to increase FA membrane thermostability [24]. As shown in Figure 4.36 for DDP:DOH::1:1 mixed system, the GP decreased from 0.58 to 0.15 upon increasing the temperature from 35°C to 65°C, at pH 4. At pH 8, the GP decreased from 0.18 to -0.61 upon increasing the temperature from 35°C to 65°C for the DDP:DOH::1:1 mixed system, which reflects a drastic decrease in the membrane order (Figure 4.37). This shows that DOH can have a dual effect on membrane packing at pH 8; at low temperature, DOH increased the membrane packing, while at high temperature it decreased the membrane packing. For the LA, the GP was found to decrease from -0.30±0.01 to -0.72±0.02 moving from 35°C to 65°C (Figure 4.37). Upon plotting the decrease in GP for all the systems, the highest degree of decrease (0.8±0.01) was found for DDP:DOH (1:1) system at pH 8 (Figure 4.38). This was followed by DDP:DOH (1:1) system at pH 4, which showed a decrease of 0.43±0.006. For the pure DDP and LA membranes (both at pH 8), the decrease in GP was 0.29±0.007 and 0.42 ±0.01, respectively, when the temperature changed from 35°C to 65°C. This highlighted that DDP membranes are relatively more resistant to temperature-induced decrease in membrane packing than LA membranes (Figure 4.38). The smallest change in GP (0.07±0.03) was observed for the MOA membrane as the membrane is loosely packed even at 35°C because of unsaturation in it (Figure 4.1).

To understand the change in vesicle morphology at elevated temperatures, we next monitored the turbidity of the suspensions and plotted the change in turbidity upon increasing the temperature from 35°C to 65°C. In all the systems, a decrease in turbidity was observed upon increasing temperature (Figure 4.39). The highest percentage of decrease was observed for DDP:DOH::1:1 mixed system at pH 4 (56.7±3.6), followed by the DDP:DOH::1:1 system at pH 8 (45.2±2.3) (Figure 4.39). The least decrease was observed for the pure DDP system at pH 8 (20.9±2.1). Using decanoic acid and decanoic acid-decanol (1:1 molar ratio) mixed membranes, studies have reported an increase in micellar and monomer population at the expense of vesicles, and also a decrease in vesicle lamellarity when heated above 60°C [32]. As vesicle lamellarity and number are both known to linearly correlate with

suspension turbidity, the decrease in turbidity observed here for all systems could therefore indicate a decrease in vesicle number and/or lamellarity [25]. Since membrane order is inversely correlated with membrane permeability, a decrease in membrane packing at elevated temperature as observed here should facilitate the exchange of matter [24]. At pH 8, DDP and DDP-DOH mixed membrane would possess high permeability similar to FAs membrane (LA). However at pH 4, because of the tight packing (high GP), DDP and DDP-DOH mixed membrane would possess extremely low permeability which can be counterbalanced by increasing the temperature.
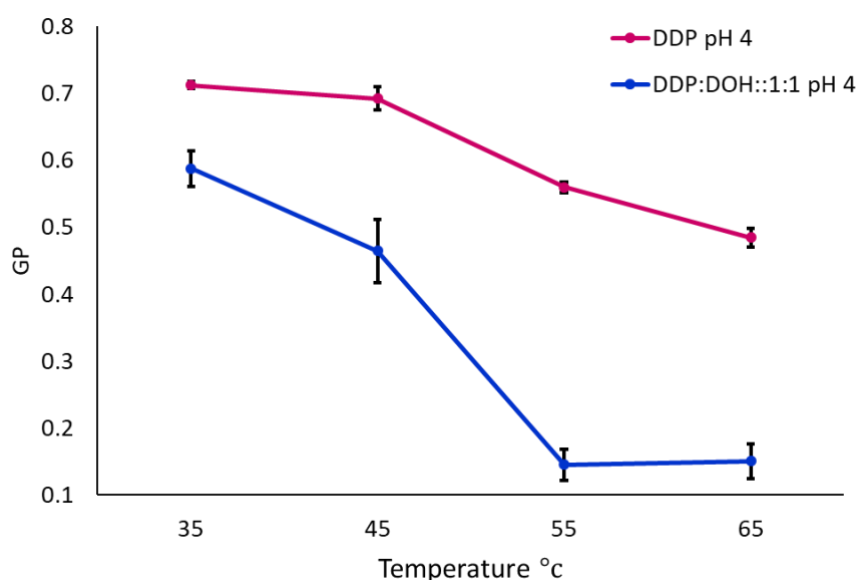

Figure 4.36: *Graph showing laurdan GP values of the pure DDP and DDP:DOH::1:1 membrane systems over varying temperatures at pH 4. N = 4, error bar = SD. Higher GP value indicates higher membrane order. With an increase in temperature, the GP value decreased showing a decrease in membrane order, for both the systems. The extent of decrease was comparatively higher for DDP:DOH::1:1 system.*
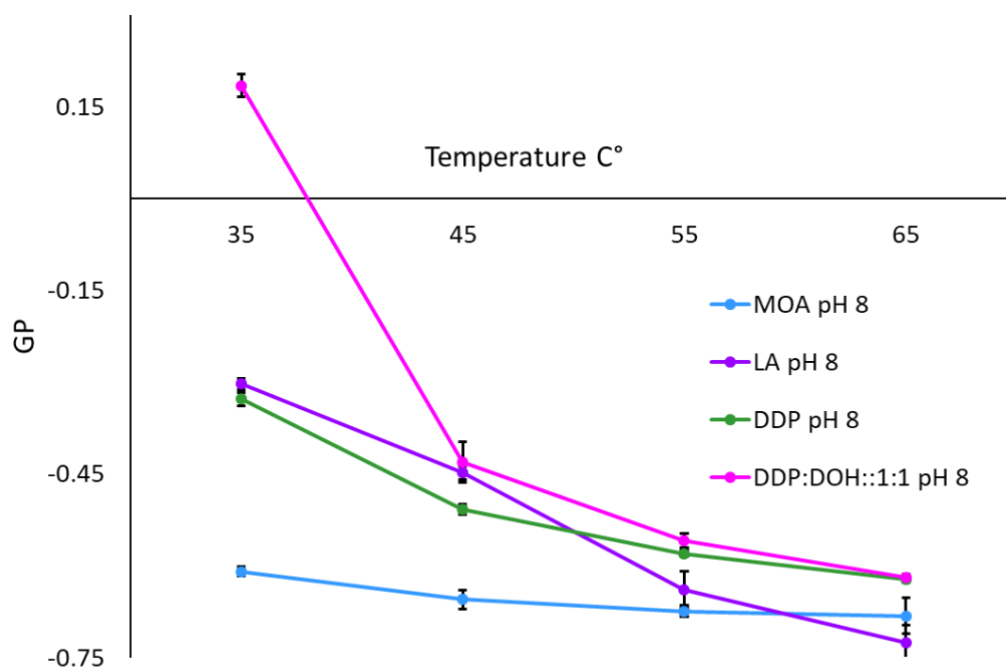
Figure 4.37: *The graph shows laurdan GP values of the different membrane systems over varying temperatures at pH 8. N = 4, error bar = SD. Higher GP value indicates higher membrane order. With an increase in temperature, the GP value decreased showing a decrease in membrane order, for all four membrane systems.*
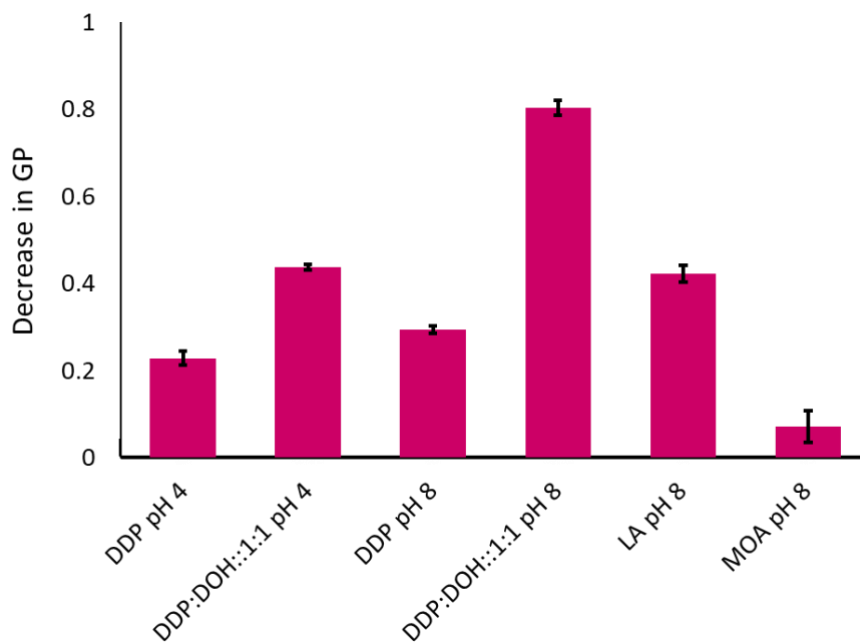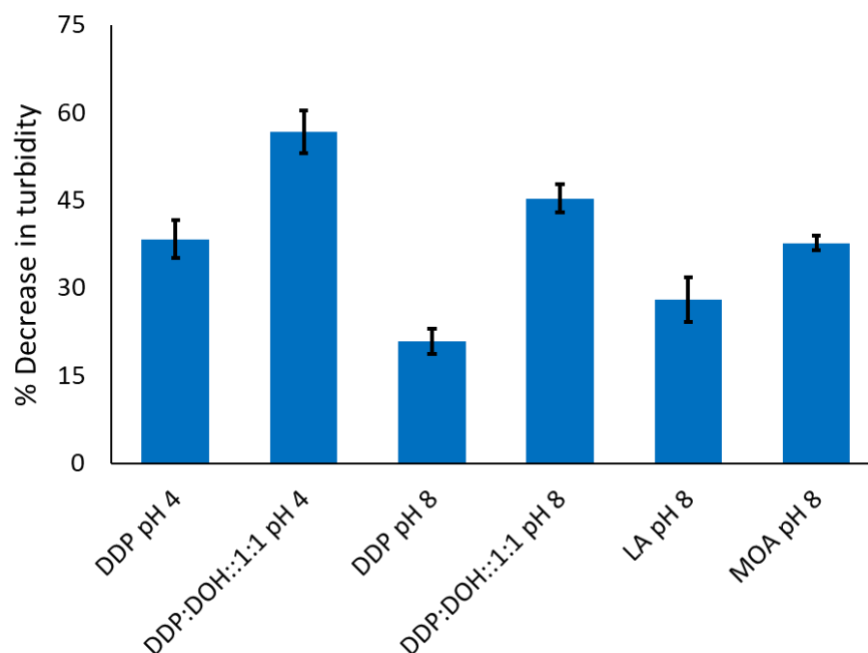
Figure 4.39: The bar plot represents the decrease in the turbidity at 600 nm for different membrane systems upon increasing the temperature from 35°C to 65°C, at pH 4 and 8, respectively. N = 4, error bar = SD.

4.4.4 Comparison of DDP membrane properties with different model protocellular membranes

In order to understand and correlate DDP membrane properties with other model protocellular membrane systems, we compared the micropolarity and order of DDP membranes with different PLs (1-palmitoyl-2-oleoyl-glycero-3-phosphocholine ,POPC; 1,2-dipalmitoyl-sn-glycero-3-phosphocholine, DPPC; 1,2-dimyristoyl-sn-glycero-3-phosphocholine, DMPC; 1,2-di-dodecanoyl-sn-glycero-3-phosphocholine, DLPC; 1,2-di-decanoyl-sn-glycero-3-phosphocholine; DDPC) and FAs (Dodecanoic acid, LA; Decanoic acid, DA; Myristoleic acid, MOA; and Oleic acid, OA) membranes, of varying chain length and melting point (Figure 4.1), both at pH 4 and 8 at 45°C. NR I_{610}/I_{660} ratio and laurdan GP for four different phospholipids were

determined at both pH 4 and 8. However, for all the four FA systems, it was determined at pH 8 as FAs don't assemble into vesicles at pH 4. As shown in the Figure 4.40 at pH 8, the NR I_{610}/I_{660} ratio for all the four FA systems was between 1.50 to 1.68, indicating high membrane micropolarity. For all the four phospholipids, the I_{610}/I_{660} ratio was between 1.86 to 2.16, indicating comparatively low membrane micropolarity (water accessibility). The I_{610}/I_{660} ratio for DDP membranes at pH 8 was 2.2, suggesting that the DDP membranes possess similar polarity as that of phospholipid membranes at this pH (Figure 4.40). In terms of membrane order (GP) for FA membranes, the highest and lowest GP values were observed for LA (-0.41) and MOA (-0.73), respectively, at pH 8. For the DDP membranes at pH 8, the GP value was -0.50, which was similar to that of decanoic acid (C10, DA membranes) (-0.5) (Figure 4.40). Interestingly, though LA membranes possess the same chain length and similar melting point as that of DDP, DDP membranes are comparatively less packed at pH 8. For the phospholipid membranes at pH 8, DMPC had the highest GP (-0.26) and DDPC had the lowest GP (-0.49) at 45°C. The GP of DLPC (-0.40) was found to be similar to that of LA membranes (-0.41), which have the same aliphatic chain length. GP of DDPC (-0.5) was similar to that of DDP (-0.5), indicating the loose packing of the membrane. All the aforementioned data essentially highlighted the unique nature of the DDP membrane, where its micropolarity resembles a phospholipid membrane but its membrane packing is similar to that of both DA and DDPC membranes at pH 8. However, at pH 4, the I_{610}/I_{660} ratio of the DDP membrane is 2.45, which is higher than the values obtained for the four phospholipid membranes used in this study (Figure 4.41). Importantly, the GP of the DDP membranes at pH 4 was much higher (0.69) than the phospholipid membranes studied here, reflecting its solid-ordered state, which was also reflected in the XRD pattern.

We next aimed to extend this unique tuneability to modulate the PL membranes by adding DDP to them. Recent studies reported an alteration in the membranes of multiple cancer cell lines resulting in increased membrane fluidity and decreased packing [43]. In this context, the selective fusion of liposomes composed of PL to different cancer cell lines, exploiting the increased membrane fluidity of cancer cells, has also been reported [44-45]. This highlights how the increase in the fluidity of the carrier liposome can lead to region-selective fusion. Therefore, to explore the

modulation of membranes using DDP, we added DDP to different PL membranes in varying molar ratios. We monitored the change in the GP to evaluate the change in the packing of the mixed membrane in response to pH change at physiological temperature (37°C). As shown in Figure 4.42 Panel a, at pH 4 and 8, the GP of pure POPC membrane was -0.23±0.01 and -0.28±0.01 respectively, at 37°C. However, upon the addition of DDP to POPC (PL:DDP::2:1), the GP value changed to 0.11±0.01 and -0.31±0.01 at pH 4 and 8, respectively. Upon increasing the ratio of DDP (PL:DDP::1:1), the GP value further changed to 0.26±0.01 and -0.32±0.01 at pH 4 and 8, respectively (Figure 4.42 Panel a). We next studied DPPC, which has a high melting point (41°C) and is also known to stay in ordered crystalline form at both pH 4 and 8 with a GP value of 0.53±0.02 for this analysis. The addition of DDP in 1:1 molar ratio resulted in a further increase in the order of the mixed DPPC membrane to 0.65±0.01 at pH 4. However, at pH 8, the GP decreased to -0.11±0.02 showing a drastic decrease in the membrane order (Figure 4.42 Panel b). Therefore, using two different PL membrane systems, with two ratios of DDP spiked in them, we demonstrated that the addition of DDP can lead to the tuneability of the resultant mixed PL membranes. At pH 4, it resulted in increased membrane packing while at pH 8 it led to a decrease in membrane packing owing to the protonation state of the DDP molecule. At pH 8, 19% of DDP stays di-deprotonated in the membrane resulting in repulsion between the doubly negatively charged headgroups, leading to loosening in the packing. Interestingly, the change in GP in response to pH when DDP is added to the milieu, is remarkably high.
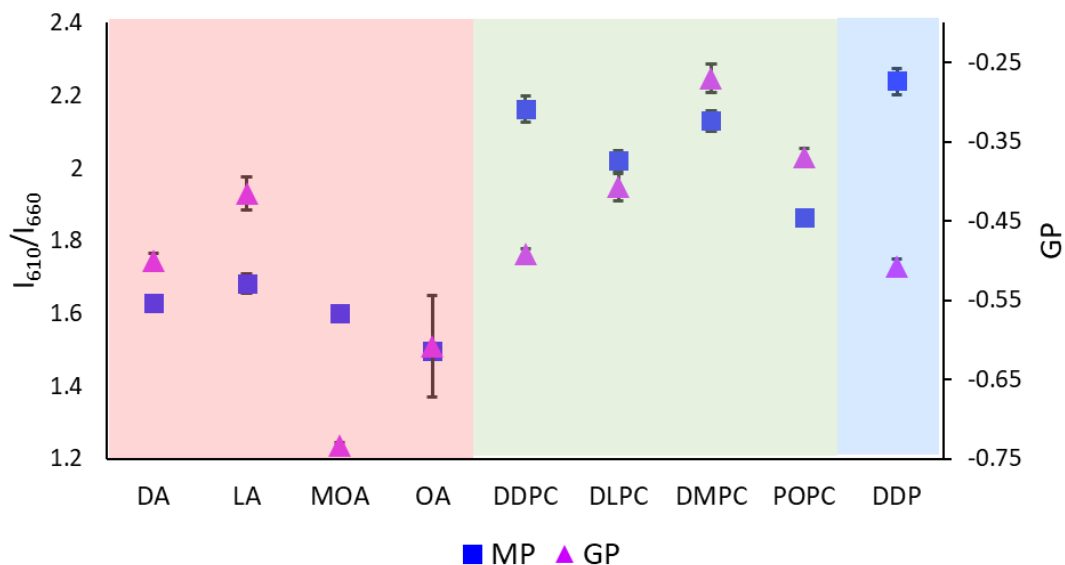
Figure 4.40: *The scatter plot shows the nile red I_{610}/I_{660} ratio (left y-axis) and laurdan GP values (right y-axis) of membranes i.e., different fatty acids, phospholipids and DDP as indicated on x-axis, at pH 8 and 45°C. N = 4, error bar = SD.*
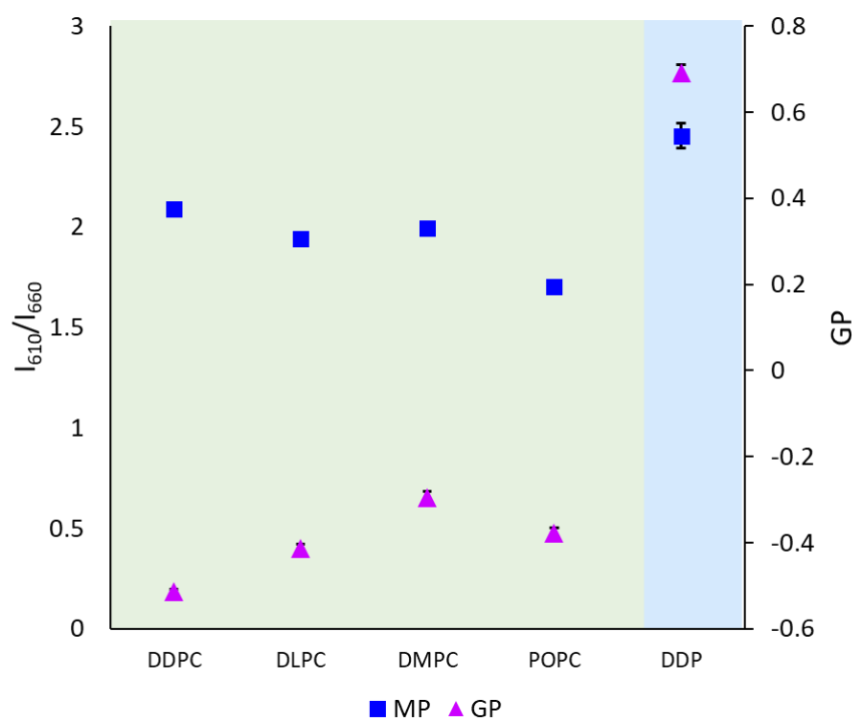

Figure 4.41: *The scatter plot showing the nile red I_{610}/I_{660} ratios (left y-axis) and the laurdan GP values (right y-axis) of different membranes i.e., for different phospholipids and DDP as indicated on x-axis, at pH 4 and 45°C. N = 4, error bar = SD. The I_{610}/I_{660} ratio of DDP membrane was higher than all the four phospholipid membranes indicating lower membrane*

micropolarity. The GP value of DDP was found to be way higher than all the phospholipid membranes investigated indicating the tighter packing of DDP membrane.
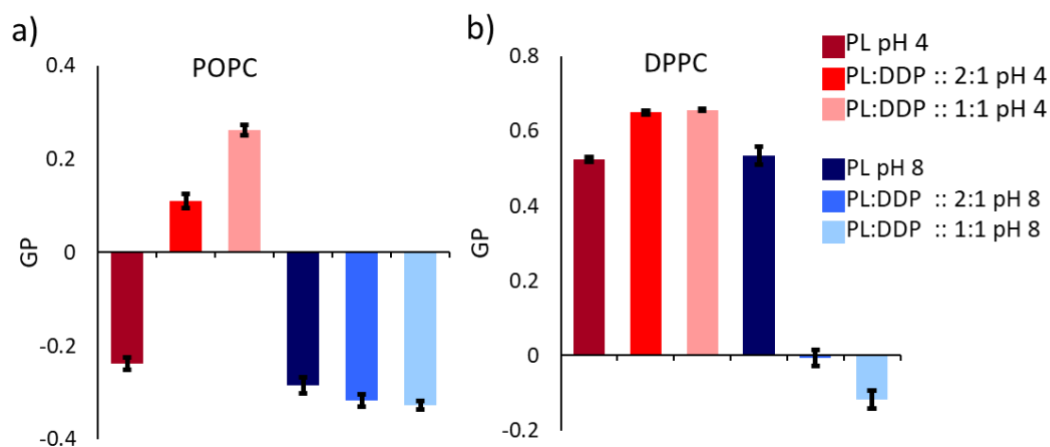

Figure 4.42: *a) The bar graph shows laurdan GP values of POPC and different POPC:DDP mixed membranes at pH 4 and 8, respectively, at 37°C. N = 4, error bar = SD. b) The bar graph shows laurdan GP values of DPPC and different DPPC:DDP mixed membranes at pH 4 and 8, at 37°C. N = 4, error bar = SD.*

4.5 Conclusions and Discussions

In this study, we characterized the pH-dependent self-assembly behaviour of DDP, an enticing candidate protocellular membrane. In contrast to FAs, which can assemble into vesicles only in a narrow regime of pH (pH 7-9), DDP alone can self-assemble into vesicles at a wide variety of pH, from pH 2 to 10. This highlights the compatibility of DDP vesicles with different prebiotically pertinent reactions that have been described to occur at a range of pH, including nonenzymatic oligomerization and replication reactions of the informational polymers occurring at a wide range. Systematic investigation of the properties of DDP membranes at varying pH revealed the markedly tunable nature of these membrane systems. The micropolarity of DDP membranes was found to be lower at pH 4 and it increased as the surrounding pH increased. The packing and fluidity of these membranes were also found to be dependent on the surrounding pH, which decreased upon increasing pH. Such pH-responsive nature can aid in the functionalization of the compartment that, in turn, facilitates robust adaptation under different environmental conditions. Significantly,

change in membrane micropolarity and packing in response to change in pH, would enable the modulation of the DDP membrane's permeability. For e.g. at acidic pH (~pH 4), an increase in DDP membrane packing would decrease membrane permeability and protect the encapsulated material from dilution and molecular parasites. On contrary, in neutral to alkaline pH (~pH 8), the decrease in DDP membrane packing would increase the exchange of materials like building blocks, between the protocell and environment, affecting the rates of encapsulated reactions like templated RNA replication. Additionally, this pH responsiveness would also directly impinge on the interaction capability and binding efficiencies of different co-solutes, including nucleotide and amino acid monomers and oligomers.

DDP assemble readily into membranes with low CBC as compared to FAs. Interestingly, the CBC varies with varying pH. The addition of DOH facilitated vesicle formation at alkaline pH by potentially H-bonding with the deprotonated DDP molecules. Further, the presence of DOH decreased the overall packing of the mixed (DDP:DOH) membranes. On similar lines, DOH also increased the overall micropolarity of the mixed membranes. DDP and DDP:DOH::1:1 membranes were more stable at elevated temperatures when compared to FA membranes. Upon increasing the temperature, the DDP membrane packing decreased, however, the extent of this decrease was dependent on the pH and also the presence of DOH. As indicated earlier, this decrease in order would increase membrane permeability to facilitated the exchange of matter between the protocellular compartment and its environment [24]. The decrease in suspension turbidity at elevated temperatures indicated the possibility of decreased membrane lamellarity. Next, we compared DDP membrane properties with different FAs and PLs membranes at pH 4 and 8, DDP membranes were found to be loosely packed and as dynamic as DA (C10) membranes at pH 8. However, the micropolarity of the membrane at this pH was similar to that of PL membranes. Nonetheless, unlike phospholipid membranes, the lower order in DDP membranes at neutral to alkaline pH, highlights its ability to support the emergence and sustenance of protocellular life forms.

Finally, we extended the pH-dependent tunable nature of DDP to phospholipid membranes by doping the phospholipid membranes with DDP. The addition of DDP allowed for controlling the membrane order of the PL:DDP mixed membranes when subjected to changing pH. In few previous studies, PL:FA mixed membrane

properties have been studied in the context of their role as model protocellular membranes [46]. We propose that DDP-phospholipid mixed membrane systems would have been even more ideal in this context, due to being a malleable and robust class of prebiotically plausible pH-responsive model protocellular membranes. This pH-responsive nature of PL:DDP mixed membranes, not only underscores the implications of these systems in the context of protocell formation, but would also be relevant for the synthetic cell engineering purposes. Pertinently, RNA oligomers have also been shown to bind more efficiently with ordered crystalline lipid membranes [47] than disordered ones. The ordered nature of the DDP membranes in acidic pH could also help in the localization and concentration of RNA molecules. Moreover, the addition of DDP in PL-membranes provides an additional component for creating adaptable artificial cells, where one could program versatile membrane functions that respond to a pH change. Finally, after undertaking more systematic research, the tunable nature of the DDP membranes can also be implemented for constructing pH-responsive synthetic cells that would allow for a selective and regiospecific release of drug molecules.

4.6 References

1. Deamer, David. "Membranes and the origin of life: a century of conjecture." *Journal of molecular evolution* 83.5 (2016): 159-168.
2. Monnard, Pierre-Alain, and Peter Walde. "Current ideas about prebiological compartmentalization." *Life* 5.2 (2015): 1239-1263.
3. Sarkar, Susovan, et al. "Prebiological membranes and their role in the emergence of early cellular life." *The Journal of Membrane Biology* 253.6 (2020): 589-608.
4. Deamer, David. "Membranes and the origin of life: a century of conjecture." *Journal of molecular evolution* 83.5 (2016): 159-168.
5. Mansy, S. S. "Cold Spring Harbor Perspect." *Biol* 2 (2010): a002188.
6. Morigaki, Kenichi, and Peter Walde. "Fatty acid vesicles." *Current Opinion in Colloid & Interface Science* 12.2 (2007): 75-80.
7. Meierhenrich, Uwe J., et al. "On the origin of primitive cells: from nutrient intake to elongation of encapsulated nucleotides." *Angewandte Chemie International Edition* 49.22 (2010): 3738-3750.
8. Apel, Charles L., David W. Deamer, and Michael N. Mautner. "Self-assembled vesicles of monocarboxylic acids and alcohols: conditions for stability and for the encapsulation of biopolymers." *Biochimica et Biophysica Acta (BBA)-Biomembranes* 1559.1 (2002): 1-9.
9. Rajamani, Sudha, et al. "Lipid-assisted synthesis of RNA-like polymers from mononucleotides." *Origins of Life and Evolution of Biospheres* 38.1 (2008): 57-74.

10. Bernhardt, Harold S. "The RNA world hypothesis: the worst theory of the early evolution of life (except for all the others) a." *Biology direct* 7.1 (2012): 1-10.

11. Bonfio, Claudia, et al. "Activation chemistry drives the emergence of functionalised protocells." *Chemical science* 11.39 (2020): 10688-10697.

12. Mariani, Angelica, et al. "pH-Driven RNA strand separation under prebiotically plausible conditions." *Biochemistry* 57.45 (2018): 6382-6386.

13. Rodriguez-Garcia, Marc, et al. "Formation of oligopeptides in high yield under simple programmable conditions." *Nature communications* 6.1 (2015): 1-7.

14. Kopetzki, Daniel, and Markus Antonietti. "Hydrothermal formose reaction." *New Journal of Chemistry* 35.9 (2011): 1787-1794.

15. Sarkar, Susovan, et al. "Compositional heterogeneity confers selective advantage to model protocellular membranes during the origins of cellular life." *Scientific reports* 10.1 (2020): 1-11.

16. Powner, Matthew W., and John D. Sutherland. "Prebiotic chemistry: a new modus operandi." *Philosophical Transactions of the Royal Society B: Biological Sciences* 366.1580 (2011): 2870-2877.

17. Cooper, George W., Wilfred M. Onwo, and John R. Cronin. "Alkyl phosphonic acids and sulfonic acids in the Murchison meteorite." *Geochimica et Cosmochimica Acta* 56.11 (1992): 4109-4115.

18. Walde, Peter, et al. "Preparation and characterization of vesicles from mono-n-alkyl phosphates and phosphonates." *The Journal of Physical Chemistry B* 101.38 (1997): 7390-7397.

19. Sakai, Takaya, et al. "Precipitate deposition around CMC and vesicle-to-micelle transition of monopotassium monododecyl phosphate in water." *The Journal of Physical Chemistry B* 116.36 (2012): 11225-11233.

20. Albertsen, Anders N., et al. "Self-assembly of phosphate amphiphiles in mixtures of prebiotically plausible surfactants." *Astrobiology* 14.6 (2014): 462-472.

21. Gao, Meihua, et al. "Vesicles composed of the single-chain amphiphile sodium monododecylphosphate: A model of protocell compartment." *Colloids and Surfaces A: Physicochemical and Engineering Aspects* 616 (2021): 126374.

22. Milshteyn, Daniel, et al. "Amphiphilic compounds assemble into membranous vesicles in hydrothermal hot spring water but not in seawater." *Life* 8.2 (2018): 11.

23. Kelley, Deborah S., et al. "An off-axis hydrothermal vent field near the Mid-Atlantic Ridge at 30 N." *Nature* 412.6843 (2001): 145-149.

24. Mansy, Sheref S., and Jack W. Szostak. "Thermostability of model protocell membranes." *Proceedings of the National Academy of Sciences* 105.36 (2008): 13351-13355.

25. Wang, Anna, Christopher Chan Miller, and Jack W. Szostak. "Core-shell modeling of light scattering by vesicles: Effect of size, contents, and lamellarity." *Biophysical journal* 116.4 (2019): 659-669.

26. Kalyanasundaram, K., and J. K. Thomas. "Environmental effects on vibronic band intensities in pyrene monomer fluorescence and their application in studies of micellar systems." *Journal of the American Chemical Society* 99.7 (1977): 2039-2044.

27. Sarkar, Susovan, Shikha Dagar, and Sudha Rajamani. "Influence of Wet–Dry Cycling on the Self-Assembly and Physicochemical Properties of Model Protocellular Membrane Systems." *ChemSystemsChem* 3.5 (2021): e2100014.

28. Arnould, Audrey, Cedric Gaillard, and Anne-Laure Fameau. "pH-responsive fatty acid self-assembly transition induced by UV light." *Journal of colloid and interface science* 458 (2015): 147-154.

29. Fameau, Anne-Laure, et al. "Smart foams: switching reversibly between ultrastable and unstable foams." *Angewandte Chemie International Edition* 50.36 (2011): 8264-8269.

30. Liu, Weiping, et al. "Flotation chemistry features in bastnaesite flotation with potassium lauryl phosphate." *Minerals Engineering* 85 (2016): 17-22.

31. Kanicky, J. R., and D. O. Shah. "Effect of premicellar aggregation on the p K a of fatty acid soap solutions." *Langmuir* 19.6 (2003): 2034-2038.

32. Misuraca, Loreto, et al. "High-temperature behavior of early life membrane models." *Langmuir* 36.45 (2020): 13516-13526.

33. Hayward, Dominic W., et al. "Neutralisation rate controls the self-assembly of pH-sensitive surfactants." *Soft Matter* 15.42 (2019): 8611-8620.

34. Xu, Huifang, et al. "Spontaneous vesicle formation and vesicle-to-micelle transition of sodium 2-ketooctanate in water." *Journal of colloid and interface science* 509 (2018): 265-274.

35. Mukherjee, Soumi, H. Raghuraman, and Amitabha Chattopadhyay. "Membrane localization and dynamics of Nile Red: effect of cholesterol." *Biochimica et Biophysica Acta (BBA)-Biomembranes* 1768.1 (2007): 59-66.

36. Parasassi, Tiziana, and Enrico Gratton. "Membrane lipid domains and dynamics as detected by Laurdan fluorescence." *Journal of fluorescence* 5.1 (1995): 59-69.

37. Harris, Faith M., Katrina B. Best, and John D. Bell. "Use of laurdan fluorescence intensity and polarization to distinguish between changes in membrane fluidity and phospholipid order." *Biochimica et Biophysica Acta (BBA)-Biomembranes* 1565.1 (2002): 123-128.

38. Ioffe, Valeriya, and Galyna P. Gorbenko. "Lysozyme effect on structural state of model membranes as revealed by pyrene excimerization studies." *Biophysical chemistry* 114.2-3 (2005): 199-204.

39. Sakai, Takaya, Youhei Kaneko, and Kaoru Tsujii. "Premicellar aggregation of fatty acid N-methylethanolamides in aqueous solutions." *Langmuir* 22.5 (2006): 2039-2044.

40. Piñeiro, Lucas, Mercedes Novo, and Wajih Al-Soufi. "Fluorescence emission of pyrene in surfactant solutions." *Advances in colloid and interface science* 215 (2015): 1-12.

41. Martins, Jorge, and Eurico Melo. "Molecular mechanism of lateral diffusion of py10-PC and free pyrene in fluid DMPC bilayers." *Biophysical Journal* 80.2 (2001): 832-840.

42. Mondal, Tathagata, et al. "Hydrogen-bonding-induced chain folding and vesicular assembly of an amphiphilic polyurethane." *Langmuir* 29.22 (2013): 6746-6753.

43. Inamura, Kosuke, et al. "Inhibitory effect of hybrid liposomes on the growth of liver cancer stem cells." *Biochemical and biophysical research communications* 509.1 (2019): 268-274.

44. Bompard, Julien, et al. "Membrane fluidity as a new means to selectively target cancer cells with fusogenic lipid carriers." *Langmuir* 36.19 (2020): 5134-5144.

45. Koitabashi, Kyoka, et al. "Acidic pH-induced changes in lipid nanoparticle membrane packing." *Biochimica et Biophysica Acta (BBA)-Biomembranes* 1863.8 (2021): 183627.

46. Jin, Lin, et al. "Fatty acid/phospholipid blended membranes: a potential intermediate state in protocellular evolution." *Small* 14.15 (2018): 1704077.
47. Janas, Tadeusz, Teresa Janas, and Michael Yarus. "Specific RNA binding to ordered phospholipid bilayers." *Nucleic acids research* 34.7 (2006): 2128-2136.

Thesis Summary

The emergence of membrane bound compartments is considered to have been crucial for the origin of early cellular life on Earth. Unlike contemporary bio-membranes, protocellular membranes are hypothesized to have been comprised of SCAs such as fatty acids, along with fatty alcohol and glycerol monoesters of fatty acids etc. Previous literature suggest that the composition and properties of protocell membranes would have been directly governed by means of complex interactions between themselves and with their environment. Towards this, I first looked at the influence of model protocells' compositional diversity, towards its ability to self-assemble into stable vesicles under different environmental constrains. I worked with a few different composite model protocell membrane systems and concocted them by mixing fatty acids of different chain lengths with their respective chain length co-surfactants. The results demonstrated that compositionally diverse membrane systems are amenable to readily form compartments that are more stable and robust under the multiple environmental conditions that we tested. Next, I evaluated the structural and chemical stability of these mixed model protocellular membranes under multiple wet-dry cycles, a geological feature with crucial importance for life's origins and early evolution. Using multiple probes, I found that the membrane composition changes upon subjecting a system to multiple wet-dry cycles. Pertinently, this led to changes in the membrane properties over the various cycles. Finally, I evaluated the membrane-forming ability of dodecyl phosphate (DDP), a minimally studied prebiotically relevant SCA. Because of multiple shortfalls that fatty acid-based membranes encounter, for e.g., especially their limitation to assemble into vesicles over a very limited pH regime, we aimed to characterize alternate membranes and DDP was a relevant choice. DDP was found to assemble into vesicles over a wide range of pH (from pH 2-10) and their membrane properties changed as a function of pH. Further, the addition of dodecanol to the DDP membrane system, enhanced vesicle formation and stability in alkaline pH regimes. This tunable nature of DDP membranes in response to pH can be effectively used to construct functional protocellular compartments. In all, our work shows that DDP was found to be a better protocell candidate than traditional fatty acid-based membranes. Towards this, the next step would be to look at the self-assembly behaviour of mixed

DDP-based membranes by adding supporting co-surfactants and looking at their self-assembly, vesicular stability and properties, under simulated prebiotic conditions. The tunable nature of the DDP membranes can also be implemented for constructing pH-responsive synthetic cells that would allow for a selective and regiospecific release of drug molecules.

PUBLICATIONS

1. Sarkar, Susovan, et al. "Compositional heterogeneity confers selective advantage to model protocellular membranes during the origins of cellular life." *Scientific reports* 10.1 (2020): 1-11.

2. Sarkar, Susovan, et al. "Prebiological membranes and their role in the emergence of early cellular life." *The Journal of Membrane Biology* 253.6 (2020): 589-608.

3. Sarkar, Susovan, Shikha Dagar, and Sudha Rajamani. "Influence of Wet–Dry Cycling on the Self-Assembly and Physicochemical Properties of Model Protocellular Membrane Systems." *ChemSystemsChem* 3.5 (2021): e2100014.

4. Sarkar, Susovan, et al. "pH-responsive self-assembled compartments as tuneable model protocellular membrane systems." *ChemBioChem* (2022): e20220037.

SPRINGER NATURE

Thank you for your order!

Dear Mr. Susovan Sarkar,

Thank you for placing your order through Copyright Clearance Center's RightsLink® service.

Order Summary

Licensee:	Mr. Susovan Sarkar
Order Date:	Jun 10, 2022
Order Number:	5325400719546
Publication:	Journal of Membrane Biology
Title:	Prebiological Membranes and Their Role in the Emergence of Early Cellular Life
Type of Use:	Thesis/Dissertation
Order Ref:	20152017
Order Total:	0.00 USD

View or print complete details of your order and the publisher's terms and conditions.
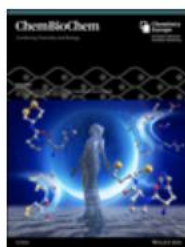
Sincerely,

Copyright Clearance Center

CCC **RightsLink®**

SPRINGER NATURE

Compositional heterogeneity confers selective advantage to model protocellular membranes during the origins of cellular life

Author: Susovan Sarkar et al

Publication: Scientific Reports

Publisher: Springer Nature

Date: Mar 11, 2020

Copyright © 2020, The Author(s)

Thank you for your order!

Dear Mr. Susovan Sarkar,

Thank you for placing your order through Copyright Clearance Center's RightsLink® service.

Order Summary

Licensee: Mr. Susovan Sarkar
Order Date: Oct 5, 2022
Order Number: 5402570225607
Publication: ChemBioChem
Title: pH-Responsive Self-Assembled Compartments as Tuneable Model Protocellular Membrane Systems**
Type of Use: Dissertation/Thesis
Order Total: 0.00 USD

View or print complete details of your order and the publisher's terms and conditions.

Sincerely,

Copyright Clearance Center

CCC RightsLink

VITA

Name: Susovan Sarkar

Address: Department of Biology,

IISER-Pune, Dr. Homi Bhabha Road,

Ward No. 8, NCL Colony, Pashan,

Pune, Maharashtra – 411008.

Email address: Susovan.sarkar@students.iiserpune.ac.in

Education: B. Sc., Microbiology, Physics, and Chemistry, 2015

M.Sc., Biological Sciences, IISER-Pune, 2022

Ph.D., Biological Sciences, IISER-Pune, 2022